Coannihilation neutralino-stop dans le MSSM : violation de saveur, corrections radiatives et leur impact sur la densité relique de matière noire

Quentin Le Boulc'H

UNIVERSITÉ DE GRENOBLE

THÈSE

Pour obtenir le grade de

DOCTEUR DE L'UNIVERSITÉ DE GRENOBLE

Spécialité : **Physique subatomique et astroparticules**

Arrêté ministériel : 7 août 2006

Présentée par

Quentin Le Boulc'h

Thèse dirigée par **Michael Klasen**

préparée au sein du **Laboratoire de Physique Subatomique et de Cosmologie** et de **l'École doctorale de Physique de Grenoble**

Neutralino-stop coannihilation in the MSSM: flavor violation, radiative corrections and their impact on the dark matter relic density.

Thèse soutenue publiquement le **23 septembre 2013**,
devant le jury composé de :

Pr. Jean Orloff

Professor, LPC, Clermont Université, Président

Pr. Manuel Drees

Professor, Bethe Center for Theoretical Physics, Universität Bonn, Rapporteur

Pr. Joakim Edsjö

Professor, Oskar Klein Centre for Cosmoparticle Physics, Stockholm University, Rapporteur

Dr. Sabine Kraml

Directeur de recherche CNRS, LPSC, Université de Grenoble, Examinateur

Dr. Geneviève Bélanger

Directeur de recherche CNRS, LAPTh, Université de Savoie, Examinateur

Pr. Michael Klasen

Professor, Institut für Theoretische Physik, Westfälische Wilhelms-Universität Münster, Directeur de thèse

"Le savant n'étudie pas la nature parce que cela est utile; il l'étudie parce qu'il y prend plaisir, et il y prend plaisir parce qu'elle est belle."

— Henri Poincaré

"There is a crack in everything
That's how the light gets in."

— Leonard Cohen

A mon fils, Malo,
pour m'avoir rappelé
que tout commence
par l'envie d'apprendre.

Acknowledgements

Je tiens tout d'abord à remercier Manuel Drees et Joakim Edsjö pour m'avoir fait l'honneur d'être mes rapporteurs, ainsi que d'avoir fait le déplacement jusque Grenoble afin d'assister à ma soutenance. La pertinence de leurs remarques sera utile à toute la collaboration lors des projets à venir, j'en suis sûr. Je remercie également Jean Orloff pour m'avoir fait le plaisir de présider mon jury de thèse, ainsi que Geneviève Bélanger et Sabine Kraml pour avoir été présentes en tant qu'examinateurs.

Je remercie ensuite Michael Klasen, mon directeur de thèse, pour m'avoir donné la possibilité de travailler sur ce projet de thèse, et pour m'avoir donné son soutien et sa confiance malgré les imprévus. Sa détermination et ses encouragements ont été précieux durant ces trois années.

Ma reconnaissance va ensuite à mes collaborateurs sans qui rien n'aurait été possible. Un grand merci à Björn Herrmann pour m'avoir encadré depuis mon arrivée en tant que stagiaire jusqu'à la fin de ma thèse. Sa disponibilité et sa pédagogie ont rendu notre collaboration très agréable. Merci également à Karol Kovařík pour son investissement sans faille dans notre projet ; je lui dois la majeure partie de ce que j'ai appris sur le calcul NLO. Avec lui également, travailler a été un plaisir. Je ne peux évidemment pas manquer de remercier Julia Harz, qui a été ma principale collaboratrice durant ces trois années. J'ai rencontré peu de personnes aussi motivées et appliquées dans leur travail, et son efficacité a été plus qu'appréciable. Je la remercie également pour nos échanges quotidiens, durant lesquels nous avons partagé les moments de réussite comme de doute. Je n'oublie pas de remercier Moritz Meinecke et Patrick Steppeler pour nos discussions ainsi que pour l'ambiance chaleureuse lors de nos réunions à Münster, Annecy ou ailleurs.

Je suis également reconnaissant envers Serge Kox, directeur du LPSC, pour m'avoir accueilli au sein du laboratoire, ainsi que tout le personnel administratif pour avoir su me guider avec patience lorsque j'étais perdu. Je remercie encore une fois Sabine Kraml, directrice du groupe de Physique théorique, pour son soutien. Mes remerciements vont ensuite à tous les membres du groupe pour les moments passés en leur compagnie durant ces trois années, grâce auxquels venir au LPSC a toujours été un plaisir. J'aimerais en particulier remercier les thésards du groupe : Béranger Dumont, Tomáš Ježo, Florian Lyonnet, Zhaoting Pan et Josselin Proudom, pour la super ambiance. Merci également à Ingo Schienbein, en particulier pour m'avoir guidé durant

mes premières expériences d'enseignement, ainsi qu'à Christopher Smith et Akin Wingerter pour toutes nos discussions. Je souhaite enfin bonne chance à Jeremy Bernon pour sa thèse à venir.

Je me dois aussi de remercier la SNCF pour m'avoir transporté de Lyon à Grenoble (non sans encombre) presque quotidiennement. Lorsque ce ne fut pas possible, le groupe de Physique Théorique de l'IPNL m'a accueilli, et je les en remercie. Merci en particulier à Guillaume Drieu La Rochelle, Martin Elmer et Ahmad Tarhini que j'ai eu le plaisir de retrouver là-bas.

Pour finir je remercie ma famille, et en particulier mes parents, pour leur soutien constant et leurs encouragements, et ce depuis très longtemps, ainsi que ma femme pour m'avoir supporté durant ces trois années, et mon fils, qui ne sait pas à quel point ses sourires m'ont aidé à avancer.

Introduction

Dark matter is one of the most important mysteries of modern Cosmology. Since the discovery of "missing mass" by F. Zwicky in 1933 after measuring the velocities of galaxies in the Coma cluster, many experimental results have confirmed that about 85% of the Universe mass was made of an unknown, invisible, stable matter called dark matter, which is now a major ingredient of the Standard Model of Cosmology. These experimental results also tell us that dark matter seems to be made of Weakly Interacting Massive Particles (WIMPs). The WMAP experiment has especially measured the exact quantity of this dark matter in our Universe, and a more precise measurement was recently performed by the Planck experiment. This quantity actually corresponds to what remains after the so-called freeze-out mechanism in the early Universe, and is therefore called "relic density". As this mechanism involves not only the expansion of the Universe but also the annihilation of dark matter, it can be predicted from theoretical models, as we will see in Chap. 1. Indeed, if one knows the nature of dark matter and its interactions, the necessary annihilation cross sections can be computed.

On the Particle Physics side, dark matter is also of great importance. It is one of the very few observations which can not be accounted for by the Standard Model of Particle Physics, which is described in detail in Chap. 2. Despite the enormous success of the latter, which thanks to the elegant framework of gauge theories can explain up to a very high precision almost everything which has been measured in Particle Physics, it is believed that there might be some New Physics beyond it. In particular none of the Standard Model particles is a good candidate for dark matter.

The most famous model of Physics beyond the Standard Model is Supersymmetry, presented in Chap. 3, which introduces a new symmetry relating bosons to fermions and therefore predicts the existence of several new particles: the supersymmetric partners of the Standard Model particles. As Supersymmetry is broken it also introduces a large number of free parameters, and studying the phenomenology of its minimal version (the MSSM) is already a huge task. One of the numerous advantages of Supersymmetry is that it provides several possible dark matter candidates, the lightest neutralino being the most studied. Indeed, an additional parity called R-parity is generally included in the MSSM, which leads to the stability of the Lightest Supersymmetric Particle (LSP). If this LSP is weakly interacting, then it can be a good dark matter candidate. This is the case of the neutralino, which is a mixing of bino, neutral wino

and higgsinos, respectively the supersymmetric partners of the B boson, the neutral W boson and the neutral Higgs bosons. As the lightest neutralino is usually mostly made of bino, its annihilation cross section is small and its relic density is in general too large. However, special mechanisms can enhance its annihilation cross section and thus reduce its relic density. One of these mechanisms is the coannihilation with another supersymmetric particle, which does not imply the annihilation of neutralinos, but new processes resulting in the diminution of the density of neutralinos. Indeed, if a supersymmetric particle has a mass close to the neutralino mass, it will not decouple before the freeze-out, and its coannihilation with the neutralino will eventually reduce the relic density.

One of the supersymmetric particles which can coannihilate with the neutralino and therefore decrease its relic density is the stop, i.e. the supersymmetric partner of the top quark. Because of its large mass (and Yukawa coupling), the top quark has a special status within the Standard Model. So does the stop, which like the top quark is strongly related to the Higgs sector by the loop corrections to its mass. In addition, for several reasons, the stop is usually the lightest squark and can also be the Next-to-Lightest Supersymmetric Particle (NLSP) and thus coannihilate with the neutralino in some parts of the MSSM parameter space. As will be discussed in Chap. 4, because of the difficulty to probe the small neutralino-stop mass splitting scenario at the LHC, and the corresponding low direct detection cross section, these regions, called neutralino-stop coannihilation regions, are still compatible with experimental constraints. For these reasons it is interesting to study the phenomenology of these regions in the MSSM.

The phenomenology of the dark matter relic density in the MSSM is quite well known, in particular in simple models like the cMSSM, based on strong theoretical assumptions. Since these models are more and more constrained, the knowledge of more general SUSY models should be improved. In particular it is necessary to study the phenomenological consequences of relaxing such assumptions: no or partial unification of soft masses, CP violation, Non Minimal Flavor Violation (NMFV), etc. In Chap. 5 we study the phenomenology of NMFV in the squark sector in the context of neutralino relic density. We consider flavor violating terms in the sectors of right handed third generation up and down squarks and show that the corresponding off-diagonal elements in the squark mass matrices can have an important impact on the thermally averaged (co)annihilation cross section of the neutralino, and in consequence can modify its predicted relic density. More precisely, large flavor mixing allows for efficient annihilation of neutralinos into final states that are forbidden in the case of MFV. Flavor violating terms are also important in the case of coannihilation of a neutralino with a squark, since they reduce the squark mass eigenvalue and therefore the neutralino-squark mass splitting, on which the importance of coannihilation processes crucially depends. All these effects lead to the opening of new regions compatible with the relic density measurement, thanks to contributions which are absent in the cMSSM with MFV (neutralino-sbottom coannihilation or neutralino annihilation into top and charm quarks for example).

In Chap. 6, we focus on the issue of the precision with which Supersymmetric parameters can be extracted from measurements of the relic density, again in the case of neutralino-stop coannihilation. Indeed, the experimental results are more and more precise, and the relic density measurement by Planck has reached a 2% accuracy. On the other hand, the theoretical predictions also need to be more accurate, which requires to compute the (co)annihilation cross sections at Next-to-Leading Order (NLO). Following earlier work in the calculation of one-loop SUSY-QCD corrections to the annihilation of neutralinos, which have shown that the impact of such corrections was larger than the experimental uncertainty, we have calculated similar corrections for the neutralino-stop coannihilation into electroweak gauge and Higgs bosons. The calculation is presented in Chap. 6, including the procedure used to cancel the Ultra-Violet (UV) and Infra-Red (IR) divergences, as well as other technical details. We also give details about the implementation of the results in a numerical Fortran code which allows us to compute the relic density in the parameter space of Supersymmetric models using these one-loop cross section thanks to `micrOMEGAs`. We also show numerical results for the corresponding NLO cross sections as well as the impact of these corrections on the relic density in a phenomenological MSSM model. We observe that this impact is larger than the current experimental uncertainty on the relic density and therefore need to be taken into account. Finally, we comment on the ongoing calculation of the one-loop corrections to neutralino-stop coannihilation into a top quark and a gluon.

The App. A contains details about the structure of our numerical code and the way our results are implemented. Apps. B and C introduce two different methods used to remove IR divergences: the dipole subtraction method, which is not used in our calculation but is part of a future project, and the two cutoff phase space slicing method, used in the case of a gluon in the final state.

We complete this introduction by noticing how exciting have been the last three years regarding experimental results in Particle and Astroparticle Physics. The results of the Planck experiment, recently released, were one of the main motivations to our precision calculation. It is fortunate that, thanks to the LHC which started running at the end of 2009, the Standard Model can now be completely described including its last piece: the Higgs boson. However these experiments also brought new constraints on the models we studied: the Higgs boson mass has been measured, strong limits on the masses of Supersymmetric particles have been derived, New Physics contributions to flavor observables have been severely constrained, etc. It is of course impossible to take into account all the latest constraints in each of the studies presented here. Nevertheless it is clear that the methods, tools and qualitative observations presented in this thesis do not depend on the specific supersymmetric scenario and will be very important for future studies.

Acronyms used in this thesis

- **WIMP: Weakly Interacting Massive Particle**
- **LHC: Large Hadron Collider**
- **SM: Standard Model**
- **EWSB: Electro-Weak Symmetry Breaking**
- **QCD: Quantum Chromo-Dynamics**
- **CKM: Cabbibo-Kobayashi-Maskawa**
- **RGE: Renormalization Group Equations**
- **SUSY: Supersymmetry**
- **LSP: Lightest Supersymmetric Particle**
- **NLSP: Next to Lightest Supersymmetric Particle**
- **GUT: Grand Unified Theory**
- **MSSM: Minimal Supersymmetric Standard Model**
- **cMSSM: constrained Minimal Supersymmetric Standard Model**
- **pMSSM: phenomenological Minimal Supersymmetric Standard Model**
- **MFV: Minimal Flavor Violation**
- **cMFV: constrained Minimal Flavor Violation**
- **NMFV: Non Minimal Flavor Violation**
- **NLO: Next-to-Leading Order**
- **UV: Ultra-Violet**
- **IR: Infra-Red**

Contents

1. Dark matter and its relic density **1**

1.1. Dark matter evidences and detection 1

1.1.1. The Standard Model of Cosmology 1

1.1.2. Evidences for dark matter 2

1.1.3. Detection of dark matter 4

1.2. The relic density of dark matter 5

1.2.1. The freeze-out mechanism 5

1.2.2. Overview of relic density calculation 6

1.2.3. Calculation of the relic density including coannihilation 7

2. The Standard Model of Particle Physics **13**

2.1. Introduction 13

2.2. Quantum Electro-Dynamics 14

2.3. Quantum Chromo-Dynamics 14

2.4. From the weak interactions to the Higgs boson 16

2.5. Unitary gauge and the Goldstone Boson Equivalence Theorem 18

2.6. Quarks and leptons 19

2.7. Beyond the Standard Model? 21

3. Supersymmetry and the MSSM **25**

3.1. Introduction 25

3.2. The Supersymmetry algebra 26

3.3. The Minimal Supersymmetric Standard Model 27

3.3.1. Multiplet content of the MSSM 27

3.3.2. Lagrangian and interactions of the MSSM 28

3.3.3. R-parity 31

3.4. Supersymmetry breaking 32

3.4.1. Soft Supersymmetry breaking 32

3.4.2. Mediation of Supersymmetry breaking 33

3.5. The MSSM mass spectrum 36

3.5.1. Mass eigenstates of the MSSM 36

3.5.2. The Higgs sector 37

3.5.3. The neutralino sector . . . 39
3.5.4. The squark sector . . . 39

4. Neutralino-stop coannihilation in the MSSM 43
4.1. Phenomenology of neutralino relic density . . . 43
4.1.1. cMSSM . . . 43
4.1.2. Non universal models . . . 44
4.2. Experimental constraints in the MSSM parameter space . . . 47
4.2.1. Relic density of dark matter . . . 47
4.2.2. Direct detection of dark matter . . . 50
4.2.3. Supersymmetric particle production and decay . . . 51
4.2.4. Higgs boson observation . . . 52
4.2.5. Flavor violating observables in B-Physics . . . 53
4.2.6. Anomalous magnetic moment of the muon . . . 54
4.3. Neutralino-stop coannihilation in the pMSSM . . . 55

5. Impact of non minimal flavor violation on the relic density 61
5.1. Introduction . . . 61
5.2. Non minimal flavor violation in the squark sector of the MSSM . . . 62
5.3. Impact on the relic density . . . 64
5.4. Numerical analysis . . . 67
5.5. Flavor violating down-squark and sbottom coannihilation . . . 73
5.6. Conclusion . . . 74

6. Impact of next-to-leading order corrections on the relic density 77
6.1. The DM@NLO project . . . 77
6.1.1. NLO cross sections for dark matter relic density . . . 77
6.1.2. Calculation and implementation: practical aspects . . . 79
6.2. Virtual corrections and renormalization . . . 80
6.2.1. Introduction . . . 80
6.2.2. Regularization of UV divergences . . . 82
6.2.3. QCD renormalization of the MSSM . . . 85
6.3. Real corrections and infrared treatment . . . 92
6.3.1. Introduction . . . 92
6.3.2. Cancellation of soft divergences . . . 93
6.3.3. Additional sources of infrared divergences . . . 96
6.4. Next-to-leading order cross sections: numerical results . . . 98
6.4.1. pMSSM scenario and tree-level cross sections . . . 98
6.4.2. Next-to-leading order cross sections . . . 101
6.5. Numerical impact on the relic density . . . 104

6.6. The gluon final state . . . 109
6.6.1. Virtual corrections and renormalization . . . 109
6.6.2. Real corrections and collinear divergences . . . 111
6.7. Conclusion . . . 113

A. The DM@NLO code **115**
A.1. Structure of the code . . . 115
A.2. General amplitudes . . . 117

B. Dipole subtraction method **119**

C. The two cutoff phase space slicing method **121**
C.1. Soft part . . . 121
C.2. Hard collinear part . . . 123
C.3. Hard non collinear part . . . 124

Conclusion and outlook **127**

List of Figures **129**

List of Tables **133**

Bibliography **135**

Chapter 1.

Dark matter and its relic density

This chapter is devoted to a short review of WIMP dark matter and its relic density. In Sec. 1.1 we briefly review some experimental evidences for dark matter and discuss the possibility of its direct or indirect detection. In Sec. 1.2 we focus on its relic density: the freeze-out mechanism is introduced, and the calculation of the relic density is presented.

1.1. Dark matter evidences and detection

1.1.1. The Standard Model of Cosmology

The Standard Model of Cosmology is based on the Big-Bang Cosmological principle and describes the evolution of the Universe from its very early state to now. It explains quantitatively many observations like the Big-Bang Nucleosynthesis (BBN), the Cosmic Microwave Background (CMB), the formation of structures, the abundance of elements, etc. Solving the Einstein equations by assuming isotropy and homogeneity leads to the the Friedmann equation which describes the expansion of the Universe:

$$H^2 + \frac{k}{a^2} = \frac{8\pi G_N}{3}\rho_{tot} \tag{1.1}$$

where $a(t)$ is the scale factor, k describes the spatial curvature, G_N is Newton's constant, ρ_{tot} is the total average energy density of the universe, and $H(t)$ is the Hubble parameter defined as

$$H(t) = \frac{\dot{a}(t)}{a(t)}. \tag{1.2}$$

Its current value is $H_0 = 67.3 \pm 1.2$ km s^{-1} Mpc^{-1} [1]. The density of matter, energy or radiation in the Universe are often expressed in units of ρ_c, the critical density, which is

defined as the total density when the Universe is flat ($k = 0$):

$$\rho_c \equiv \frac{3H^2}{8\pi G_N}. \tag{1.3}$$

For a substance i we then have

$$\Omega_i \equiv \frac{\rho_i}{\rho_c}. \tag{1.4}$$

The quantities Ω_i evolve with time and their equations of evolution depend on the equation of state of the substance i.

This model is also denoted as the $\Lambda-$CDM model, where Λ represents the cosmological constant which could explain the so-called dark energy, and CDM stands for "Cold Dark Matter". Dark energy and dark matter are the two most important ingredients of the Standard Model of Cosmology, but also the two least known. The History of Universe as described by the Standard Model of Cosmology can be summarized as the following:

- $T \sim 10^{16}$ GeV: breaking of a grand unified group into the Standard Model gauge groups.
- $T \sim 10^2$ GeV: electroweak symmetry breaking.
- $T \sim 10^1 - 10^3$ GeV: freeze-out of WIMP dark matter with GeV-TeV mass.
- $T \sim 0.3$ GeV: QCD phase transition (confinement of quarks and gluons into hadrons).
- $T \sim 1$ MeV: neutrons freeze-out.
- $T \sim 100$ keV: Big Bang Nucleosynthesis (creation of light elements from protons and neutrons).
- $T \sim 1$ eV: beginning of structure formation.
- $T \sim 0.4$ eV: Cosmic Microwave Background produced by photon decoupling.
- $T = 2.7K \sim 10^{-4}$ eV: today.

Some of these steps are well known and experimentally tested (Big Bang Nucleosynthesis for instance), others are still speculative (Grand Unification Theories). As can be seen at a temperature of about a TeV occurs the freeze-out of a hypothetical dark matter particle, this mechanism being described in Sec. 1.2.

1.1.2. Evidences for dark matter

We will now give some of the major observations supporting the idea of dark matter [2]. The first hints for dark matter came from an observation of the velocity dispersion of galaxies in the Coma cluster by F. Zwicky in 1933 [3]. Indeed, the virial mass of the cluster derived from the velocities of galaxies did not agree with the mass observed from luminous matter. The expression "dark matter" then appeared. More recently, more refined measurements have been

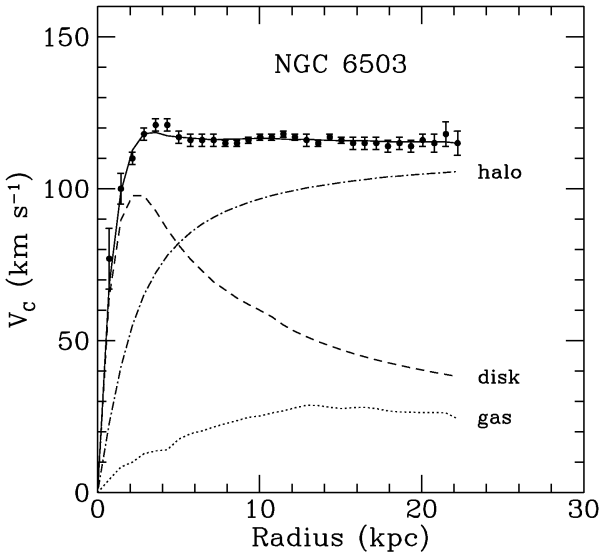

Figure 1.1.: Rotation curve of the spiral galaxy NGC 6503. The dotted, dashed and dash-dotted lines are the contributions of gas, disk and dark matter, respectively. Figure taken from [5].

done using gravitational lensing and X-ray observations. They all agree on this conclusion and on the dark matter content of the Coma cluster.

One of the most striking evidences for dark matter comes from the recent observation of the Bullet cluster, which is in fact made of two interacting clusters. The gravitational potential is measured from gravitational lensing, while the quantity of baryonic (luminous) matter is measured from X-rays observations. They do not coincide, which can be explained by the presence of a large amount of non baryonic collisionless matter [4].

At smaller scales, the measurement of the circular velocity of matter as a function of its distance from the galactic center is in disagreement with the velocity expected from Newtonian dynamics. Indeed, the rotation curve is expected to fall as $r^{-1/2}$ beyond the visible disk, while the observations show a flat behavior (see Fig. 1.1). This discrepancy can be explained by assuming the presence of a halo of invisible matter with a mass density $\rho(r) \sim r^{-2}$, which is one of the strongest evidences for dark matter. However the exact shape of this density in the inner part of the galaxies is still poorly known.

The total amount of dark matter in the Universe can be determined only by observations on cosmological scales, and in particular from the Cosmic Microwave Background. This radiation, discovered by A. Penzias and E. Wilson in 1965, comes from the decoupling of photons in the early Universe. The CMB is described with a very good precision by a black body spectrum of temperature $T = 2.726\ K$ and is almost perfectly isotropic. Its small anisotropies can be however analyzed and provide crucial information about the matter and energy content of the

early Universe. In particular, the density of dark matter can be extracted from the analysis of its spectrum. The WMAP experiment extracts the 7 parameters of the Cosmological Standard Model from their measurement of the CMB, and after combination with the measurement of the Hubble constant H_0 and Baryon Acoustic Oscillations (BAO) they obtain [6]:

$$\Omega_{\mathrm{CDM}} h^2 \;=\; 0.1126 \;\pm\; 0.0036. \tag{1.5}$$

More recently, the Planck experiment has released more accurate results [1]:

$$\Omega_{\mathrm{CDM}} h^2 \;=\; 0.1199 \;\pm\; 0.0027. \tag{1.6}$$

Again, "CDM" stands for "Cold Dark Matter". Indeed, the observation of large scale structures are in disagreement with the idea of a hot (i.e. relativistic) dark matter, and it is usually assumed that dark matter is made of rather heavy particles (even though the possibility of "warm" dark matter is still under discussion).

1.1.3. Detection of dark matter

As it is obvious that dark matter carries neither a strong charge (otherwise it would interact with baryonic matter) nor an electromagnetic one (otherwise it would not be dark), it is often considered that dark matter interacts only through the weak interaction (a strong argument for this is given in Sec. 1.2.3), in which case it is a Weakly Interacting Massive Particle (WIMP).

The idea of detecting directly WIMPs [7, 8], first mentioned in [9], provides the most promising way of identifying dark matter. As the Milky Way is expected to be embedded within a dark matter halo, dark matter particles should travel through the solar system and even across the earth. The expected galactic velocity of dark matter leads to an energy transfer to an atomic nucleus of about ~ 10 keV, which could in principle be detected by experiments. However, using rough estimations for the local mass density of dark matter, and considering weakly interacting dark matter, one obtains a typical cross section for a WIMP scattering on nuclei below about 10^{-8} pb. These small cross sections imply that detecting directly dark matter on earth would require heavy target nuclei, large detectors and long measurement times.

The main experimental challenge is to reduce the background from environmental radioactivity and cosmic radiation which is much higher than the expected signal and requires to run such experiments deep underground. As this background most likely consists in electron recoil, one can also try to discriminate it from the WIMP induced nuclear recoil. The three main effects used to detect the scattering of WIMPs with a nucleus are ionization, production of scintillation light, and production of heat. Many experiments use two of these methods in order to improve the background rejection. Annual modulation of the signal is also used to discriminate it from the background.

These experiments have made enormous progress in the last years and have started to exclude interesting regions of the parameter space of dark matter models. In particular, the XENON100 [10] experiment provides the most stringent constraints up to now. However several experiments have claimed to have observed dark matter. Indeed, DAMA [11], CoGeNT [12, 13] and CRESST [14] see hints of dark matter with a mass around 10 GeV, which is however excluded by the limits put by the XENON100, CDMS [15–17] and EDELWEISS [18] experiments. These three claims are also not compatible between each other and no single dark matter model is able to explain all of these discrepancies.

Another possibility is to detect indirectly dark matter via its annihilation into detectable particles like gamma rays, electrons and positrons, protons and antiprotons, or neutrinos. The stable particles will be directly detected ("primary products"), while the unstable ones will decay into secondary products which will be detected. All these particles are of course of very different nature and will therefore imply very different production mechanisms, propagation models, detection techniques, etc. For a review of indirect detection of WIMPs, see [2] and [8].

1.2. The relic density of dark matter

1.2.1. The freeze-out mechanism

It has been known since almost half a century that a stable particle in thermal equilibrium in the early Universe can have a significant abundance today, due to the so-called freeze-out mechanism. The thermal equilibrium is possible when the thermal energy of the primordial plasma is higher than the mass of the stable (dark matter) particle. The equilibrium is guaranteed by annihilation of dark matter into lighter (Standard Model) particles, and the opposite process: production of dark matter through annihilation of Standard Model particles. The latter process is possible only since the thermal energy is sufficiently high. As the Universe expands, its temperature decreases, and when the thermal energy becomes smaller than the mass of the dark matter particle, its production starts to be thermally suppressed by the Boltzmann distribution. Annihilation is however not suppressed and the (comoving) number density of dark matter particles drops exponentially. As the annihilation rate is proportional to the number density it also decreases, and when it falls below the expansion rate the annihilation stops and the dark matter particle decouples from the plasma: this is the freeze-out. The comoving number density of dark matter particles remains then constant until today, and the density which is measured today is called relic density (see Fig. 1.2).

Here we have assumed that other non-Standard-Model particles were much heavier so that they decouple long before the dark matter particle and therefore do not play any role during the freeze-out mechanism. However if it happens that one of these particles is close in mass to the

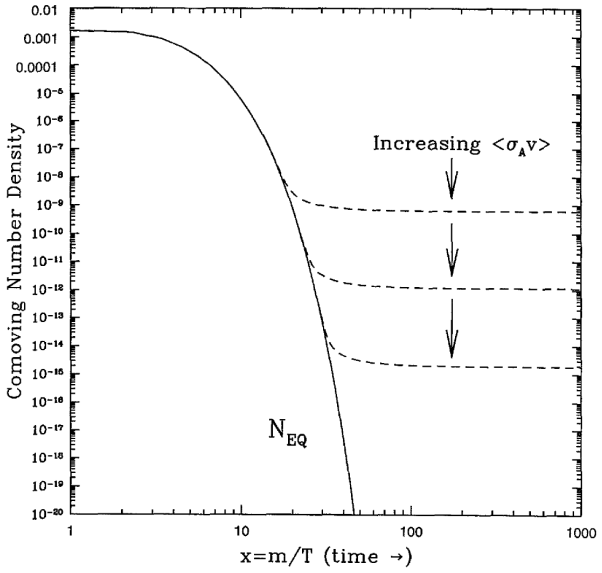

Figure 1.2.: Comoving number density of a WIMP in the early Universe. The dashed curves are the actual abundance, and the solid curve is the equilibrium abundance. Taken from [19].

dark matter one, it can be thermally accessible at the time of freeze-out, and their interactions with the dark matter particle will modify the phenomenology of the decoupling. In this case these so-called coannihilation processes have to be taken into account when computing the relic density of dark matter, which will be presented in the next section.

1.2.2. Overview of relic density calculation

A approximate calculation of the dark matter relic density has been developed several decades ago (see [20] for example). It was however shown in [21] and [22] that the approximations traditionally used were not justified in several cases. In particular, the thermal averaging of the annihilation cross section was generalized to the relativistic case, which is necessary for a proper treatment of thresholds and resonances. In [22] was also pointed out that the whole calculation method had to be generalized in the case of coannihilation, first noticed in [23]. Coannihilation occurs when another particle is slightly heavier than the dark matter particle and can interact with it. Indeed, as explained above, if their mass difference is of the same order of magnitude than the freeze-out temperature, this additional particle is thermally accessible and will play a role during the freeze-out mechanism. Griest and Seckel generalized the calculation of relic density to the case when the neutralino can coannihilate with another supersymmetric particle and applied it to the case of neutralino-squark coannihilation. The resulting general calculation method has been rewritten in a more convenient way and applied to neutralino-chargino coannihilation processes in [24].

An automation of the relic density calculation based on the formalism developed in [21], [24] in which resonances, thresholds and coannihilation with all possible initial states are included has been implemented in tools such as `micrOMEGAs` [25, 26], `DarkSUSY` [27], `IsaRED` [28, 29] or `SuperIso Relic` [30]. The first version of `micrOMEGAs` was using the freeze-out approximation which uses an approximate solution to the evolution equation by estimating the freeze out temperature. Now both codes solve numerically the full evolution equation. This calculation procedure is summarized in the following section.

1.2.3. Calculation of the relic density including coannihilation

This procedure consists in several steps: deriving the evolution equation for the number density of the dark matter particle and reformulating it in terms of entropy density, expressing the thermally averaged (co)annihilation cross section, and integrating numerically the resulting equation from early to present times. To take into account potential coannihilation of dark matter with other supersymmetric particles we first consider a set of N particles χ_i with masses m_i and internal degrees of freedom g_i. These N particles are ordered in mass such that χ_1 (the lightest neutralino in our case) is the lightest one and is stable due to R-parity. Standard Model particles will be denoted as X or Y. The abundances of the χ_i are determined by the three following $R-$parity conserving processes: the annihilation of supersymmetric particles into Standard Model particles $\chi_i\chi_j \to XY$, the scattering of supersymmetric particles off the thermal background $\chi_i X \to \chi_j Y$, and the decay processes $\chi_i \to \chi_j X$. One can then write an evolution equation for each of the n_i which will depend on the relevant cross section and decay rates. However, as all the supersymmetric particles decay quite quickly into the LSP χ_1, its final abundance will be expressed as the sum of the densities of all supersymmetric particles:

$$n = \sum_{i=1}^{N} n_i. \tag{1.7}$$

Its evolution equation is then expressed as the sum of all the evolution equations for the n_i and simplifies as:

$$\frac{dn}{dt} = \sum_{i=1}^{N} \frac{dn_i}{dt} = -3Hn - \sum_{i,j=1}^{N} \langle \sigma_{ij} v_{ij} \rangle \left(n_i n_j - n_i^{\mathrm{eq}} n_j^{\mathrm{eq}} \right). \tag{1.8}$$

Here the first term on the right-hand side corresponds to the dilution due to the expansion of the Universe, H being the Hubble parameter. The second term describes $\chi_i\chi_j$ annihilation with a total annihilation cross section

$$\sigma_{ij} \quad = \quad \sum_{X} \sigma(\chi_i\chi_j \to XY) \tag{1.9}$$

which has to be thermally averaged. The scattering and decay processes do not contribute since we sum over all the n_i. v_{ij} are the relative velocities and $n_i^{\rm eq}$ are the number densities at equilibrium. Since the annihilation rate determines the freeze-out and is much slower than the other processes, one can assume that the ratio of the n_i to the total density n keeps its equilibrium value before, during and after freeze-out:

$$\frac{n_i}{n} \simeq \frac{n_i^{\rm eq}}{n^{\rm eq}}. \tag{1.10}$$

Eq. (1.8) can be then rewritten as

$$\frac{dn}{dt} = -3Hn - \langle\sigma_{\rm eff} v\rangle \left(n^2 - n_{\rm eq}^2\right) \tag{1.11}$$

where

$$\langle\sigma_{\rm eff} v\rangle = \sum_{ij} \langle\sigma_{ij} v_{ij}\rangle \frac{n_i^{\rm eq}}{n^{\rm eq}} \frac{n_j^{\rm eq}}{n^{\rm eq}}. \tag{1.12}$$

This equation nicely resembles to the one we would have obtained without taking coannihilation into account, in which the effective cross section $\sigma_{\rm eff}$ is replaced by the usual annihilation cross section. Because of entropy conservation it is more convenient to reformulate the equation Eq. (1.11) in term of the variable $Y = n/s$ where s is the entropy density. We obtain

$$\dot{Y} = -s\langle\sigma_{\rm eff} v\rangle \left(Y^2 - Y_{\rm eq}^2\right). \tag{1.13}$$

It is also convenient to use the temperature T instead of the time t as independent variable. Defining $x = m_1/T$ we obtain

$$\frac{dY}{dx} = -\frac{m_1}{x^2} \frac{1}{3H} \frac{ds}{dT} \langle\sigma_{\rm eff} v\rangle \left(Y^2 - Y_{\rm eq}^2\right). \tag{1.14}$$

After expressing the Hubble constant in terms of the pressure, and the pressure and entropy content in terms of effective degrees of freedom $g_{\rm eff}(T)$ and $h_{\rm eff}(T)$, we arrive to the final evolution equation:

$$\frac{dY}{dx} = -\sqrt{\frac{\pi}{45G}} \frac{g_*^{1/2} m_1}{x^2} \langle\sigma_{\rm eff} v\rangle \left(Y^2 - Y_{\rm eq}^2\right) \tag{1.15}$$

where $Y_{\rm eq}$ can be written as

$$Y_{\rm eq} = \frac{n_{\rm eq}}{s} = \frac{45x^2}{4\pi^4 h_{\rm eff}(T)} \sum_i g_i \left(\frac{m_i}{m_1}\right)^2 K_2\left(x\frac{m_i}{m_1}\right) \tag{1.16}$$

and $g_*^{1/2}$ as

$$g_*^{1/2} = \frac{h_{\rm eff}}{\sqrt{g_{\rm eff}}}\left(1 + \frac{T}{3h_{\rm eff}}\frac{dh_{\rm eff}}{dT}\right). \tag{1.17}$$

The thermal averaged effective cross section appearing in (Eq. 1.15) can be written as

$$\langle\sigma_{\rm eff} v\rangle = \frac{\int_0^\infty dp_{\rm eff} p_{\rm eff}^2 W_{\rm eff} K_1\left(\frac{\sqrt{s}}{T}\right)}{m_1^4 T\left[\sum_i \frac{g_i}{g_1}\frac{m_i^2}{m_1^2}K_2\left(\frac{m_i}{T}\right)\right]^2}. \tag{1.18}$$

Here $p_{\rm eff} \equiv p_{11}$ with p_{ij} defined as the momentum of χ_i in the center-of-mass frame of $\chi_i\chi_j$. $W_{\rm eff}$ is the effective annihilation rate defined as

$$W_{\rm eff} = \sum_{ij}\frac{p_{ij}}{p_{11}}\frac{g_i g_j}{g_1^2}W_{ij} \tag{1.19}$$

where W_{ij} is a normalized annihilation rate related to the cross section through

$$W_{ij} = 4E_i E_j \sigma_{ij} v_{ij}. \tag{1.20}$$

In Eq. (1.18) one also used K_1 and K_2 which are respectively the modified Bessel functions of the second kind of order 1 and 2. One of the advantages of this formulation is that $W_{\rm eff}$ does not depend on the temperature T: it can therefore be calculated before thermally averaging.

Integrating numerically the Eq. (1.15) from very early times ($x = 0$) to now ($x = m_1/T_0$, where T_0 is the present photon temperature) gives Y_0. The relic density, i.e. the present abundance of dark matter, is then

$$\Omega_{\rm CDM} = m_1 s_0 Y_0/\rho_{\rm crit}, \tag{1.21}$$

where $\rho_{\rm crit} = 3H^2/8\pi G$ is the critical density and s_0 is the entropy density today. With $T_0 = 2.726$ K we finally obtain

$$\Omega_{\rm CDM}h^2 = 2.755 \times 10^8 m_1 Y_0 \tag{1.22}$$

with m_1 given in GeV. It is also possible to make an order-of-magnitude estimation of the relic density to obtain

$$\Omega_{\rm CDM}h^2 \approx \frac{3 \times 10^{-27}{\rm cm}^3{\rm s}^{-1}}{\langle\sigma v\rangle}. \tag{1.23}$$

The observed relic density corresponds then to a cross section value which is typically obtained for weak interactions, which is an argument for WIMP dark matter.

Now we would like to make some comments about the weighting factor entering in the averaged effective cross section in Eq. (1.12). For simplicity we consider a set of two particles with masses m_1 and m_2 (with $m_1 < m_2$) and internal degrees of freedom g_1 and g_2. In a non-relativistic approximation this factor can be expressed as [22]:

$$r_i\, r_j \equiv \frac{n_i^{\rm eq}}{n^{\rm eq}} \frac{n_j^{\rm eq}}{n^{\rm eq}} = \frac{g_i\, g_j \left(\frac{m_i}{m_1}\right)^{3/2} \left(\frac{m_j}{m_1}\right)^{3/2} e^{-(m_i+m_j-2m_1)/T}}{\left(\sum_{k=1,2}\, g_k \left(\frac{m_k}{m_1}\right)^{3/2} e^{-(m_k-m_1)/T}\right)^2} \tag{1.24}$$

$$= \frac{g_i\, g_j \left(\frac{m_i}{m_1}\right)^{3/2} \left(\frac{m_j}{m_1}\right)^{3/2} e^{-(m_i+m_j-2m_1)/T}}{\left(g_1 + g_2 \left(\frac{m_2}{m_1}\right)^{3/2} e^{-(m_2-m_1)/T}\right)^2}. \tag{1.25}$$

It is trivial to show that in the case of two degenerate particles ($m_1 = m_2$) one has

$$r_i\, r_j = \frac{g_i\, g_j}{(g_1+g_2)^2}. \tag{1.26}$$

On the other hand, when $m_2 \gg m_1$, the $r_i\, r_j$ have the following behavior:

$$r_1\, r_1 \sim 1, \tag{1.27}$$

$$r_1\, r_2 \sim \frac{g_2}{g_1} \left(\frac{m_2}{m_1}\right)^{3/2} e^{-(m_2-m_1)/T}, \tag{1.28}$$

$$r_2\, r_2 \sim \left(\frac{g_2}{g_1}\right)^2 \left(\frac{m_2}{m_1}\right)^3 e^{-2(m_2-m_1)/T}. \tag{1.29}$$

We clearly see that the coannihilation of dark matter with this second particle (associated with the weighting factor $r_1\, r_2$ in Eq. (1.28)) is Boltzmann suppressed and will be relevant only when $m_2 \approx m_1$.

Although this formalism allows for a rigorous and precise calculation of the relic density of dark matter, via a numerical solving of the Boltzmann Eq. (1.8), this procedure is unfortunately subject to several uncertainties. The first source of uncertainty lies in the extraction of the relic density of dark matter from cosmological data. The extraction is based on a simple cosmological model which uses a minimal set of six parameters to fit the available cosmological data and bases its conclusions on the Standard Model of cosmology [6]. It has been shown that changing either the number of free parameters of the model used to fit the cosmological data [31] or modifying the assumptions contained in the Standard Model of cosmology (e.g., altering the expansion rate or the entropy content in the primordial Universe or later, but still before Big Bang Nucleosynthesis [32, 33]), may change the extracted central value of $\Omega_{\rm CDM}h^2$ along with the confidence levels. Another possibility is that the dark matter abundance is

enhanced by some non-thermal production mechanism in the early Universe. For instance, they could be produced by decay of heavier particles (gravitino [34] or axino [35] for example). Another important source of uncertainty is obviously the precision of the calculation of the cross section. We will review in detail the different sources of uncertainty in the calculation of the cross section in the framework of supersymmetric models in Sec. 4.2.1.

Chapter 2.

The Standard Model of Particle Physics

In this chapter we first recall how gauge theories are used to describe consistently QED (Sec. 2.2) and QCD (Sec. 2.3), and detail the Glashow-Salam-Weinberg model of the weak interactions and its associated Brout-Englert-Higgs mechanism (Sec. 2.4 and Sec. 2.5). We then discuss the fermionic sector of the Standard Model, with an emphasize on the quark mixing (Sec. 2.6). Lastly, we comment on some theoretical and experimental hints about Beyond the Standard Model Physics (Sec. 2.7). The main references used in this chapter are [36], [37] and [38].

2.1. Introduction

Allowing for neutrino masses, and discarding inconclusive deviations in precision measurements, the Standard Model explains all experimental results in Particle Physics. It describes consistently the electromagnetic, weak and strong interactions in the single framework of gauge theories. By definition the latter are invariant under local transformations of the charged fields, which leads to the existence of massless vector bosons: the gauge fields. A simple case of gauge theory is the electromagnetism, which is invariant under $U(1)$, and associated with the photon. "Quantum Chromo-Dynamics" (QCD) is an example of a non-abelian gauge theory, invariant under $SU(3)$ and associated with the gluons. The strongly interacting particles (i.e. those interacting with the gluon) carry a strong charge called "color". The case of the weak interaction is different since it is a short-range interaction, therefore associated with massive gauge bosons. The Brout-Englert-Higgs mechanism states that the gauge symmetry is spontaneously broken, the gauge bosons acquiring a mass. As a consequence, a scalar particle, relic of this mechanism, exists: the Higgs boson. In this chapter we describe the different components of the Standard Model Lagrangian, starting by the simplest one: the Lagrangian of Quantum Electro-Dynamics (or QED).

2.2. Quantum Electro-Dynamics

By requiring the Dirac Lagrangian to be invariant under local $U(1)$ transformations, one is forced to introduce a new vector field A_μ called "gauge field", associated with the photon:

$$\mathcal{L} = \bar{\psi}(i\gamma^\mu D_\mu - m)\psi \tag{2.1}$$

where $D_\mu \equiv \partial_\mu + ieA_\mu$. Its gauge and Lorentz invariant kinetic term is then $\frac{1}{4}F_{\mu\nu}F^{\mu\nu}$, with $F_{\mu\nu} = \partial_\mu A_\nu + \partial_\nu A_\mu$, the factor 1/4 being chosen so that the resulting Lagrangian matches with the relativistic Maxwell's equations.

Note that A_μ has four components, whereas a physical photon has only two polarization states (the ones which are transverse). In fact, in a theory with a local symmetry, some degrees of freedom can be modified by gauge transformations without any consequences: they are therefore unphysical. This subtlety forbids us to define a propagator for the photon without fixing the gauge, which is done by the following Lagrangian:

$$\mathcal{L}_{GF} = -\frac{1}{2\xi}(\partial^\mu A_\mu)^2. \tag{2.2}$$

That leads to the following expression for the photon propagator:

$$\frac{-i}{p^2} \times \left(g_{\mu\nu} - (1-\xi)\frac{p^\mu p^\nu}{p^2} \right). \tag{2.3}$$

This general gauge fixing formulation is known as R_ξ-gauge; common choices for the gauge fixing parameter are $\xi = 1$ (Feynman gauge) or $\xi = 0$ (Landau gauge). However, as physical observables do not depend on the gauge, the ξ parameter can be kept as general. This property of gauge theories is expressed by the Ward identities, which state that the degrees of freedom of the photon proportional to its four-momenta (see the second term in the propagator) will cancel in the amplitude.

We finally obtain the Lagrangian of QED:

$$\mathcal{L}_{QED} = \frac{1}{4}F_{\mu\nu}F^{\mu\nu} + \bar{\psi}(i\not{D} - m)\psi - \frac{1}{2\xi}(\partial^\mu A_\mu)^2. \tag{2.4}$$

2.3. Quantum Chromo-Dynamics

QCD is described by a non abelian gauge theory (invariant under local $SU(3)$ transformations) with massless self-interacting gauge bosons (the gluons) [39–41]. Its starting point is a

Lagrangian similar to the one of QED:

$$\mathcal{L} = \bar{\psi}(i\gamma^\mu \mathbf{D}_\mu - m)\psi, \tag{2.5}$$

ψ being in fact here a triplet of fermions (each of them carrying a different $SU(3)$ charge called "color"), and $\mathbf{D}$ being a 3×3 matrix: $\mathbf{D}_\mu \equiv \mathbf{I}\partial_\mu + ig\mathbf{A}_\mu$ where $\mathbf{A}_\mu = \mathbf{T}^a A^a_\mu$. $\mathbf{T}^a$ are the 8 generators of $SU(3)$, associated with the 8 gluons A^a_μ. In analogy to the case of QED, these vector fields ensure that the Lagrangian given above is invariant under local $SU(3)$ gauge transformations. The gluons can interact with themselves, as indicated by the non-zero commutator of two $SU(3)$ generators:

$$[\mathbf{T}^a, \mathbf{T}^b] = if^{abc}\mathbf{T}^c \neq 0. \tag{2.6}$$

f^{abc} are the structure constants of $SU(3)$ and, as the generators, obey to special relations.

The kinetic term is

$$-\frac{1}{4}F^a_{\mu\nu}F^{a\ \mu\nu}, \text{ with } F^a_{\mu\nu} = \partial_\mu A^a_\nu + \partial_\nu A^a_\mu - gf^{abc}A^b_\mu A^c_\nu. \tag{2.7}$$

It contains the two terms

$$gf^{abc}(\partial_\mu A^a_\nu)A^b_\mu A^c_\nu - \frac{1}{4}g^2 f^{abc}f^{ade}A^b_\mu A^c_\nu A^d_\mu A^e_\nu, \tag{2.8}$$

corresponding to three-point and four-point self-interactions. As in QED we need a gauge fixing Lagrangian:

$$\mathcal{L}_{GF} = -\frac{1}{2\xi}(\partial^\mu A^a_\mu)^2 \tag{2.9}$$

which enters the propagator of Eq. (2.3) for the gluon. However the cancellations required by the Ward identities in QED are more complex in the case of QCD. A prescription suggested by Faddeev and Popov [42] to ensure these cancellations imply unphysical particles called Faddeev-Popov ghosts. These are scalar particles behaving according to the Fermi-Dirac statistics, appearing only in loops, and can be seen as negative degrees of freedom canceling the unphysical time-like and longitudinal polarization degrees of freedom of the gluons. Their corresponding Lagrangian is

$$\mathcal{L}_{\text{ghost}} = \bar{c}^a(-\partial^\mu D^{ac}_\mu)c^c, \text{ with } D^{ac}_\mu = \partial_\mu \delta^{ac} + gf^{abc}A^b_\mu. \tag{2.10}$$

We have now obtained the total QCD Lagrangian:

$$\mathcal{L}_{QCD} = \bar{\psi}(i\gamma^\mu \mathbf{D}_\mu - m)\psi - \frac{1}{4}F^a_{\mu\nu}F^{a\ \mu\nu} - \frac{1}{2\xi}(\partial^\mu A^a_\mu)^2 + \bar{c}^a(-\partial^\mu D^{ac}_\mu)c^c. \tag{2.11}$$

2.4. From the weak interactions to the Higgs boson

As we have seen in the previous sections, gauge symmetries require the existence of a massless vector field for each generator of the symmetry group. As a consequence gauge theories can not be used naively to describe weak interactions since the weak bosons are massive (weak interaction is a very short range interaction). Adding a mass term by hand in the Lagrangian for these fields would break the gauge symmetry as needed, but it would also lead to non-renormalizability of the theory. The model of weak interactions introduced by Glashow, Salam and Weinberg [43–45] makes use of spontaneously breaking of a local symmetry (the so-called Brout-Englert-Higgs mechanism [46–48]) to create a renormalizable mass term for the weak bosons. In addition, as we will see, the electromagnetic and weak interactions are unified in a single larger symmetry group.

Let us start by defining a complex $SU(2)$ doublet of scalar fields ϕ, with a weak hypercharge Y = +1, called the Higgs field:

$$\Phi = \begin{pmatrix} \phi^+ \\ \phi^0 \end{pmatrix}. \tag{2.12}$$

Its corresponding Lagrangian is:

$$\mathcal{L}_\Phi = (D^\mu \Phi)^\dagger (D_\mu \Phi) - V(\Phi^\dagger \Phi) \quad \text{with } V(\Phi^\dagger \Phi) = \lambda[\Phi^\dagger \Phi - \mu^2/(2\lambda)]^2. \tag{2.13}$$

The covariant derivative is $D_\mu = \partial_\mu - \frac{i}{2} g_2 W_\mu^a \sigma^a - \frac{i}{2} g_1 B_\mu$ where W_μ^a and B_μ are the gauge fields associated with the $SU(2)$ and $U(1)_Y$ generators.

When spontaneously breaking a local (gauge) symmetry, the Lagrangian remains invariant under the gauge transformations, but the lowest energy state (the "vacuum"), is not a singlet of the gauge symmetry. There is an infinite number of ground states with the same energy, and the symmetry breaking chooses one of these states as the "true" vacuum. In our case, as can be seen from the potential (2.13), for $\mu^2 > 0$ the field Φ develops a non-zero vacuum expectation value (VEV) which breaks the $SU(2) \times U(1)_Y$ symmetry. One combination of the 4 generators has to stay unbroken by the vacuum, so that the theory contains one massless gauge boson (the photon), while the three others gauge bosons will acquire a mass from the VEV. In order to obtain a massless gauge boson which is uncharged under $U(1)_{\text{em}}$, the VEV should be developed by the neutral component of Φ:

$$\langle \Phi \rangle = \frac{1}{\sqrt{2}} \begin{pmatrix} 0 \\ v \end{pmatrix} \text{ with } \; v = \left(-\frac{\mu^2}{\lambda} \right)^{1/2} = 246 \text{ GeV}. \tag{2.14}$$

We can expand Φ around its VEV and apply a gauge transformation by using the three degrees of freedom from $SU(2)$ (the electromagnetic gauge remains to be fixed). We choose a specific gauge called "unitary gauge" which will be explained later. We obtain the following expression:

$$\Phi = \frac{1}{\sqrt{2}} \begin{pmatrix} 0 \\ v + H(x) \end{pmatrix}. \tag{2.15}$$

If we expand $\mathcal{L}_\Phi$ using this expression for Φ we obtain:

$$\begin{aligned} \mathcal{L}_\Phi = -\frac{1}{2}\partial_\mu H \partial^\mu H + \frac{1}{4} g_2^2 (v+H)^2 W_\mu^+ W_\mu^- + \\ \frac{1}{8}(g_1^2 + g_2^2)(v+H)^2 Z_\mu^0 W_\mu^0 - \lambda v^2 H^2 - \lambda v H^3 - \frac{\lambda}{4} H^4 \end{aligned} \tag{2.16}$$

with

$$W_\mu^\pm = \frac{W_\mu^1 \mp i W_\mu^2}{\sqrt{2}} \text{ and } Z_\mu^0 = \frac{g_2 W_\mu^3 - g_1 B_\mu}{\sqrt{g_2^2 + g_1^2}}. \tag{2.17}$$

The bilinear terms in these fields give us the masses of the vector fields:

$$m_W = \frac{g_2 v}{2},\ m_Z^2 = \frac{1}{4}(g_1^2 + g_2^2) v^2. \tag{2.18}$$

Note that these mass eigenstates are obtained by a rotation of an angle θ_W called the Weinberg angle, which is experimentally measured and satisfies the relation $\cos\theta_W = m_W/m_Z$. There is a fourth vector boson orthogonal to Z^0 without mass term which is identified as the photon:

$$A_\mu = \frac{g_2 W_\mu^3 + g_1 B_\mu}{\sqrt{g_2^2 + g_1^2}}. \tag{2.19}$$

The photon is associated with the generator $Q = T_3 + Y/2$, where T_3 is the weak isospin third component and Y is the weak hypercharge, which is precisely the combination which is not broken by the vacuum.

By acquiring a mass, each of the weak vector bosons increases its number of degrees of freedom by 1. These 3 degrees of freedom correspond to the ones which are "lost" during the symmetry breaking. Indeed, the Goldstone theorem states that for every spontaneously broken continuous symmetry, the theory contains a number of massless scalar particles (the "Goldstone bosons"), this number being equal to the number of broken generators (3 in our case). These non-observed Goldstone bosons are in fact "eaten" by the gauge bosons to increase their number of degrees of freedom. As the Higgs field defined in Eq. (2.12) contained 4 degrees of freedom, one of them should be still present: it is the so-called scalar Higgs boson. In the Lagrangian (2.16) there is also a bilinear term in H which give rise to a mass for the Higgs

boson: $m_H^2 = 2\lambda v^2 = 2\mu^2$. The remaining terms in $\mathcal{L}_\Phi$ correspond to its trilinear and quartic self-interactions, and to interactions between Higgs and gauge bosons.

2.5. Unitary gauge and the Goldstone Boson Equivalence Theorem

We should now comment a bit on the unitary gauge which has been used without giving any detail. The unitary gauge is a particular choice of the gauge which makes the Goldstone bosons disappear (they actually become infinitely heavy as we will see later).

We can naively generalize the propagator given in Eq. (2.3) in $R_\xi-$gauge for a massive vector boson:

$$\frac{-i}{p^2 - m^2} \times \left(g_{\mu\nu} - (1-\xi)\frac{p^\mu p^\nu}{p^2} \right). \tag{2.20}$$

However it is obvious that some ingredients are missing: in the Feynman gauge, the terms proportional to p^μ do not cancel as in the case of massless vector boson, since the massive one have some longitudinal polarization components. The derivation of a propagator in a theory with spontaneously broken symmetry is actually more complicated and one needs to apply the Faddeev-Popov method carefully. The gauge fixing Lagrangian contains then additional terms, and as in QCD there are ghost particles associated with each vector boson which appear only in loops. This Lagrangian contains terms of interaction between these particles, but also mass terms for the Goldstone bosons and the ghosts particles which give $m = \sqrt{\xi} m_{W,Z}$ for the Goldstone bosons and ghosts associated with the W and Z bosons. The propagators of the massive vector bosons, Higgs bosons, Goldstone bosons, and ghosts are then respectively:

$$\frac{-i}{p^2 - m^2} \times \left(g_{\mu\nu} - (1-\xi)\frac{p^\mu p^\nu}{p^2 - \xi m^2} \right) \text{ with } m = m_W \text{ or } m_Z, \tag{2.21}$$

$$\frac{i}{p^2 - m_h^2}, \tag{2.22}$$

$$\frac{-i}{p^2 - m^2} \text{ with } m = \sqrt{\xi} m_W \text{ or } \sqrt{\xi} m_Z, \tag{2.23}$$

$$\frac{-i}{p^2 - m^2} \text{ with } m = \sqrt{\xi} m_W \text{ or } \sqrt{\xi} m_Z. \tag{2.24}$$

Now we see that in the Feynman gauge ($\xi \to 1$), the propagators of massive vector bosons reduce to the expression given in Eq. (2.20), but there is also a contribution from a Goldstone boson with the same mass. When using the appropriate Feynman rules for their interaction,

their contributions exactly match with the contribution from the missing longitudinal polarization states of the massive vector bosons.

There is however another choice of gauge which has the advantage of absorbing these contributions within the massive vector boson. Indeed in the unitary gauge ($\xi \to \infty$), the propagators of the massive vector bosons are

$$\frac{-i}{p^2 - m^2} \times \left(g_{\mu\nu} - \frac{p^\mu p^\nu}{m^2} \right) \tag{2.25}$$

which contains in the last term the missing degrees of freedom. On the other hand the Goldstone bosons become infinitely heavy since they have $m \sim \sqrt{\xi}$: they do not contribute in that particular gauge. It is easier now to understand that the Goldstone bosons are "eaten" by the vector bosons which become massive.

The Goldstone Boson Equivalence Theorem [49–51] states that for energies much higher than the vector boson mass, the amplitude for emission or absorption of a longitudinally polarized massive gauge boson is equal to the same amplitude with the Goldstone boson which has been eaten by the gauge boson. It is related to the fact that the longitudinal component of a massive vector boson becomes dominant when the boson is moving relativistically. This theorem has been proved and is a consequence of the gauge invariance.

2.6. Quarks and leptons

We have seen that the Standard Model, which is made of QCD and electroweak interactions, is based on the gauge group $U(1)_Y \times SU(2) \times SU(3)$. That means that each fermion of the Standard Model will lie in a given representation of each of these groups. In the following we give the weak hypercharge eigenvalue, the $SU(2)$ and the $SU(3)$ representations for each kind of fermion:

$$l_L \equiv \begin{pmatrix} \nu_L \\ e_L \end{pmatrix} = (-1, \mathbf{2}, \mathbf{1}),\ e_R = (-2, \mathbf{1}, \mathbf{1}),\ \nu_R = (0, \mathbf{1}, \mathbf{1}),$$

$$q_L \equiv \begin{pmatrix} u_L \\ d_L \end{pmatrix} = (\frac{1}{3}, \mathbf{2}, \mathbf{3}),\ d_R = (-\frac{2}{3}, \mathbf{1}, \mathbf{3}),\ u_R = (\frac{4}{3}, \mathbf{1}, \mathbf{3}).$$

Note that these quantum numbers are the same for the 3 families of fermions of the same kind, only their masses being different. Also, a gauge singlet right-handed neutrino has been introduced only for the sake of neutrinos masses.

The left-handed fermions are $SU(2)$ doublets whereas the right-handed fermions are singlet because the weak gauge bosons $W^1_\mu, W^2_\mu, W^3_\mu$ couples only to left-handed fermions. Adding a mass term by hand for the fermions would break gauge invariance since a mass term mixes left- and right-handed fermions which lie in different representation of $SU(2)$. As for the vector bosons, we can use the spontaneous breaking of the $SU(2) \times U(1)_Y$ symmetry via the Higgs mechanism to give a mass to the fermions. The mass terms are in fact written as an interaction between the fermions and the Higgs field ("Yukawa interaction"), which give mass to the fermions when the Higgs gets its VEV. For instance for the up and down quarks we have:

$$\mathcal{L} = -Y_d \bar{q}_L \Phi d_R - Y_u \bar{q}_L \tilde{\Phi} u_R + h.c. \tag{2.26}$$

where Y_u and Y_d are the Yukawa couplings of the up and down quarks, Φ is the Higgs scalar field, and $\tilde{\Phi} = i\sigma_2 \Phi^*$. The up and down quarks then acquire a mass given by $m_u = Y_u\, v/\sqrt{2}$ and $m_d = Y_d\, v/\sqrt{2}$ respectively. By generalizing this procedure we can generate masses for all the fermions of the Standard Model.

There is however a subtlety arising when including additional families of fermions, in particular when considering charged currents (i.e. transition between up- and down-type quarks). The reason is that the mass eigenstates do not coincide with the interaction eigenstates. Indeed, the mass terms generated by the Yukawa couplings of fermions to the Higgs are in general not diagonal in the generation space. They can be diagonalized by redefining the quarks fields using unitary matrices:

$$u^m_L = V_{u_L} u^i_L,\ u^m_R = V_{u_R} u^i_R \tag{2.27}$$

$$d^m_L = V_{d_L} d^i_L,\ d^m_R = V_{d_R} d^i_R \tag{2.28}$$

where q^m are the quarks mass eigenstates and q^i are their interaction eigenstates. The Yukawa matrices can then be diagonalized by

$$V_{u_L} Y_u V^\dagger_{u_R} = Y_u^{\text{diag}} \tag{2.29}$$

$$V_{d_L} Y_d V^\dagger_{d_R} = Y_d^{\text{diag}}. \tag{2.30}$$

The charged interactions (i.e. the one relating up-type and down-type quarks u^i and d^i), when expressed in the mass eigenstates basis, implies a unitary 3×3 matrix $V_{\text{CKM}} = V_{u_L} V_{d_L}$ called the Cabbibo-Kobayashi-Maskawa (CKM) matrix [52, 53]. Because the up and down quarks are not rotated in the same way, this matrix is non-diagonal. As a consequence, the charged interactions are "flavour violating": they are responsible for transitions between different generations of quarks. The CKM matrix is the unique source of flavor violation in

the Standard Model. Its standard parametrization is:

$$V_{\text{CKM}} = \begin{pmatrix} c_{12}c_{13} & s_{12}c_{13} & s_{13}e^{-i\delta} \\ -s_{12}c_{23} - c_{12}s_{23}s_{13}e^{i\delta} & c_{12}c_{23} - s_{12}s_{23}s_{13}e^{i\delta} & s_{23}c_{13} \\ s_{12}s_{23} - c_{12}c_{23}s_{13}e^{i\delta} & -c_{12}s_{23} - s_{12}c_{23}s_{13}e^{i\delta} & c_{23}c_{13} \end{pmatrix}, \tag{2.31}$$

where $c_{ij} \equiv \cos\theta_{ij}$ and $s_{ij} \equiv \sin\theta_{ij}$. The CKM matrix has 4 parameters: three angles θ_{ij} and a CP phase δ. Another parametrization is the Wolfenstein parametrization where the four mixing parameters are (λ, A, ρ, η) where η represents the CP violating phase. The Wolfenstein parametrization is an expansion in the small parameter, $\lambda \approx 0.22$. To $O(\lambda^3)$ the parametrization is given by

$$V_{\text{CKM}} = \begin{pmatrix} 1 - \frac{1}{2}\lambda^2 & \lambda & A\lambda^3(\rho - i\eta) \\ -\lambda & 1 - \frac{1}{2}\lambda^2 & A\lambda^2 \\ A\lambda^3(1 - \rho - i\eta) & -A\lambda^2 & 1 \end{pmatrix}. \tag{2.32}$$

In analogy to the quark sector, the transitions between different generations in the lepton sector is described by a unitary matrix called the Pontecorvo-Maki-Nakagawa-Sakata (PMNS) matrix [54].

2.7. Beyond the Standard Model?

Before trying to motivate the search for Physics beyond the Standard Model, one should first point out its enormous success as a theory describing the particles we know and their interactions. It includes the strong and electroweak interactions, generates masses via the Higgs mechanism, describes precisely the transitions between the different fermions families, etc. The Standard Model has been experimentally tested with an incredibly high precision and a huge variety of observables. There are, however, a few hints that there could ("should"?) be a more general model describing Particle Physics at a higher energy scale. Before detailing briefly some of these arguments, let us give a non-exhaustive list of fundamental questions which are not answered by the Standard Model:

- Why is the Standard Model based on the specific group structure $U(1) \times SU(2) \times SU(3)$, with three different coupling constants? Can the Standard Model particles be described by a single representation?
- Why are there three families? Why is there a strong mass hierarchy between them? Why are the neutrino masses so small?
- Why are these specific mixing patterns in the quark and lepton sectors realized?

- Why is the Higgs boson so light in comparison to the Planck scale?
- Why does QCD not seem to break $CP-$symmetry?
- Why is the electric charge quantized?
- How is gravity quantized and how is it unified with the Standard Model?
- What is the nature of dark matter, which can not be explained by the Standard Model?

Dark matter

As we stated in the last chapter, the WIMP paradigm of dark matter requires the existence of a heavy stable particle, neutral under the electric and color interactions. There is no such candidate in the Standard Model, the neutrinos being much too light. In addition, we have seen that observations point out the non-baryonic nature of dark matter. As a consequence, assuming that dark matter is made of WIMPs requires the introduction of New Physics.

In particular, assuming that dark matter was in thermal equilibrium in the early Universe, its relic density can be related to its mass and annihilation cross section (see Chap. 1). A particle with weak interactions and mass ~ 100 GeV obtained naturally the correct order of magnitude for the relic density: this is called the *WIMP miracle*, which is often cited as a strong argument in favor of new Physics at the electroweak scale.

Hierarchy problem

The Higgs boson being a scalar, the one-loop corrections to its mass give quadratic divergences with the energy. When regularizing the divergent integrals by a cutoff scale, we obtain a correction to the Higgs mass proportional to this cutoff scale squared. Assuming the Standard Model to be valid up to the GUT scale, with New Physics describing the theory at higher scale, the Higgs mass correction is then extremely large compared to the observed mass (~ 125 GeV). This gap between Planck and electroweak scale is the origin of the *Hierarchy problem*. One solution would be to require the large divergent terms to cancel very precisely in order to give the correct mass, which is known as *fine-tuning*, and lead to the problem of *naturalness* of the theory. Another solution, as we will see in Chap. 3, is to introduce new particles contributing in loops in a way which naturally cancels the divergence.

Unification of gauge couplings

After several centuries spent merging apparently distinct phenomena into more general and predictive frameworks (Maxwell's electro-magnetism, Newton's universal gravitational interaction, Einstein space-time, theory of electro-weak interactions, etc.) it seems quite natural to ask if the strong and the electroweak interactions could be described by a unified theory.

The Standard Model describes both of them but separately, as their description is based on a direct product of three gauge groups.

One could therefore expect a Grand Unified Theory (GUT) to describe these interactions as a single gauge group, with only one coupling constant. The three coupling constants of the Standard Model should then meet at a common point at high energy. Unfortunately, the renormalization group equations (RGE) predict that this is not the case.

Chapter 3.

Supersymmetry and the MSSM

Supersymmetry and the Minimal Supersymmetric Standard Model (MSSM) are introduced in this chapter. The algebra of Supersymmetry, extension of the Poincaré algebra, is presented in Sec. 3.2, and the MSSM is discussed in details in Sec. 3.3. In particular, its particle content and interaction Lagrangian are described. The question of Supersymmetry breaking is addressed in Sec. 3.4, where examples of different breaking scenarios are given. Finally, the spectrum of the relevant MSSM sectors are discussed in Sec. 3.5. The main reference used to write this chapter is [55].

3.1. Introduction

As we have seen in Chap. 2, despite of the obvious experimental success of the Standard Model, there are hints that there might be some new Physics beyond it. A possible extension of the Standard Model is obtained by requiring a new symmetry in the Lagrangian, called Supersymmetry, which is the unique extension of the Poincaré symmetry using graded Lie algebras. In this chapter we will shortly describe the supersymmetric algebra, and describe the Lagrangian of the minimal supersymmetric extension of the Standard Model (the MSSM), and the interactions it implies. The breaking of Supersymmetry and its mediation will be then discussed. Finally, we will describe the resulting spectrum of the MSSM and its implication for neutralino dark matter. We will see that in addition to its mathematical motivation, Supersymmetry provides several attractive features such as the possibility of gauge coupling unification, the presence of dark matter candidates in the spectrum, a (partial) solving of the hierarchy problem, an explanation of the origin of electroweak symmetry breaking (which is introduced by hand in the Standard Model), and the possibility of supergravity.

3.2. The Supersymmetry algebra

Quantum Field Theories are based on the Poincaré group, which includes Lorentz transformations and translations in space-time, whose generators are respectively $M^{\mu\nu}$ and P^{μ}. These objects satisfy specific commutation relations:

$$\begin{aligned}
[P^{\rho}, P^{\sigma}] &= 0, && (3.1)\\
[P^{\rho}, M^{\nu\sigma}] &= i(g^{\rho\nu}P^{\sigma} - g^{\rho\sigma}P^{\nu}), && (3.2)\\
[M^{\mu\nu}, M^{\rho\sigma}] &= -i(g^{\mu\rho}M^{\nu\sigma} + g^{\nu\sigma}M^{\mu\rho} - g^{\mu\sigma}M^{\nu\rho} - g^{\nu\rho}M^{\mu\sigma}), && (3.3)
\end{aligned}$$

which tell us that the Lorentz transformations and the translations are linked together. The Poincaré group is a non-trivial extension of the group made of rotations and space translations, which is also realized in nature. The symmetry can be extended further, by including the gauge symmetries (see Chap. 2). In the Standard Model, the extended symmetry group is a direct product of the Poincaré group with the gauge groups. In other words, the extension is trivial, and the generators of the gauge groups commute with the generators of the Poincaré group:

$$\begin{aligned}
\left[T^{a}, T^{b}\right] &= i\, f^{abc}T^{c} && (3.4)\\
[T^{a}, P^{\rho}] &= 0 && (3.5)\\
[T^{a}, M^{\rho\sigma}] &= 0. && (3.6)
\end{aligned}$$

According to the *no-go theorem* from Coleman and Mandula, the construction of a non-trivial extension of the Poincaré group, in which the new generators mix with $M^{\mu\nu}$ and P^{μ}, is not possible. However they were assuming that only bosonic generators (i.e. which do not change the spin of the states on which they act) were involved. If we consider a set of fermionic generators Q_{α} (which change the spin of a state by 1/2) it becomes possible to extend the Poincaré algebra in a non-trivial way. In this way we obtain a $\mathcal{N} = 1$ supersymmetric theory. The $\mathcal{N} = 1$ Supersymmetry algebra (also called super-Poincaré algebra) is a graded Lie algebra defined by the following commutation relations:

$$\begin{aligned}
[Q_{\alpha}, P^{\rho}] &= 0 && (3.7)\\
\left\{Q_{\alpha}, \bar{Q}_{\dot{\beta}}\right\} &= 2(\sigma^{\rho})_{\alpha\dot{\beta}}P_{\rho} && (3.8)\\
[M^{\rho\sigma}, Q_{\alpha}] &= -i(\sigma^{\rho\sigma})_{\alpha}^{\ \beta}Q_{\beta} && (3.9)\\
\{Q_{\alpha}, Q_{\beta}\} &= \left\{\bar{Q}_{\dot{\alpha}}, \bar{Q}_{\dot{\beta}}\right\} = 0. && (3.10)
\end{aligned}$$

Here Q_{α} and $\bar{Q}_{\dot{\beta}}$ are two Weyl spinor with $\alpha, \dot{\beta} \in \{1, 2\}$ which are related by $(Q_{\alpha})^{\dagger} = \bar{Q}_{\dot{\alpha}}$.

Adding a new set of generators require the introduction of a new coordinates, which are described by two Grassmann spinors θ^{α} and $\bar{\theta}^{\dot{\alpha}}$. The obtained extended space is called *superspace*,

and the fields living on that space are called *superfields*. The irreducible representations of the Supersymmetry algebra are called supermultiplets. Supermultiplets contain both fermion and boson states, superpartners of each other. As the operator P^2 commutes with the Q_α, all particles in a same supermultiplet will have the same mass. In addition, all the gauge group generators commute with the Q_α, which means that superpartners will also have the same quantum numbers, only their spin will differ. It can also be shown that each supermultiplet must contain an equal number of fermionic and bosonic degrees of freedom ($d.o.f$). A possibility is then to construct a supermultiplet from a Weyl fermion and a complex scalar field (each having two $d.o.f$), which is called a chiral (or matter) supermultiplet. Another possibility is a supermultiplet containing a massless vector field and a massless Weyl fermion (each having two $d.o.f$), which is called a vector (or gauge) supermultiplet.

A nice feature of Supersymmetry is that it solves the Hierarchy problem described in Sec. 2.7. Indeed, in addition to the one-loop contributions from Standard Model particles, the Higgs mass will receive corrections from superpartners of same masses. The different spin of the superpartners will give a different overall sign to the correction, and the couplings are related to the Standard Model one in such a way that the corrections cancel each other. If Supersymmetry is an exact symmetry of nature it protects the Higgs mass from receiving quadratic divergences and therefore offers a solution to the Hierarchy problem.

3.3. The Minimal Supersymmetric Standard Model

3.3.1. Multiplet content of the MSSM

The Minimal Supersymmetric Standard Model (MSSM) is a minimal supersymmetric $\mathcal{N} = 1$ extension of the Standard Model. In that framework each of the particles from the Standard Model lies in one chiral or vector supermultiplet, and must therefore have a superpartner with spin differing by 1/2. The fermions are part of chiral supermultiplets and have scalar partners called sfermions and denoted $\tilde{f}$. In particular the left-handed and right-handed fermions are separate Weyl fermions with different gauge transformation properties, each having their own complex scalar partner with the same gauge properties. The Higgs boson is also part of a chiral supermultiplet, and have a fermionic partner called higgsino. In fact, in order to cancel gauge anomalies, a second Higgs supermultiplet is needed. Another reason is that a second Higgs doublet is needed in order to give mass to up and down fermions in Supersymmetry. We have therefore two $SU(2)_L$ doublet complex scalar fields with weak hypercharge $\pm 1/2$ denoted by H_u and H_d. They both have a neutral and a charged component, the neutral ones combining into the Standard Model Higgs boson. The particle content of chiral supermultiplets in the MSSM is summarized in Tab. 3.1.

Names		spin 0	spin 1/2
squarks, quarks	Q	$(\widetilde{u}_L \;\; \widetilde{d}_L)$	$(u_L \;\; d_L)$
($\times$3 families)	$\overline{u}$	$\widetilde{u}^*_R$	$u^\dagger_R$
	$\overline{d}$	$\widetilde{d}^*_R$	$d^\dagger_R$
sleptons, leptons	L	$(\widetilde{\nu} \;\; \widetilde{e}_L)$	$(\nu \;\; e_L)$
($\times$3 families)	$\overline{e}$	$\widetilde{e}^*_R$	$e^\dagger_R$
Higgs, higgsinos	H_u	$(H^+_u \;\; H^0_u)$	$(\widetilde{H}^+_u \;\; \widetilde{H}^0_u)$
	H_d	$(H^0_d \;\; H^-_d)$	$(\widetilde{H}^0_d \;\; \widetilde{H}^-_d)$

Table 3.1.: Chiral supermultiplets in the Minimal Supersymmetric Standard Model.

Names	spin 1/2	spin 1
gluino, gluon	$\widetilde{g}$	g
winos, W bosons	$\widetilde{W}^\pm \;\; \widetilde{W}^0$	$W^\pm \;\; W^0$
bino, B boson	$\widetilde{B}^0$	B^0

Table 3.2.: Gauge supermultiplets in the Minimal Supersymmetric Standard Model.

The gauge bosons of the Standard Model are part of gauge supermultiplets, and have fermionic partners called gauginos (see Tab. 3.2). After electroweak symmetry breaking, the neutral wino W^0 and the bino B^0 mix to give the Z^0 boson and the photon γ, and their superpartners the zino $\tilde{Z}^0$ and the photino $\tilde{\gamma}$.

In the MSSM these extra particles will contribute to the RGE evolution of the gauge couplings constants. It is well known that in the Standard Model the three gauge couplings constants do not meet at a common point at high scale. One success of the MSSM is to ensure the unification of the coupling constants at a unification scale $M_{\text{GUT}} \sim 2 \times 10^{16}$ GeV, which can be taken as a hint for Grand Unification Theories.

3.3.2. Lagrangian and interactions of the MSSM

To construct the Lagrangian of the MSSM we start from the general expression of the Lagrangian density of a renormalizable supersymmetric theory:

$$\mathcal{L} = \mathcal{L}_{\text{chiral}} + \mathcal{L}_{\text{gauge}} - \sqrt{2}g(\phi^* T^a \psi)\lambda^a - \sqrt{2}g\lambda^{\dagger a}(\psi^\dagger T^a \phi) + g(\phi^* T^a \phi)D^a \tag{3.11}$$

where each term will be described in the following.

The first term in Eq. (3.11) is $\mathcal{L}_{\text{chiral}}$ which is the Lagrangian involving chiral supermultiplets. It is given by

$$\mathcal{L}_{\text{chiral}} = -D^{\mu}\phi^{*i}D_{\mu}\phi_i + i\psi^{\dagger i}\overline{\sigma}^{\mu}D_{\mu}\psi_i - \frac{1}{2}\left(W^{ij}\psi_i\psi_j + W^{*}_{ij}\psi^{\dagger i}\psi^{\dagger j}\right) - W^{i}W^{*}_{i} \tag{3.12}$$

where i, j label the different chiral supermultiplets. ϕ_i and ψ_i are then respectively the scalar and fermionic degrees of freedom of the multiplet i. The covariant derivatives are defined by

$$D_{\mu}\phi_i = \partial_{\mu}\phi_i - igA^{a}_{\mu}(T^{a}\phi)_i \tag{3.13}$$

$$D_{\mu}\phi^{*i} = \partial_{\mu}\phi^{*i} igA^{a}_{\mu}(\phi^{*}T^{a})^{i} \tag{3.14}$$

$$D_{\mu}\psi_i = \partial_{\mu}\psi_i - igA^{a}_{\mu}(T^{a}\psi)_i \tag{3.15}$$

where A^{a}_{μ} are the gauge field and T^{a} the generators of the gauge groups. The first two terms in Eq. (3.12) are given by the Wess-Zumino model for a free chiral supermultiplet and contain only kinetic terms. The remaining terms are interaction terms which are expressed in function of W^{i} and W^{ij}, both being related to the superpotential W by

$$W^{i} = \frac{\delta W}{\delta\phi_i},\ W^{ij} = \frac{\delta^2}{\delta\phi_i\delta\phi_j}W. \tag{3.16}$$

The latter is defined as

$$W = \frac{1}{2}M^{ij}\phi_i\phi_j + \frac{1}{6}y^{ijk}\phi_i\phi_j\phi_k. \tag{3.17}$$

The superpotential (which is not a potential) is an holomorphic function containing all interactions, including fermions and bosons masses. Note that the last term in Eq. (3.12) contains only scalar fields and therefore contribute to the scalar potential $V(\phi, \phi^{*})$. It can be shown using the equations of motion that the chiral supermultiplet Lagrangian is invariant under supersymmetric transformation of the fields. However, Supersymmetry has to be a valid symmetry at the quantum level, i.e. also off-shell, when these equations are not respected. The trick is to introduce a new complex scalar auxiliary field F (the "F-term"), with no propagating degree of freedom (i.e. unphysical), which allows the Supersymmetry algebra to close off-shell. Its corresponding Lagrangian is then $\mathcal{L}_{\text{auxiliary}} = F^{*}F$, and F follows specific transformation rules which make the Lagrangian supersymmetric even when off-shell. Using the equation of motion for the field F one can show that $F_i = -W^{*}_{i}$ and $F^{*i} = -W^{i}$. The field F is therefore eliminated from the Lagrangian, as can be seen from the Eq. (3.12).

The second term in Eq. (3.11) is the Lagrangian density for a gauge supermultiplet, given by

$$\mathcal{L}_{\text{gauge}} = -\frac{1}{4}F^{a}_{\mu\nu}F^{\mu\nu a} + i\lambda^{\dagger a}\overline{\sigma}^{\mu}D_{\mu}\lambda^{a} + \frac{1}{2}D^{a}D^{a} \tag{3.18}$$

where λ^a are the fermionic degrees of freedom of the gauge multiplets (A^a_μ being the bosonic degrees of freedom). The field strength is defined as

$$F^a_{\mu\nu} = \partial_\mu A^a_\nu - \partial_\nu A^a_\mu g f^{abc} A^b_\mu A^c_\nu \tag{3.19}$$

and the covariant derivative as

$$D_\mu \lambda^a = \partial_\mu \lambda^a + g f^{abc} A^b_\mu \lambda^c. \tag{3.20}$$

In analogy to the F-term in the case of chiral supermultiplets, one needs to introduce here a real bosonic auxiliary field D^a (the "D-term") in order for Supersymmetry to be consistent off-shell. The equation of motion for D^a gives then $D^a = 0$, but this relation is modified when one introduces couplings between gauge chiral supermultiplets, which are contained in the last three terms of Eq. (3.11). Supersymmetry imposes that the couplings involved in these interactions are equal to the gauge couplings. The first two terms are couplings between gauginos and matter fields and can be seen as the supersymmetric equivalent of the Standard Model gauge interactions. The last term modifies the equation of motion for the field D^a and gives rise to the equality $D^a = -g(\phi^* T^a \phi)$. By using this expression for the field D^a, one can eliminate it from the Lagrangian and the last terms of Eqs. (3.18) and (3.11) combine to give

$$\frac{1}{2} \sum_a g_a^2 (\phi^* T^a \phi)^2. \tag{3.21}$$

This term also contributes to the scalar potential which therefore receives contribution from the F- and D-term:

$$V(\phi, \phi^*) = F^{*i} F_i + \frac{1}{2} \sum_a D^a D^a = W_i^* W^i + \frac{1}{2} \sum_a g_a^2 (\phi^* T^a \phi)^2. \tag{3.22}$$

As a consequence, the Yukawa interactions, fermion masses and gauge couplings determine the scalar potential of supersymmetric theories. This is precisely the reason why the Higgs boson mass can be predicted by Supersymmetry.

The Lagrangian given in Eq. (3.11) implies several kinds of interactions which we summarize in the following.

- Yukawa (i.e. scalar-fermion-fermion) couplings determined by the dimensionless symmetric parameter y^{ijk}.
- A quartic scalar coupling given by $y^{ijn} y^*_{kln}$.
- Another contribution to the quartic scalar coupling given by the gauge couplings.
- A cubic scalar coupling given by $M^*_{in} y^{jkn}$.
- A fermion mass term M^{ij}.
- A scalar squared mass term $M^*_{ik} M^{kj}$.

- Standard Model coupling between gauge bosons and fermions given by the gauge couplings.
- Standard Model non-abelian coupling between gauge bosons given by the gauge couplings.
- A coupling between gaugino and gauge boson, given by the gauge couplings.
- A coupling between a gauge boson and one or two scalars given by the gauge couplings.
- A coupling between a gaugino, a chiral fermion and a complex scalar given by the gauge couplings.

The Lagrangian Eq. (3.11) is entirely fixed by the superpotential W, which is the following for the MSSM:

$$W_{\text{MSSM}} = \tilde{u}_R^* Y_u \tilde{Q} H_u - \tilde{d}_R^* Y_d \tilde{Q} H_d - \tilde{e}_R^* Y_e \tilde{L} H_d + \mu H_u H_d. \tag{3.23}$$

The first three terms in Eq. (3.23) correspond to the second term in Eq. (3.17). They involve Y_u, Y_d and Y_e which are 3×3 matrices in the family space, containing the masses and CKM mixings of the quarks and leptons. We see that the term $W^i W_i^*$ in Eq. (3.12) gives a quartic scalar coupling as expected, which couples either four squark together, or two squark with two Higgs. On the other hand, the terms $W^{ij}\psi_i\psi_j$ are responsible not only for Yukawa couplings but also for their supersymmetric version: higgsino-sfermion-fermion couplings. The last term, called "μ-term", corresponds to the first term in Eq. (3.17) and provides a squared-mass term for the Higgs, and a mass term for the higgsinos.

3.3.3. R-parity

We could have considered additional terms in the superpotential, but they would violate baryon and lepton number, which is strongly constrained experimentally, in particular from the non-observation of proton decay. Therefore the MSSM contains a new symmetry called "R-parity" which forbids such terms. R-parity is a discrete Z_2 symmetry, associated with a multiplicatively conserved quantum number defined as

$$P_R = (-1)^{3(B-L)+2s} \tag{3.24}$$

where B is the baryon number, L is the lepton number, and s is the spin. All Standard Model particles have $P_R = +1$, while all their supersymmetric partners have $P_R = -1$. If R-parity is exactly conserved, mixing between particles of different P_R is forbidden, and vertices must contain an even number of particles with $P_R = -1$. This has extremely important phenomenological consequences:

- As stated above, the problem of proton decay is solved.
- All supersymmetric particles will decay into a final state containing the Lightest Supersymmetric Particle (LSP)

- The LSP is stable since it can not decay into Standard Model particles. If massive and weakly interacting it can provide a good dark matter candidate.
- When colliding Standard Model particles, supersymmetric particles can be produced only in an even number (in pairs for example).
- As a consequence, if the LSP is weakly interacting, collider signatures of Supersymmetry with R-parity will often imply missing energy.

It is of course possible that R-parity is violated, which is then strongly constrained by observations such as proton decay, and leads to different signatures at collider.

3.4. Supersymmetry breaking

3.4.1. Soft Supersymmetry breaking

The Lagrangian that we have described does not provide a realistic theory. Indeed, as all the supersymmetric particles must have the same mass as their Standard Model partners, Supersymmetry has been excluded by far by observations: a selectron with mass identical to the electron mass should have been already discovered. The conclusion is that if Supersymmetry exist, it has to be spontaneously broken. The last piece we need to derive the MSSM Lagrangian is therefore a Supersymmetry breaking Lagrangian.

As we have seen before, one of the motivation for Supersymmetry comes from the Hierarchy problem, which was solved by introducing new particles differing from the Standard Model particles only by their spin. In particular, an important condition was that the couplings of the Standard Model particles and their superpartners must fulfill some special relations. If Supersymmetry is broken, one can require the breaking terms to maintain these relations, to avoid introducing new quadratically divergent corrections to the Higgs mass. This is called *soft* Supersymmetry breaking, meaning that $\mathcal{L}_{\text{breaking}}$ contains only mass terms and coupling parameters with positive dimension, and is therefore denoted $\mathcal{L}_{\text{soft}}$. Another important condition for Supersymmetry in order to cancel exactly the one-loop corrections to the Higgs mass and stabilize it was the equality of masses between superpartners. The mass terms in $\mathcal{L}_{\text{soft}}$ will therefore introduce new divergent terms proportional to m^2_{soft}, where m_{soft} is the largest mass scale associated with the soft Supersymmetry breaking terms. As a consequence the mass scale of supersymmetric particles should not be too high, otherwise the Hierarchy problem would come back again. In other words, the observations tell us that Supersymmetry has to be broken, which forbids the theory to fix the Hierarchy problem, unless supersymmetric particles are not too heavy, in which case the naturalness of the theory can be acceptable. This is actually one argument that convince people that Supersymmetry could be observable at the LHC. One has however to keep in mind that what is *natural* or not is a highly subjective notion.

The breaking of Supersymmetry involves new particles and interactions at some high scale. As this mechanism is still unknown, it is convenient to parametrize Supersymmetry breaking by introducing a new effective Lagrangian $\mathcal{L}_{\text{soft}}$ which breaks Supersymmetry explicitly. Its general form is

$$\mathcal{L}_{\text{soft}} = -\left(\frac{1}{2}M_a\,\lambda^a\lambda^a + \frac{1}{6}a^{ijk}\phi_i\phi_j\phi_k + \frac{1}{2}b^{ij}\phi_i\phi_j + t^i\phi_i\right) + c.c. - (m^2)^i_j\phi^{j*}\phi_i. \tag{3.25}$$

The most general gauge invariant and R-parity conserving soft Supersymmetry breaking Lagrangian for the MSSM is

$$\begin{aligned}
\mathcal{L}^{\text{MSSM}}_{\text{soft}} &= && (3.26)\\
&- \frac{1}{2}\left(M_3\widetilde{g}\widetilde{g} + M_2\widetilde{W}\widetilde{W} + M_1\widetilde{B}\widetilde{B} + c.c.\right)\\
&- \left(\widetilde{\overline{u}}\,T_U\,\widetilde{Q}H_u - \widetilde{\overline{d}}\,T_D\,\widetilde{Q}H_d - \widetilde{\overline{e}}\,T_E\,\widetilde{L}H_d + c.c.\right)\\
&- \widetilde{Q}^\dagger\,M^2_{\widetilde{Q}}\,\widetilde{Q} - \widetilde{L}^\dagger\,M^2_{\widetilde{L}}\,\widetilde{L} - \widetilde{\overline{u}}\,M^2_{\widetilde{U}}\,\widetilde{\overline{u}}^\dagger - \widetilde{\overline{d}}\,M^2_{\widetilde{D}}\,\widetilde{\overline{d}}^\dagger - \widetilde{\overline{e}}\,M^2_{\widetilde{E}}\,\widetilde{\overline{e}}^\dagger\\
&- m^2_{H_u}H^*_uH_u - m^2_{H_d}H^*_dH_d - (bH_uH_d + c.c.)\,. && (3.27)
\end{aligned}$$

The first line contains M_1, M_2 and M_3 which are respectively the bino, wino and gluino mass terms. The second line contains cubic scalar couplings T_U, T_D and T_E which are 3×3 complex matrices in the family space, related to the soft-breaking matrices $A_{u,d}$ and the respective Yukawa matrices $Y_{u,d}$ through $T_{U,D} = A_{u,d}\,Y_{u,d}$. The third line contains mass terms for the squarks and sleptons: $M^2_{\widetilde{Q}}$, $M^2_{\widetilde{L}}$, $M^2_{\widetilde{U}}$, $M^2_{\widetilde{D}}$ and $M^2_{\widetilde{E}}$ are 3×3 complex hermitian matrices in the family space. The last line contains contributions to the Higgs potential.

While Supersymmetry does not introduce new parameters as compared to the Standard Model, the Supersymmetry breaking Lagrangian implies a very large number (105) of free parameters (masses, CP phases, mixing angles) in the theory. However many of them are strongly constrained from experiment and thus can not take arbitrary values. In particular this is the case for the flavor and CP violating parameters: off diagonal matrix elements and CP phases must be suppressed by some unknown mechanism. This so-called "flavour problem" in Supersymmetry is often solved in an effective way by considering "Minimal Flavour Violation" (MFV) scenario in which no additional flavor violating sources are added as compared to the Standard Model, the number of parameters being then drastically reduced. Some aspects of the flavor sector of the MSSM and the related issues will be discussed in more details in Chap. 5.

3.4.2. Mediation of Supersymmetry breaking

For phenomenological reasons the spontaneous breaking of Supersymmetry has to happen in a hidden sector distinct from the MSSM. The breaking has then to be communicated to

the MSSM (the "visible" sector). The particles in the hidden sector have very small (or no) direct couplings to the MSSM particles, and some interaction mediates the breaking of Supersymmetry to the visible sector. There are three main ways to mediate the breaking which we will now briefly describe.

Gravity mediated Supersymmetry breaking So far we have been considering Supersymmetry as a global symmetry. However it can be promoted to a local symmetry, in which case it includes gravity and is called "supergravity" (SUGRA). As gravity couples with all the fields that leads to the most popular model of Supersymmetry breaking mediation in which the interactions that mediates the breaking of Supersymmetry to the visible sector are gravitational. Assuming $m_{\text{soft}} \sim 100$ GeV, the scale at which the breaking occurs is then expected to be roughly $M_{\text{SSB}} \sim 10^{11}$ GeV. As gravity is sensitive to flavor, in principle one can expect large flavor violating terms in the resulting soft breaking terms which are in contradiction with the observations: this is the "flavour problem". It is nevertheless often assumed that soft terms are flavor diagonal. In the minimal framework called "constrained MSSM" (cMSSM), the soft terms also satisfy very strict relations:

$$M_3 = M_2 = M_1 = m_{1/2}, \tag{3.28}$$

$$M_{\tilde{Q}}^2 = M_{\tilde{L}}^2 = M_{\tilde{U}}^2 = M_{\tilde{D}}^2 = M_{\tilde{E}}^2 = m_0^2\,\mathbf{1}, \tag{3.29}$$

$$m_{H_u}^2 = m_{H_d}^2 = m_0^2, \tag{3.30}$$

$$T_U = A_0\,Y_u,\ T_D = A_0\,Y_d,\ T_E = A_0\,Y_e, \tag{3.31}$$

$$b = B_0\,\mu. \tag{3.32}$$

The soft breaking terms are defined at the scale $\sim M_{\text{Pl}}$, and using the Renormalization Group Equations (RGE) for these terms will predict the MSSM spectrum at the electroweak scale. However, the RGE are usually used only from the Unification scale $M_U \sim 2 \times 10^{16}$ GeV since they are badly known above this scale. Nicely, non-observed large flavor and CP violating terms are absent in this model. However these very strong assumptions are theoretically not very well motivated. In the MSSM the electroweak symmetry breaking condition fixes B_0 and $|\mu|$ but let $\tan\beta \equiv v_u/v_d$ (which is the ratio of the VEVs of the two Higgs doublets) as a free parameter. We are therefore left with the following 5 free parameters:

$$m_{1/2},\ m_0,\ A_0,\ \tan\beta,\ \text{sign}(\mu). \tag{3.33}$$

Note that in supergravity scenario there is a supersymmetric partner for the graviton (the spin 2 particle associated with the gravitational interaction) of spin 3/2 called the gravitino. In the cMSSM, the gravitino has a mass $m_{3/2} \sim M_{\text{SSB}} \sim 10^{11}$ GeV so that it does not play any phenomenological role. It is therefore usually not counted in the number of free parameters.

An even more constrained model is mSUGRA for "minimal supergravity", in which the bilinear and trilinear soft terms are related by $B_0 = A_0 - m_0$. $\tan\beta$ is then fixed by the electroweak symmetry breaking condition. In the mSUGRA model, one also assumes the equality $m_{3/2} = m_0$ so that the gravitino is expected to be rather light, even often the LSP.

Gauge mediated Supersymmetry breaking Another possibility is that the Supersymmetry breaking is mediated to the visible sector by the gauge interactions. In that context one introduces new chiral multiplets ("messengers"), which couples to the hidden sector and to the visible one through radiative corrections involving gauge interactions. A nice features of Gauge Mediated Supersymmetry Breaking (GMSB) models is that due to the flavor blind gauge interactions the flavor problem is avoided. The gauginos soft breaking masses are generated by one-loop diagrams, while the scalars masses come from two-loop diagrams. The minimal models of GMSB are defined by six parameters: the SUSY breaking scale in the messenger sector, the number of messenger pairs, the messenger mass scale, the Universal mass scale of SUSY particles, $\tan\beta$ and the sign of μ. Because gauge interactions are much stronger than gravity, the SUSY breaking scale can be much lower. As a consequence the gravitino can be very light and is usually the LSP, which has very important phenomenological implications for cosmology and collider Physics.

Anomaly mediated Supersymmetry breaking In the superconformal Anomaly mediated Supersymmetry breaking (AMSB) there are extra spatial dimensions and the visible and hidden sectors are living on different branes. It is then possible that supergravity mediate the Supersymmetry breaking between these different sectors, the resulting soft terms can then be understood in terms of the anomalous violation of a local superconformal invariance.

The phenomenological MSSM We should say a few words here about the phenomenological MSSM (pMSSM) which is not a model of Supersymmetry breaking mediation, but rather a simplified effective description of the soft breaking terms at low scale. In the pMSSM the soft breaking parameters are given at low scale, and no assumption is made about the relations they fulfill at the GUT scale. However, the number of parameters is reduced to a reasonable number, i.e. compatible with a numerical analysis in the parameter space. The reduction is made by applying some assumptions derived from experimental constraints (MFV for instance), but also by selecting only the relevant parameters for the study one wants to perform. Different versions of the pMSSM can exist, depending on the phenomenological aspects of the model one is interested in. Some general characteristics of pMSSM models are the assumption of MFV and CP-conserving MSSM, and degenerate soft masses as well as zero trilinear couplings for the first two generations of sfermions. In that case one would ends up with a 19 parameters model, which is still a rather large number of parameters for a numerical study.

Interaction eigenstates		Mass eigenstates	
Notation	Name	Notation	Name
$\tilde{q}_L$, $\tilde{q}_R$	left and right handed squarks	$\tilde{q}_1$, $\tilde{q}_2$	squarks 1 et 2
$\tilde{l}_L$, $\tilde{l}_R$	left and right handed sleptons	$\tilde{l}_1$, $\tilde{l}_2$	sleptons 1 et 2
$\tilde{\nu}$	sneutrinos	$\tilde{\nu}$	sneutrinos
$\tilde{g}$	gluino	$\tilde{g}$	gluino
$\tilde{W}^{\pm}$	charged winos	$\tilde{\chi}^{\pm}_{1,2}$	charginos
$\tilde{H}^{-}_1$	higgsino −		
$\tilde{H}^{+}_2$	higgsino +		
$\tilde{B}$	bino	$\tilde{\chi}^{0}_{1,2,3,4}$	neutralinos
$\tilde{W}^3$	neutral wino		
$\tilde{H}^{0}_{1,2}$	neutral higgsinos		

Table 3.3.: Interaction and mass eigenstates of the superpartners of the Standard Model particles.

3.5. The MSSM mass spectrum

3.5.1. Mass eigenstates of the MSSM

After EWSB, the interactions eigenstates of the MSSM that share common quantum numbers mixe to give mass eigenstates. The left and right eigenstates of each of the squarks and sleptons mixe into mass eigenstates denoted by 1 and 2. The neutral higgsinos ($\widetilde{H}^0_u$ and $\widetilde{H}^0_d$) and gauginos ($\widetilde{B}^0$ and $\widetilde{W}^0$) combine into four neutral mass eigenstates called neutralinos ($\tilde{\chi}^0_i$). The charged higgsinos ($\widetilde{H}^+_u$ and $\widetilde{H}^-_d$) and winos ($\widetilde{W}^+$ and $\widetilde{W}^-$) combine into two charged mass eigenstates called charginos ($\tilde{\chi}^{\pm}_i$). The gluino is a unique case within the MSSM in the sense that it is a color octet fermion, therefore it does not mix and its interaction and mass eigenstates coincide. The case of the sneutrino is a bit more subtle since it depends if one includes right-handed neutrinos in the Standard Model or not; we do not focus on these issues here. The interaction and corresponding mass eigenstates of the MSSM are summarized in Tab. 3.3.

After detailing the Higgs sector of the MSSM, we will discuss in details the two most relevant sectors of the MSSM for our study: the neutralino and the squark sectors, with an emphasize on the case of third generation squarks.

3.5.2. The Higgs sector

Electroweak symmetry breaking in the MSSM The Higgs part of the MSSM scalar potential can be expressed in function of the four components of the two Higgs doublets:

$$\begin{aligned} V = \quad & |\mu|^2 \left(|H_u^0|^2 + |H_u^+|^2 + |H_d^0|^2 + |H_d^-|^2\right) \\ & + \frac{1}{8}\left(g^2 + g'^2\right)\left(|H_u^0|^2 + |H_u^+|^2 - |H_d^0|^2 - |H_d^-|^2\right)^2 + \frac{1}{2}g^2\left|H_u^+ H_d^{0*} + H_u^0 H_d^{-*}\right|^2 \\ & m_{H_u}^2\left(|H_u^0|^2 + |H_u^+|^2\right) + m_{H_d}^2\left(|H_d^0|^2 + |H_d^-|^2\right) + \left[b\left(H_u^+ H_d^- - H_u^0 H_d^0\right) + c.c.\right]. \end{aligned} \tag{3.34}$$

The first and second lines are respectively the contributions of the F- and D-term (see Eq. (3.22)), and the third line is the contribution of the soft breaking terms (last line of Eq. (3.27)). The minimum of V has to break the electroweak symmetry (see Sec. 2.4 for a description of the Higgs mechanism). We can first require V to be bounded from below, which leads to the following relation between the potential parameters:

$$2b < 2|\mu|^2 + m_{H_u}^2 + m_{H_d}^2. \tag{3.35}$$

Electroweak symmetry breaking occurs if there is a combination of H_u^0 and H_d^0 with negative squared mass term, which is expressed by

$$b^2 > (|\mu|^2 + m_{H_u}^2)(|\mu|^2 + m_{H_d}^2). \tag{3.36}$$

Note that the $b-$term helps EWSB to occur. Note also that these constraints can not be satisfied if $m_{H_u}^2 = m_{H_d}^2$. As a consequence it is not possible to have EWSB without breaking of Supersymmetry (i.e. $m_{H_u}^2 = m_{H_d}^2 = 0$): Supersymmetry breaking is needed to break gauge symmetry. Let us also point out that in models like the cMSSM where the soft breaking Higgs squared masses $m_{H_u}^2$ and $m_{H_d}^2$ are equal at high energy, the EWSB is triggered by the RGE running which brings $m_{H_u}^2$ to small or negative value. This mechanism, called "radiative electroweak symmetry breaking", is more natural compared to the Standard Model where one has to impose by hand the condition $\mu^2 < 0$.

The field H_u^0 and H_d^0 can now acquire non-zero VEVs which are denoted

$$v_u = \langle H_u^0 \rangle, v_d = \langle H_d^0 \rangle \tag{3.37}$$

while their ratio is written as $\tan\beta \equiv v_u/v_d$. We can now require that the potential minimum leads to the correct value for the Z boson mass and derive the two following relations:

$$m_{H_u}^2 + |\mu|^2 - b\cot\beta - (m_Z^2/2)\cos(2\beta) = 0, \tag{3.38}$$

$$m_{H_d}^2 + |\mu|^2 - b\tan\beta + (m_Z^2/2)\cos(2\beta) = 0. \tag{3.39}$$

These relations are compatible with Eqs. (3.35) and (3.36) and allow us to eliminate the two parameters b and $|\mu|$ in favor of $\tan\beta$ and $\text{sign}(\mu)$.

Higgs mass eigenstates Out of the eight degrees of freedom of the Higgs fields in the MSSM (two complex $SU(2)$ doublets), three are absorbed by the gauge bosons during electroweak symmetry breaking. The remaining five degrees of freedom gives five scalar mass eigenstates: two CP-even neutral h^0 and H^0 (where h^0 is the lightest), one CP-odd neutral A^0, and two charged $H^\pm$. The expressions of their tree-level masses can be obtained from the minimization of the potential (at tree-level):

$$m^2_{A^0} = 2b/\sin(2\beta) = 2|\mu|^2 + m^2_{H_u} + m^2_{H_d} \tag{3.40}$$

$$m^2_{h^0,H^0} = \frac{1}{2}\Big(m^2_{A^0} + m^2_Z \mp \sqrt{(m^2_{A^0} - m^2_Z)^2 + 4m^2_Z m^2_{A^0}\sin^2(2\beta)}\Big), \tag{3.41}$$

$$m^2_{H^\pm} = m^2_{A^0} + m^2_W. \tag{3.42}$$

An important feature of $m^2_{h^0}$ is that it is bounded from above:

$$m_{h^0} < m_Z|\cos(2\beta)|, \tag{3.43}$$

which is excluded by the LEP experiment, and is not compatible with $m_{h^0} = 125$ GeV, as suggested by the LHC discovery. Note that the identification of h^0 as the observed Higgs boson is possible since in the MSSM h^0 is often behaving like the Standard Model Higgs boson (same couplings), in particular in the "decoupling limit" where $m_{A^0} >> m_Z$ in which $m_{h^0} = m_Z|\cos(2\beta)|$ at tree-level. What we are still missing here are the radiative corrections to the Higgs mass. They can be calculated from the quantum correction to the Higgs potential, which are known at two loops. These corrections can be significantly large and the dominant contribution, come from the one-loop diagrams with top squarks and quarks. Taking into account these one-loop corrections, the lightest Higgs mass in the decoupling limit becomes

$$m^2_{h^0} = m^2_Z\cos^2 2\beta + \frac{3g^2 m^4_t}{8\pi^2 m^2_W}\left[\log\frac{M^2_{\text{SUSY}}}{m^2_t} + \frac{X^2_t}{M^2_{\text{SUSY}}}\left(1 - \frac{X^2_t}{12\,M^2_{\text{SUSY}}}\right)\right] \tag{3.44}$$

where $X_t = A_t - \mu/\tan\beta$ is the stop mixing parameter (see Sec. 3.5.4) and $M_{\text{SUSY}} = \sqrt{m_{\tilde{t}_1} m_{\tilde{t}_2}}$ is the average mass of the two top squarks. One possibility to enhance the one-loop contribution and reach 125 GeV is to have a large M_{SUSY}, i.e. heavy stops. However it is often seen as theoretically unsatisfactory since it worsens the naturalness of the theory.

3.5.3. The neutralino sector

As said in the introduction there are 4 neutralinos $\tilde{\chi}_i^0, \widetilde{\chi}_i^0,\ i = 1, 2, 3, 4$, ordered by increasing mass, which are mixture of bino, neutral wino and neutral higgsinos. In the gauge-eigenstate basis $(\widetilde{B}, \widetilde{W}^0, \widetilde{H}_d^0, \widetilde{H}_u^0)$, the neutralino mass matrix is

$$\mathcal{M}_{\widetilde{\chi}^0} = \begin{pmatrix} M_1 & 0 & -c_\beta\, s_W\, m_Z & s_\beta\, s_W\, m_Z \\ 0 & M_2 & c_\beta\, c_W\, m_Z & -s_\beta\, c_W\, m_Z \\ -c_\beta\, s_W\, m_Z & c_\beta\, c_W\, m_Z & 0 & -\mu \\ s_\beta\, s_W\, m_Z & -s_\beta\, c_W\, m_Z & -\mu & 0 \end{pmatrix} \tag{3.45}$$

with $s_\beta = \sin\beta$, $c_\beta = \cos\beta$, $s_W = \sin\theta_W$, and $c_W = \cos\theta_W$. M_1, M_2 and μ are respectively the bino, wino and higgsino soft masses. The remaining terms are Higgs-higgsino-gaugino couplings which mix higgsinos with bino and wino. The mass matrix $\mathcal{M}_{\widetilde{\chi}^0}$ can be diagonalized by a unitary matrix $U^{\widetilde{\chi}^0}$ to obtain mass eigenstates:

$$U^*_{\widetilde{\chi}^0} \mathcal{M}_{\widetilde{\chi}^0} U^{-1}_{\widetilde{\chi}^0} = \mathrm{diag}(m_{\tilde{\chi}_1^0}, m_{\tilde{\chi}_2^0}, m_{\tilde{\chi}_3^0}, m_{\tilde{\chi}_4^0}). \tag{3.46}$$

In principle μ is complex and its phase is unknown, but strongly constrained by experiment. We will always consider here that μ is a real parameter. In the limit $m_Z \ll |\mu \pm M_1|, |\mu \pm M_2|$, which happens often in the cMSSM for example, the gauginos mixing is negligible and the four neutralinos are said to be "bino-like", "wino-like" and "higgsino-like" with respective mass M_1, M_2 and $|\mu|$.

3.5.4. The squark sector

As the squarks of the MSSM share the same quantum numbers, they can mix and the mass eigenstates are obtained after diagonalization of two 6×6 mass matrices, for the up and down type squarks. However we will here assume diagonal soft terms in the family space so that one only needs to consider 2×2 matrices, neglecting the mixing between different generations (the general case of non-diagonal soft terms will be considered later in Chap. 5). The mass matrices of the up and down type squarks then read

$$\mathcal{M}^2_{\tilde{q}_i} = \begin{pmatrix} M^2_{\tilde{Q}_i} + (I_q^{3L} - e_q\, s^2_W) \cos 2\beta\, m_Z^2 + m^2_{q_i}\,, & m_{q_i}\big(A_{q_i} - \mu\,(\tan\beta)^{-2I_q^{3L}}\big) \\ m_{q_i}\big(A_{q_i} - \mu\,(\tan\beta)^{-2I_q^{3L}}\big) & M^2_{\tilde{U}_i, \tilde{D}_i} + e_q\, s^2_W \cos 2\beta\, m_Z^2 + m^2_{q_i} \end{pmatrix}, \tag{3.47}$$

with $q = u, d$ and $i = 1, 2, 3$ is the generation index. Here e_q is the fractional charge of the squark in units of e, I_q^{3L} is the weak isospin of the squark, $M_{\tilde{Q}_i}$, $M_{\tilde{U}_i}$, and $M_{\tilde{D}_i}$ are the soft-breaking mass terms of the squarks, and A_{u_i}, A_{d_i} are the soft-breaking trilinear couplings. In this notation the $M_{\tilde{Q}_i}$, $M_{\tilde{U}_i}$, $M_{\tilde{D}_i}$, A_{u_i} and A_{d_i} are the i^{th} diagonal elements of the soft breaking 3×3 matrices $M^2_{\tilde{Q}}$, $M^2_{\tilde{L}}$, $M^2_{\tilde{U}}$, $M^2_{\tilde{D}}$, $M^2_{\tilde{E}}$, A_u and A_d respectively, which are involved in the soft breaking Lagrangian (3.27).

The soft-breaking mass terms obviously give contributions to the diagonal elements of the mass matrix. The off-diagonal terms proportional to m_Z^2 correspond to a mass splitting between the components of $SU(2)_L$ doublets and come from the D-term contribution to the scalar potential, while the diagonal term proportional to m_q^2 come from the F-term contribution (see Eq. (3.22)). The latter also gives a term in $m_q\,\mu$ in the diagonal elements after the Higgs get a VEV (combination of first and last term of Eq. (3.23) for instance). Finally, the soft-breaking trilinear couplings give a contribution to the off-diagonal elements, after the Higgs get a VEV.

For each generation this mass matrix can be diagonalized by a unitary matrix $U^{\tilde{q}}$ to give mass eigenstates (here the generation index has been suppressed for clarity):

$$U^{\tilde{q}}\,\mathcal{M}^2_{\tilde{q}}\,(U^{\tilde{q}})^\dagger = \text{diag}(m^2_{\tilde{q}_1}, m^2_{\tilde{q}_2}), \tag{3.48}$$

with $m^2_{\tilde{q}_1} < m^2_{\tilde{q}_2}$. The interaction and mass eigenstates basis being related by a mixing angle $\theta_{\tilde{q}}$:

$$\begin{pmatrix} \widetilde{q}_1 \\ \widetilde{q}_2 \end{pmatrix} = \begin{pmatrix} \cos\theta_{\tilde{q}} & -\sin\theta_{\tilde{q}} \\ \sin\theta_{\tilde{q}} & \cos\theta_{\tilde{q}} \end{pmatrix} \begin{pmatrix} \widetilde{q}_L \\ \widetilde{q}_R \end{pmatrix}. \tag{3.49}$$

As the mixing between the left and right squarks is proportional to their Yukawa coupling, the mass eigenstates will differ from the interaction eigenstates only for the third generation squarks. The second reason why the case of third generation squarks is peculiar is that their large Yukawa and trilinear couplings enhance the RGE running of their masses:

$$16\pi^2 \frac{d}{dt} m^2_{Q_3} = X_t + X_b - \frac{32}{3} g_3^2 |M_3|^2 - 6 g_2^2 |M_2|^2 - \frac{2}{15} g_1^2 |M_1|^2 + \frac{1}{5} g_1^2 S, \tag{3.50}$$

$$16\pi^2 \frac{d}{dt} m^2_{\widetilde{u}_3} = 2X_t - \frac{32}{3} g_3^2 |M_3|^2 - \frac{32}{15} g_1^2 |M_1|^2 - \frac{4}{5} g_1^2 S, \tag{3.51}$$

$$16\pi^2 \frac{d}{dt} m^2_{\widetilde{d}_3} = 2X_b - \frac{32}{3} g_3^2 |M_3|^2 - \frac{8}{15} g_1^2 |M_1|^2 + \frac{2}{5} g_1^2 S \tag{3.52}$$

where M_1, M_2, M_3 are the gaugino masses,

$$S = m^2_{H_u} - m^2_{H_d} + \text{Tr}[\mathbf{m}^2_Q - \mathbf{m}^2_L - 2\mathbf{m}^2_{\bar{u}} + \mathbf{m}^2_{\bar{d}} \mathbf{m}^2_{\bar{e}}] \tag{3.53}$$

and

$$X_t = 2|y_t|^2(m_{H_u}^2 + m_{Q_3}^2 + m_{\widetilde{u}_3}^2) + 2|a_t|^2, \tag{3.54}$$

$$X_b = 2|y_b|^2(m_{H_d}^2 + m_{Q_3}^2 + m_{\widetilde{d}_3}^2) + 2|a_b|^2. \tag{3.55}$$

It is clear that as X_t depends on y_t and a_t it will be large for third generation, which will decrease their masses at low energy. Also note that the right handed stop mass has a factor 2 in front of X_t and does not receive negative contribution from M_2, thus it will be lighter than the left handed one.

Chapter 4.

Neutralino-stop coannihilation in the MSSM

This chapter is devoted to the phenomenology of neutralino relic density in the MSSM and its interplay with other experimental constraints, with an emphasize on the neutralino-stop coannihilation. In Sec. 4.1 we discuss in detail the constraint from the relic density of neutralino and its phenomenology in the cMSSM and several other well-studied MSSM models. In Sec. 4.2 we list the existing experimental constraints that can be applied on the parameter space of MSSM models, including the relic density of dark matter, and focus on the neutralino-stop coannihilation regions. In Sec. 4.3, we finally perform a numerical analysis of the neutralino-stop coannihilation regions in the pMSSM.

4.1. Phenomenology of neutralino relic density

4.1.1. cMSSM

In constrained models such as the cMSSM, the unification of gaugino masses at high scale imposes strong constraints on the lightest neutralino content (see Eq. (3.28)). That often leads to a neutralino which is mainly a bino, and as the bino does not couple to gauge bosons the typical annihilation cross section is too low for the relic density to reach the upper limit of Eq. (1.6) in the parameter space. As a consequence a special mechanism like resonances or coannihilation [1] is required in order to enhance the cross section, which can then be sufficiently large in specific parts of the parameter space. In the following we list the possible mechanisms which can happen in the cMSSM and potentially give the correct relic density.

[1] Note that in some situations coannihilation can also increase the relic density. See [56] for an example in Supersymmetry, and [57] for a non supersymmetric model.

- In a large part of the parameter space (historically called the "Bulk"), light sleptons can enhance the t-channel annihilation of neutralinos into leptons final states. Such light sleptons are however excluded by far.

- For low $m_{1/2}$ a s-channel resonance with a light CP-even Higgs boson h^0 can occurs, which is however in contradiction with the Higgs boson observation at LHC, and is excluded by the limits on the squarks and gluino masses (and other constraints).

- For large $\tan\beta$ the CP-odd Higgs boson A^0 is lighter and a s-channel resonance can occurs ("A-funnel"). In addition, large values of $\tan\beta$ enhance couplings of A^0 to down-type fermions. As a result neutralino annihilation into b quark pairs or tau lepton pairs can be significantly enhanced.

- For large m_0 the RGEs result in a rather small value of μ ("focus point" [58]) which increases the higgsino content of the lightest neutralino, enhancing the annihilation into fermion pairs via Z boson or A^0 exchange. Also, the splitting with the lightest chargino is reduced, enhancing the coannihilation of the lightest neutralino with the lightest chargino into electroweak gauge bosons final states.

- For low m_0 the lightest stau is light (NLSP) and the coannihilation between neutralino and stau becomes significant [59, 60].

- For large A_0 the stop mixing is increased (see Sec. 3.5.4) and the lightest stop becomes light (NLSP), which enhances the coannihilation between neutralino and stop [56, 61, 62].

This is illustrated in Fig. 4.1 where are shown in blue the regions of the cMSSM parameter space favored by the measurement of the dark matter relic density by Planck, for two different set of parameters. Because of the very narrow experimental 1σ range (see Eq. 1.6), we use here a 10σ range so that the corresponding region is clearly visible. On the left side of Fig. 4.1, three of the regions discussed above are visible: the Higgs resonance is seen as vertical lines at low $m_{1/2}$, the focus-point is seen at $m_0 > 3$ TeV, and the stau coannihilation region is seen as a very narrow band along the stau-LSP region (in red), where there is no dark matter candidate. On the right side, due to the large (negative) value of A_0, there is a stop coannihilation region along the stop-LSP region in red. We also show in green the regions in which the predicted Higgs mass falls within the range $123 < m_{h^0} < 129$ GeV, using a rough approximation of the experimental and theoretical precision. It is clear that most of the cosmologically favored regions are excluded or strongly disfavored by the Higgs boson observation.

4.1.2. Non universal models

As the cMSSM is not very well motivated and strongly constrained by experiments it is interesting to consider more general models in which some of the relations between the soft breaking

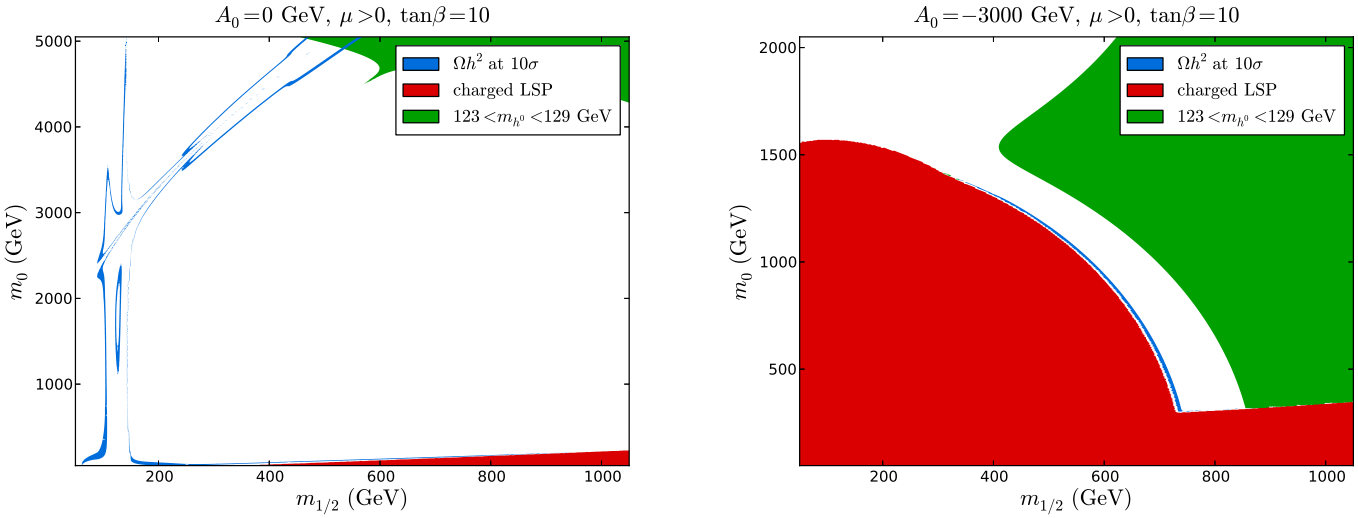

Figure 4.1.: Cosmologically favored region in the $(m_0, m_{1/2})$ plane of the cMSSM for $\mu > 0$, $\tan\beta = 10$, $A_0 = 0$ GeV (left) and $A_0 = -3000$ GeV (right).

parameters at the GUT scale are relaxed. One then ends up with a larger number of free parameters, and more possibilities to enhance the annihilation cross section. For example, stop coannihilation can be achieved without large A_0 either through RGE effects, or by relaxing the universality of squark masses at the GUT scale. New coannihilation channels can also appear, like coannihilation with bottom squarks, or with sleptons other than the stau. Also, there is more freedom to increase the higgsino or wino component of the neutralino (especially if there is no gaugino mass unification), in which case its annihilation cross section is enhanced. In the following we describe some features of simple non universal models in which only a few assumptions from the cMSSM are relaxed.

Non Universal Gaugino Mass models When considering $SO(10)$ GUT the properties of the SUSY breaking mechanism are related to the breaking of an $SU(5)$ subgroup into the Standard Model gauge group $SU(3)\times SU(2)\times U(1)$. The relations between the gaugino masses M_i $(i = 1, 2, 3)$ at the unification scale are given by the embedding coefficients of the Standard Model groups in $SU(5)$. In particular, in Non Universal Gaugino Masses (NUGM) models, the unification constraint $M_i = m_{1/2}$ of the cMSSM can be relaxed without spoiling the unification of the gauge couplings. Three independent parameters are then needed to fully parameterize the gaugino sector. Previous studies have shown that NUGM models have an interesting dark matter phenomenology [63, 64].

Choosing $M_1 > M_2$ for instance leads to a lightest neutralino with a significant wino component, which can open new annihilation channels due to the larger coupling of the neu-

tralino with the electroweak gauge bosons. Coannihilation channels with other neutralinos or charginos can also be important [65]. Modifying the value of M_3 has a strong impact on the whole SUSY spectrum through RGE effects. For instance, choosing $M_3 < M_2$ decreases μ and leads to a LSP with a large higgsino component, as for the focus point in the cMSSM. The stop mass is also strongly affected by the value of M_3, and can be reduced without the need for large trilinear couplings as in the cMSSM. Another effect is the decreasing of the mass of A^0, the A-funnel becoming then available even for intermediate values of $\tan\beta$. In NUGM it is also possible to have a gluino NLSP and therefore neutralino-gluino coannihilation which is a very efficient coannihilation process, as discussed in [66].

Non Universal Higgs Mass models Similarly to the mechanism leading to non-universal gaugino masses, in $SO(10)$ SUSY GUTs, depending on the exact representation to which the Higgs doublets belong, their corresponding SUSY breaking masses m_{H_D} and m_{H_U} need not necessarily be the same. In non-universal Higgs mass models they can therefore be treated as independent parameters at the high scale [67, 68].

Since the parameters in the Higgs sector are related to the gaugino masses (in particular M_3) via the RGE, many effects seen in NUGM models can be reproduced in NUHM by choosing the correct set of parameters. Indeed, as in the case of NUGM models, new contributions to the RGE appears, which can considerably modify the spectrum of SUSY particles. These additional contributions will modify the masses of SUSY particles at the electroweak scale. In the stop sector for instance, $m^2_{H_u}$ and $m^2_{H_d}$ appears in the quantity defined in Eq. (3.53) (which is equal to zero in the cMSSM, but equal to $m^2_{H_u} - m^2_{H_d}$ in NUHM) and in the quantity X_t defined in Eq. (3.54). By choosing a large negative value for $m^2_{H_u} - m^2_{H_d}$ one can reduce the stop mass through the RGE and enhance the neutralino stop coannihilation by keeping $A_0 = 0$ GeV. These new contributions can also lead to coannihilation processes between neutralino and first or second generation sleptons or squarks, for instance.

Non Universal Sfermion Mass models It is also possible to relax the assumption that all squark and slepton soft masses are equal at GUT scale. In [69] a minimal scenario of non universal sfermion masses (mNUSM) inspired by $SU(5)$ GUT is described. In this model the sfermions are described by two different representations, which result in a specific pattern for the sfermion masses at the GUT scale. In particular the masses of the left-handed sleptons and right-handed down type squarks are not equal to m_0, which allows important contributions from new coannihilating partners like the sbottom, the stau or the tau sneutrino.

Another example of phenomenologically interesting possibility would be to modify the up-type squark soft masses at GUT scale to end up with a lighter stop at the electroweak scale, which could then coannihilate with the neutralino even for $A_0 = 0$.

4.2. Experimental constraints in the MSSM parameter space

In this section we discuss the relevant experimental constraints in the MSSM and their phenomenological implications, in particular for the neutralino-stop coannihilation regions. We first focus on the constraint coming from the measurement of the dark matter relic density, and describe the processes relevant for the calculation of the relic density in the neutralino-stop coannihilation regions. We then discuss the phenomenology of various experimental results as the one from LHC, the Higgs boson mass and flavor Physics results. Note that a typical scenario of neutralino-stop coannihilation and the relevant experimental constraints have been discussed in detail in [70].

The first constraints that should be applied on the parameter space of SUSY models are trivial: there must be EWSB[2], the high scale parameters must lead to a valid (i.e. non tachyonic) spectrum at low scale, and there must be a dark matter candidate (the neutralino in our case). Further constraints can be derived from different experimental measurements, the most relevant for our study being detailed in the next sections.

4.2.1. Relic density of dark matter

The lightest neutralino $\tilde{\chi}_1^0$ is often considered as the LSP because it would then provide a good dark matter candidate. In addition it often naturally emerges as the LSP in many supersymmetric models like the cMSSM. As explained in the Chap. 1 it is possible to constrain supersymmetric models by assuming that it provides a viable dark matter candidate, and comparing the obtained predictions to different experimental results related to dark matter. In particular, if one assume that this dark matter candidate is the only source of the missing mass in the Universe, the calculated relic density must be compatible with the numerical value extracted from the CMB observation. Another possibility, which we shall not consider here, is to impose only an upper bound on the relic density since in principle dark matter can be made of several particles of different nature. We recall that, assuming that the Standard Model of cosmology is valid, the experimentally measured relic density of dark matter is [1]:

$$\Omega_{\rm CDM} h^2 \;=\; 0.1199 \;\pm\; 0.0027. \tag{4.1}$$

Following the procedure described in Sec. 1.2, one can then predict the relic density of neutralinos in a specific supersymmetric model with some particular choice of parameter values, and compare it with the given experimental value. In this way constraints on the models can

[2]The public tool `Vevacious`, recently released [71], allows to check if the considered potential minimum is a global one, and if it not the case, it computes the tunneling time. To be valid the lifetime of this minimum must be longer that the Universe one. We do not consider this constraint here, even though this is particularly interesting since light stops can be responsible for color breaking minima.

be derived, and can be used together with other constraints to obtain informations about the compatibility of the models with observations.

One of the key ingredients needed in the calculation of relic density is the cross section of the processes involved in the freeze-out mechanism. This cross section, calculated in the usual perturbation theory, can be then convoluted with the thermal distribution to obtain the effective thermally averaged cross section involved in the Boltzmann Eq. (1.18). The relic density calculation tools described in Sec. 1.2 are also able to calculate these cross sections. They are either hard-coded (`DarkSUSY`, `SuperIso Relic`), or automatically calculated by another program (`CalcHEP` [72] in the case of `micrOMEGAs`, `CompHEP` [73] in the case of `IsaRed`), so that efficient scanning of parameter space of supersymmetric models can be performed. Indirectly, another important ingredient is needed: the calculation of the supersymmetric particles spectrum, i.e. their masses and mixings. Indeed, these quantities are required when calculating the cross sections. Fortunately, such calculation can also be automatically performed by tools such as `SPheno` [74, 75], `Suspect` [76], or `SoftSUSY` [77]. `SPheno` for instance, solves the renormalization group equations (RGE) numerically to two-loop order with boundary conditions defined by high scale theories. The calculation of the supersymmetric spectrum includes one-loop correction to all masses, and even two-loop corrections to some parameters in the Higgs sector. These programs can write the obtained spectrum in a standardized way (SUSY Les Houches Accord [78] for instance) which can then be passed to a relic density calculator. However the relic density calculation public tools often have several limitations when computing the necessary cross sections in Supersymmetry:

- exact $R-$parity is assumed, i.e. $R-$parity violating terms are forbidden. If $R-$parity violation can seems in contradiction with the requirement of a stable dark matter, it has been shown that gravitino can be a good dark matter candidate in $R-$parity violating models [79].

- the CP conserving limit is taken (CP violating models are implemented in `micrOMEGAs`.)

- minimal flavor violation is assumed, i.e. the flavor violating terms come from the CKM matrix (this point will be discussed in Chap. 5).

- only two-body final states are considered. It has been shown in [80] that in some specific kinematic configurations, annihilation of dark matter into three-body final states can become dominant. This situation also occurs in the inert doublet model [81, 82] and has been implemented in the latest version of `micrOMEGAs`.

- Even if some effective corrections are taken into account, especially in `micrOMEGAs`, cross sections are calculated at leading order (this point will be discussed in the Chap. 6).

The latest version of `micrOMEGAs` also includes the possibility to calculate the relic density of an asymmetric dark matter, and in the case of semi-annihilation.

We now focus on the neutralino-stop coannihilations where the relic density is reduced by annihilation processes involving stops. Let us first describe the processes which are relevant in these regions (a similar discussion can be found in [62]). When the mass splitting between the lightest neutralino and the lightest stop is small, processes involving the stop play an important role in the freeze-out mechanism and have to be taken into account. In this situation, in addition to the annihilation of two neutralinos (which here proceeds mostly through t-channel stop exchange producing top pairs), two other kind of scattering processes become relevant: the coannihilation between a neutralino and a stop, and the annihilation of two stops. As detailed in Sec. 1.2 these two processes are Boltzmann suppressed by exponential factors (see Eq. (1.28) and (1.29)):

$$\exp\left[-\frac{m_i + m_j - 2\,m_{\tilde{\chi}_1^0}}{T}\right] \tag{4.2}$$

where m_i and m_j are the masses of the two initial particles, and T is the freeze-out temperature which can be roughly approximated by $T \approx m_{\tilde{\chi}_1^0}/20$. Defining

$$\Delta m \equiv \frac{m_{\tilde{t}_1} - m_{\tilde{\chi}_1^0}}{m_{\tilde{\chi}_1^0}} \tag{4.3}$$

one can then easily check that the cross section of coannihilation (i.e. with $m_i = m_{\tilde{\chi}_1^0}$, $m_j = m_{\tilde{t}_1}$) is suppressed by less than a factor 10 when $\Delta m < 10\%$. On the other hand, stop annihilation ($m_i = m_j = m_{\tilde{t}_1}$) is "doubly" suppressed and will be suppressed by a factor 100 for the same mass difference. However, because of the different kind of couplings which are involved, the typical stop annihilation cross section is much larger than the neutralino stop coannihilation cross section which is much larger than the neutralino annihilation cross section. Therefore for relatively small Δm neutralino-stop coannihilation will contribute significantly to the total cross section, and for even smaller mass differences the stop annihilation will become dominant. In addition, in this region the neutralino annihilation cross section is usually too low to reduce sufficiently the relic density by itself, and the stop annihilation cross section is too large so that the relic density quickly becomes too small. As a result the correct relic density will be typically achieved when $\Delta m \approx 10 - 15\%$ and will involve a mixture of these three kind of contributions, the neutralino-stop coannihilation being often the dominant one. This is illustrated in Fig. 4.2 where the contributions of neutralino annihilation (red dot-dashed line), neutralino-stop coannihilation (blue solid line) and stop annihilation (green dashed line) to the relic density are shown in function of the neutralino-stop mass splitting. The orange shaded area correspond to mass splittings for which the relic density is favored at 2σ. It is clear that neutralino annihilation is insensitive to the mass splitting, excepted for small splitting where the weighting factor is not equal to one but depends on the internal degrees of freedom (see Eq. 1.26). The contribution from neutralino-stop coannihilation and stop-stop annihilation decrease exponentially with the splitting, as explained above. In this example the relic density

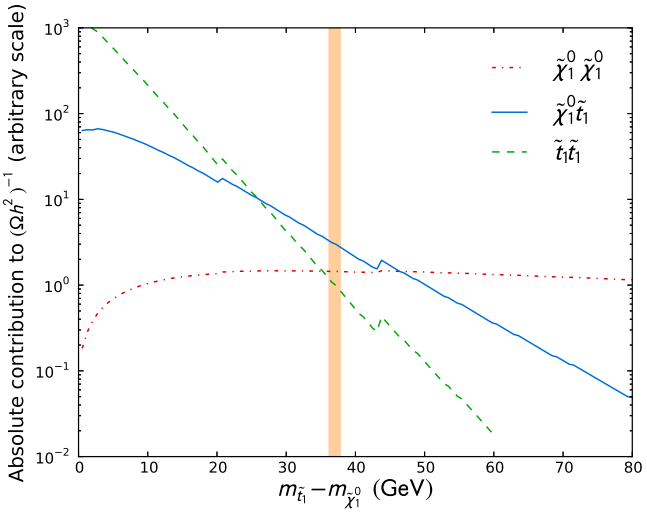

Figure 4.2.: Evolution of different contributions to the relic density of neutralino with the neutralino-stop mass splitting.

measurement favors a mass splitting of $\Delta m = 15\%$, for which the total cross section is indeed a mixture of these three processes, with the neutralino-stop coannihilation being the dominant one. To summarize, using relic density as an experimental constraint in the coannihilation region is equivalent to selecting a specific value for Δm. It can be interesting then to combine this constraint with other experimental constraints, as will be seen in the next sections.

We now show the different possible coannihilation channels and final states in Fig. 4.3. The possible final states always contain a quark and a gauge or Higgs boson. There are four different Higgs and four different gauge bosons which make eight possible final states, assuming a diagonal CKM matrix. The associated quark is either a top quark (in the case of a neutral boson) or a bottom quark (in the case of charged boson). The coannihilation occurs through s-, t- and u-channels involving respectively an internal top quark, top or bottom squark, and neutralino or chargino. Because neutralino and chargino do not couple to photon and gluon the u-channel is absent for such final state.

4.2.2. Direct detection of dark matter

As explained in the previous section, in the neutralino-stop coannihilation region the neutralino annihilation cross section is rather small and the total effective cross section is driven mostly by the neutralino-stop coannihilation process. As the neutralino-quark scattering cross section, which is involved in direct detection, is correlated with the neutralino annihilation cross section, the detection rate in the neutralino-stop coannihilation region is much lower than in the other

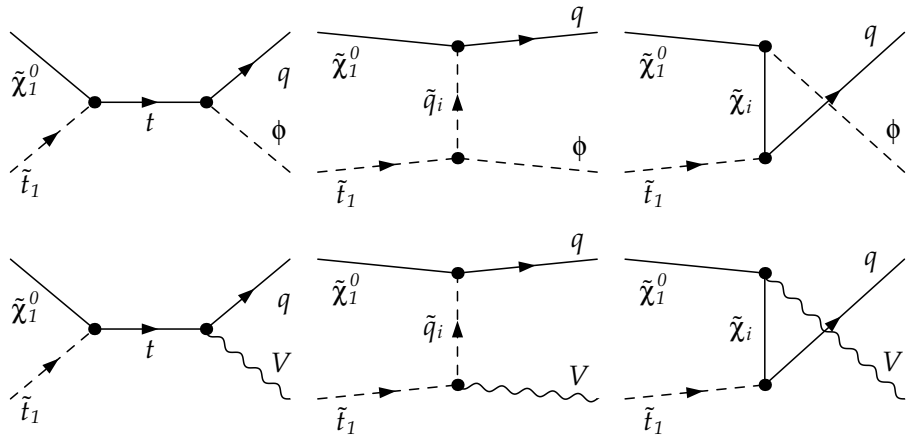

Figure 4.3.: Leading-order Feynman diagrams for neutralino-stop coannihilation into a quark and a Higgs boson ($\phi = h^0, H^0, A^0, H^\pm$) or a gauge boson ($V = g, \gamma, Z^0, W^\pm$). $q \equiv t$ or b if the outgoing boson is respectively neutral or charged. The u-channel is absent for a photon or a gluon in the final state.

regions favored by the relic density measurement. As a result the neutralino-stop coannihilation region is still completely unconstrained by the latest direct detection results [83].

4.2.3. Supersymmetric particle production and decay

Until now there has not been any direct evidence for Supersymmetry at the LHC, and the ATLAS and CMS experiments are setting limits on the masses of superpartners by looking at many possible signatures. In the standard searches for Supersymmetry one usually assumes the production of colored superparticles which then decay into other superparticles (cascade decays), the decay chain ending in a LSP which is seen as a large missing transverse energy. Most of the parameter space of the simplest constrained low energy supersymmetric models are excluded or strongly disfavored by the LHC. In particular, the gluino and squarks of first and second generations have to be heavier that ~ 1 TeV [84, 85]. These limits are however derived assuming degeneracy between different flavors and mass eigenstates, which can not be applied to the third generation squarks, as seen in Sec. 3.5.4.

At the LHC, stops can be produced by pairs through $q\,\bar{q}$ and $g\,g$ annihilation. If the stop is light a rather large production cross section is expected [86]. However, if the stop is almost degenerate with the neutralino LSP, its decay products will be soft and the reconstructed missing transverse energy will be small. As such signals are hard to trigger and detect, the LHC constraints on the stop mass are less stringent in the coannihilation region. It might be then possible that a light stop has been already copiously produced at the LHC but no excess has been seen so far [87].

Indeed, if $\Delta m \sim 10$ GeV, many decay channels of the stop are forbidden: $\tilde{t}_1 \to t\ \tilde{\chi}_1^0$ of course, but also $\tilde{t}_1 \to b\ \tilde{\chi}_1^0\ W$ and $\tilde{t}_1 \to \nu_l\ \tilde{l}^*\ b$. The decay $\tilde{t}_1 \to l\ \nu_l\ b\ \tilde{\chi}_1^0$ is kinematically accessible but strongly phase space suppressed. The dominant decay final state is then usually $\tilde{t}_1 \to c\ \tilde{\chi}_1^0$ which occurs at one loop, and the resulting signature is two soft jets with missing transverse energy. In [70] it was however shown that the decays $\tilde{t}_1 \to l\ \nu_l\ b\ \tilde{\chi}_1^0$ and $\tilde{t}_1 \to q\ \bar{q}\ b\ \tilde{\chi}_1^0$ can compete with $\tilde{t}_1 \to c\ \tilde{\chi}_1^0$ and provide a charged lepton improving the identification of the stop.

Other alternative methods have been developed to constrain light stops. In the first one gluino pair production is considered, followed by gluino decay into a top quark and a stop, which lead to same-sign top quarks and same-sign stops. However if the gluino is heavier than 600 GeV its production cross section is too small to apply this search. The other possibility is to consider stop pair production in association with a hard jet. In [88] this last method is employed to derive limit on the stop mass in the coannihilation region using monojet searched from ATLAS with 1 fb^{-1}. Their obtained excluded limit reach 160 GeV. A similar search is performed in [89] and a limit of 220 GeV is derived at the LHC at 7 TeV with 5 fb^{-1}. A "razor" analysis is performed in [70] and a upper limit of 250 GeV on the stop mass is derived in the cosmologically interesting region. In [90] they consider the production of two stops in association with two b (anti)quarks. They require the b jets to be tagged in order to suppress the Standard Model background and study the LHC discovery potential for such scenario. In [91] they perform a direct stop search using a quantity called dileptonic m_{T2} which is optimized for the coannihilation region.

To summarize, there are many different methods to constrain the stop mass in the challenging neutralino-stop coannihilation region, but the strongest limits are still below 300 GeV. Thus the neutralino-stop coannihilation still need to be explored at the LHC. Similar conclusions can be drawn from analyses of the neutralino-sbottom coannihilation region [92–94].

4.2.4. Higgs boson observation

The Higgs boson has been observed recently by the ATLAS [95] and CMS [96] experiments at the LHC and its mass has been measured to be [97, 98]

$$m_h = 125.5 \pm 0.2^{+0.5}_{-0.6}\ \text{GeV (ATLAS)}, \tag{4.4}$$

$$m_h = 125.7 \pm 0.3 \pm 0.3\ \text{GeV (CMS)}, \tag{4.5}$$

which imposes strong constraints on supersymmetric models since, as explained in Sec. 3.3.2, this quantity is a prediction of the MSSM. In the context of the MSSM, 125 GeV is typically a rather large mass (for instance minimal models of anomaly and gauge mediation are strongly disfavored [99]), and large one-loop corrections are needed to reach such high value

(see Eq. (3.44)). As a result, in addition to the Higgs sector, the stop and sbottom sectors of the MSSM are also strongly constrained. In particular, either the SUSY breaking scale M_S or the stop mixing parameter X_t has to be large [100]. More precisely, the stop mixing parameter should satisfy $|X_t| \approx 2M_S$. This second possibility is favored from naturalness arguments and is called maximal mixing scenario. Implications of such requirement for GUT models have been studied in [101]. Note that the Eq. (3.44) holds only for small splitting between the two stops. For larger splitting the value of $|X_t|/M_S$ corresponding to maximal mixing is larger.

In [102], [83] and [103] it was shown that in constrained supersymmetric models such as cMSSM or NUHM the constraint $m_{h^0} \approx 125$ GeV exclude most of the coannihilation regions. It has been however noticed in [104] that in less constrained models with inverted sfermion mass hierarchy (i.e. first two generations of squarks and sleptons much heavier than the third one), neutralino-stop coannihilation was generically present and often corresponds to the maximal mixing scenario. In general, more general models like pMSSM allows for neutralino-stop coannihilation regions compatible with experimental constraints and where the Higgs mass can be pushed up to 125 GeV. Up to now there has been however no dedicated study of the phenomenology of these regions in the pMSSM.

The measurements of the Higgs boson decay rates can also provide informations about the validity of supersymmetric models. For instance the presence of a light stop in the spectrum can modify Higgs production via gluon fusion (see [105]), however we will not consider this kind of constraints.

4.2.5. Flavor violating observables in B-Physics

Due to very high experimental and theoretical accuracies, flavor violating observables involving B mesons became a very efficient way to constraint indirectly New Physics models. In particular, we will describe here two major observables which are the branching ratios $\mathrm{BR}(B \to X_s\gamma)$ and $\mathrm{BR}(B_s \to \mu^+\mu^-)$.

$\mathrm{BR}(B \to X_s\gamma)$ involves transition of the kind $b \to s\gamma$ which occurs only at one loop in the Standard Model. The current experimental average is [106]

$$\mathrm{BR}(B \to X_s\gamma) = (3.55 \pm 0.24 \pm 0.09) \cdot 10^{-4}. \tag{4.6}$$

As contributions from the MSSM are also at one loop one can expect significant deviation from the Standard Model value, especially at large $\tan\beta$ where the MSSM contributions are enhanced. In the Standard Model this "penguin" decay process involve a W boson, while in the MSSM charged Higgs boson, chargino, neutralino and gluino can contribute.

BR($B_s \to \mu^+\mu^-$) is a rare decay which has a very small value in the Standard Model because of helicity suppression [107, 108]:

$$\mathrm{BR}(B_s \to \mu^+\mu^-)_{\mathrm{SM}} = (3.53 \pm 0.38) \cdot 10^{-9}. \tag{4.7}$$

The dominant Standard Model contribution come from a top quark loop with a Z boson. The MSSM contributions are enhanced by a factor $\tan^6\beta$ and can be more than one order of magnitude higher. In particular, this observable is very sensitive to the extra Higgs boson contributions in the MSSM. However the LHCb experiment has recently observed this decay, and the measured branching ratio is close to the Standard Model prediction, which excludes large deviation from New Physics contributions [109][3]:

$$\mathrm{BR}(B_s \to \mu^+\mu^-) = \left(3.2^{+1.4}_{-1.2}(\mathrm{stat})^{+0.5}_{-0.3}(\mathrm{syst})\right) \times 10^{-9}. \tag{4.8}$$

Note that a more stringent upper limit of 4.2×10^{-9} has been derived from previous studies [112].

As the neutralino-stop coannihilation can be important for moderate values of $\tan\beta$, it is compatible with many low energy flavour observables. In addition, even if the stop is rather light it is mostly right-handed, which is also less constrained by many of these measurements. Lastly, chargino and Higgses do not need to be light. As a consequence, flavor violating observables constraint have to be taken into account but they do not represent a major issue.

4.2.6. Anomalous magnetic moment of the muon

The muon anomalous magnetic moment, defined as

$$a_\mu = \frac{g_\mu - 2}{2} \tag{4.9}$$

where g_μ is the magnetic moment of the muon, is one of the most precisely measured quantities in Particle Physics: its average experimental value is [113, 114]

$$a_\mu^{\mathrm{EXP}} = 11\,659\,208.9(5.4)(3.3) \times 10^{-10}. \tag{4.10}$$

Computing accurately a_μ in the Standard Model is not an easy task and the theoretical prediction suffers from several uncertainties. Up to recently the accepted value was [115]

$$a_\mu^{\mathrm{SM}} = 11\,659\,180.2(4.2)(2.6)(0.2) \times 10^{-10}\,, \tag{4.11}$$

[3] More precise results have been published very recently in [110, 111].

where the first error is from the lowest order hadronic contribution, the second from all other hadronic terms, and the third is due to all non-hadronic terms. The resulting disagreement between experimental measurement and theoretical prediction is

$$\Delta a_\mu \equiv a_\mu^{\mathrm{EXP}} - a_\mu^{\mathrm{SM}} = 28.7(8.0) \times 10^{-10} \,, \tag{4.12}$$

which corresponds to a $3.6\,\sigma$ discrepancy. It is the only known observable showing an incompatibility with the Standard Model prediction of more than $3\,\sigma$. However, due to the difficulty of reaching such high theoretical precision, and the lack of recent dedicated experiment, it is not clear whether this discrepancy should be taken as a hint for Physics beyond the Standard Model or not. Indeed, for instance, recent study reexamined the calculation of the lowest order hadronic contribution (which is the main source of theoretical error) in the framework of operator product expansion [116], and found a smaller discrepancy of $\Delta a_\mu = 20.6(8.0) \times 10^{-10}$, or $2.6\,\sigma$. It is however tempting to interpret this discrepancy as a new contribution to a_μ from supersymmetric particles. In the MSSM, the one-loop contributions which come from loops with neutralino-higgsino-smuon or chargino-higgsino-sneutrino can be positive and fill the gap between a_μ^{EXP} and a_μ^{SM} [117]. In addition, it is well known that this requirement favors $M_2 \times \mu > 0$, which will always be considered here.

4.3. Neutralino-stop coannihilation in the pMSSM

In order to quantify the relative importance of the processes shown in Fig. 4.3, we have performed a random scan in a phenomenological MSSM which has been introduced in Sec. 3.4.2. In the following we describe the settings and discuss in detail the results of our scan. According to the SPA convention [118] we define the soft-breaking parameters at the scale $Q = 1$ TeV. We have made a few simplifying assumptions, which bring the number of MSSM parameters down to eight. In the squark sector, we use a common mass parameter $M_{\tilde{q}_{1,2}}$ for the squarks of the first and second generation, leaving the common mass parameter $M_{\tilde{q}_3}$ for the left- and right-handed squarks of the third generation independent. In contrast, the slepton sector is characterized by a single mass parameter $M_{\tilde{\ell}}$ for all three generations. All trilinear couplings are set to zero except for the A_t in the stop sector, which enters our calculations through the relation $T_t = Y_t A_t$ with the top Yukawa coupling Y_t. All gaugino masses are defined through the bino mass parameter M_1. The wino and gluino masses are then fixed by the relation $2M_1 = M_2 = M_3/3$, which is deduced from gaugino mass unification at the GUT scale. Finally, the Higgs sector is specified by the pole mass of the pseudoscalar Higgs boson m_A, μ as well as $\tan\beta$. In order to explore the parameter space, we have randomly generated about 1.3

million parameter points within the following ranges for the eight input parameters:

$$\begin{aligned}
500\ \text{GeV} \leq M_{\tilde{q}_{1,2}} &\leq 4000\ \text{GeV}, \\
100\ \text{GeV} \leq M_{\tilde{q}_3} &\leq 2500\ \text{GeV}, \\
500\ \text{GeV} \leq M_{\tilde{\ell}} &\leq 4000\ \text{GeV}, \\
|T_t| &\leq 5000\ \text{GeV}, \\
200\ \text{GeV} \leq M_1 &\leq 1000\ \text{GeV}, \\
100\ \text{GeV} \leq m_A &\leq 2000\ \text{GeV}, \\
|\mu| &\leq 3000\ \text{GeV}, \\
2 \leq \tan\beta &\leq 50.
\end{aligned} \tag{4.13}$$

For each set of parameters, the physical mass spectrum and the related mixing matrices have been obtained using `SPheno` (version `3.2.3`). The neutralino relic density $\Omega_\chi h^2$ as well as the contributions from the individual (co)annihilation channels have been computed using `micrOMEGAs` (version `2.4.1`). For a substantial number of these scenarios, coannihilation of the lightest neutralino with a stop plays an important role. This can be seen in the upper plot of Fig. 4.4, where we show the relative contributions of the different final states channels to the total (co)annihilation cross section as a function on the phenomenologically most relevant input parameters. Note that these plots are projections on one parameter, which means that different points correspond to different values of the 8 parameters. The two most important final states, i.e. the Higgs (in red) and the gluon (in green) follow a similar distribution, excepted that the former is dominant for high values of the trilinear couplings, while the latter is dominant for the low values. This is explained by the enhancement of the Higgs final state t-channel diagram (see Fig. 4.3) by large trilinear coupling which enters into the Higgs-stop-stop coupling. The dependence on $\tan\beta$, on the other hand, is generally less pronounced. For coannihilation (mostly into top quarks), lower values of $\tan\beta$ are slightly preferred, since $b\bar{b}$ final states become more important for $\tan\beta \gtrsim 40$ [119]. The highest contributions from a single coannihilation channel are larger than 60%, and they are obtained for rather small masses, large (negative) trilinear couplings, and moderate $\tan\beta$. Due to the low stop mass and the large mixing which leads to a high value of X_t^2/M_{SUSY}, and therefore to a negative contribution to the Higgs mass (see Eq. (3.44)), these peculiar scenario feature a very light Higgs mass (less than 80 GeV). As a consequence the Higgs final state contribution is enhanced and can reach high values. As we will see these scenario are obviously not compatible with the Higgs mass measurement from LHC. The influence of the remaining input parameters, such as those related to first and second generation squarks, sbottoms, and sleptons, as well as the higgsinos, is less important in this context. Therefore the corresponding dependencies are not shown here.

Experimentally viable scenarios have to satisfy a number of additional constraints. In order to see whether coannihilation scenarios can survive these constraints we therefore impose rough selections on several observables. First, in the middle plot of Fig. 4.4 we require the relic density to be in agreement with the Planck measurement in Eq. 4.1 within a 5σ confidence interval. As a consequence, 99% of the original 1.3 million points disappear. In particular the highest contributions of all channels are excluded and the maximum contribution is now 50%. The very low masses and trilinear couplings are also partially affected.

In the lower plot of Fig. 4.4 we impose an interval for the Higgs boson mass of $122.5 < m_{h^0} < 128.5$ GeV. This very conservative mass range is motivated by the rather large theoretical uncertainty on the mass calculation which is estimated to be about 3 GeV within `SPheno`. With this constraint 68% of the points appearing in the first plot are excluded. Again, the highest contributions are removed, and the maximum contribution is here 40%. The low masses, low trilinear couplings and low $\tan\beta$ regions are severely affected, due to the role of these parameters in the stop loop contribution to the Higgs mass in Eq. (3.44). The example of the trilinear coupling parameter is particularly striking, since there is no viable coannihilation scenario for $|T_t| \lesssim 1$ TeV. One obtains two favored regions with $T_t < 0$ and $T_t > 0$. Since the light Higgs final state is important for the large values of $|T_t|$, this channel is dominant in both regions. The region with $T_t < 0$ also has important contributions from the gluon and heavy Higgs final states, while the one with $T_t > 0$ has important contributions from the heavy Higgs and Z^0 final states. It is important to note that the maximal mixing required by $m_{h^0} \sim 125$ GeV favors the light Higgs final state since its t-channel is enhanced by a large trilinear coupling.

In the upper plot of Fig. 4.5 we impose constraints on two flavor observables. First, we impose limits on the branching ratio of $B \to X_s\gamma$ corresponding to a 3σ interval around the observed value given in Eq. 4.6. In addition, we impose an upper limit of 6×10^{-9} on the branching ratio of $B_s \to \mu^+\mu^-$. Since the experimental result given in Eq. 4.8 is compatible with zero at 3σ we do not impose any lower limit. The upper limit is a 3σ estimation of the result given in [112]. The effect of these constraints is to remove 33% of the points present in the original plot. Without any surprise the most affected regions are the low masses and high $\tan\beta$ regions. Globally the distribution does not change significantly, and as pointed out in Sec. 4.2.5 flavor Physics measurements are not in contradiction with neutralino-stop coannihilation.

Finally, we show in the lower plot of Fig. 4.5 the scenario which passes all the constraints mentioned above (relic density, light Higgs mass and flavor observables). Only 0.2% of the original points are now present on this plot. To summarize, the effects of imposing all the constraints are:

- Excluding the scenario with the highest contributions, resulting in the absence of contributions higher than $\sim 25\%$.
- Excluding the low masses regions ($M_1 \lesssim 450$ GeV or $M_{\tilde{q}_3} \lesssim 1$ TeV).
- Excluding the regions with $|T_t| \lesssim 1$ TeV, which result in a dominance of the light Higgs final state.
- Disfavoring the regions with very low or high $\tan\beta$.
- Excluding all scenario with significant contributions from charged Higgs final state, mostly due to the relic density and flavor constraints.

As can be seen, after imposing all constraints, the statistically most important final state is a top quark together with a light Higgs boson, followed by top quark and a gluon, a heavy Higgs boson, or a Z-boson. The coannihilation into a bottom quark and a W-boson is somehow subdominant whereas final states including a charged Higgs boson or a photon are even less important.

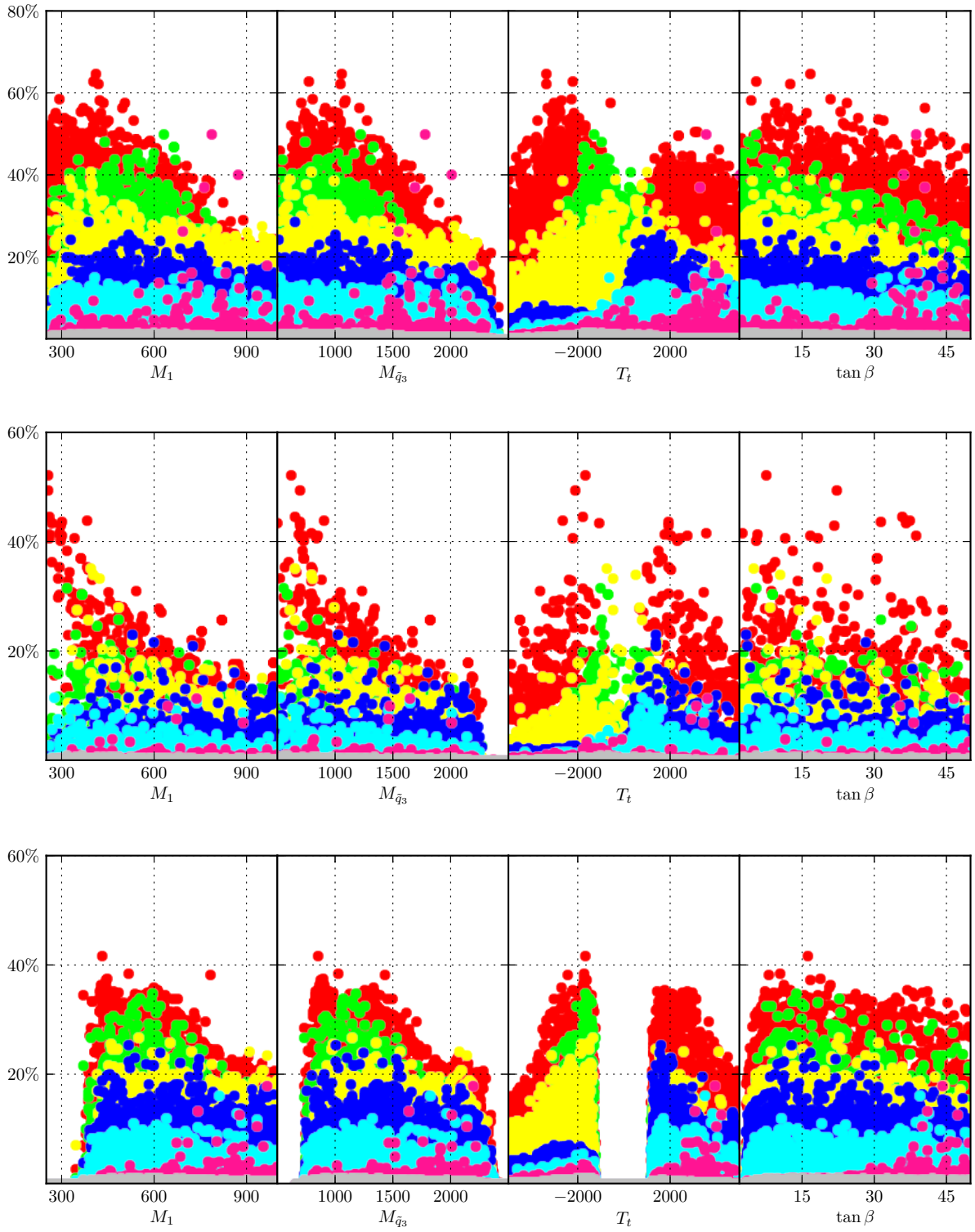

Figure 4.4.: Relative contributions of the neutralino-stop coannihilation channels for the generated parameter points as a function of the input parameters M_1, $M_{\tilde{q}_3}$, T_t, and $\tan\beta$ before (top) and after applying the relic density (middle) and Higgs mass (bottom) constraints. Shown are the contributions from th^0 (red), tg (green), tZ^0 (blue), tH^0 and tA^0 (yellow), bW^+ (cyan), bH^+ (pink), and $t\gamma$ (gray) final states. The parameters M_1, $M_{\tilde{q}_3}$, and T_t are given in GeV. The constraints are detailed in the text.

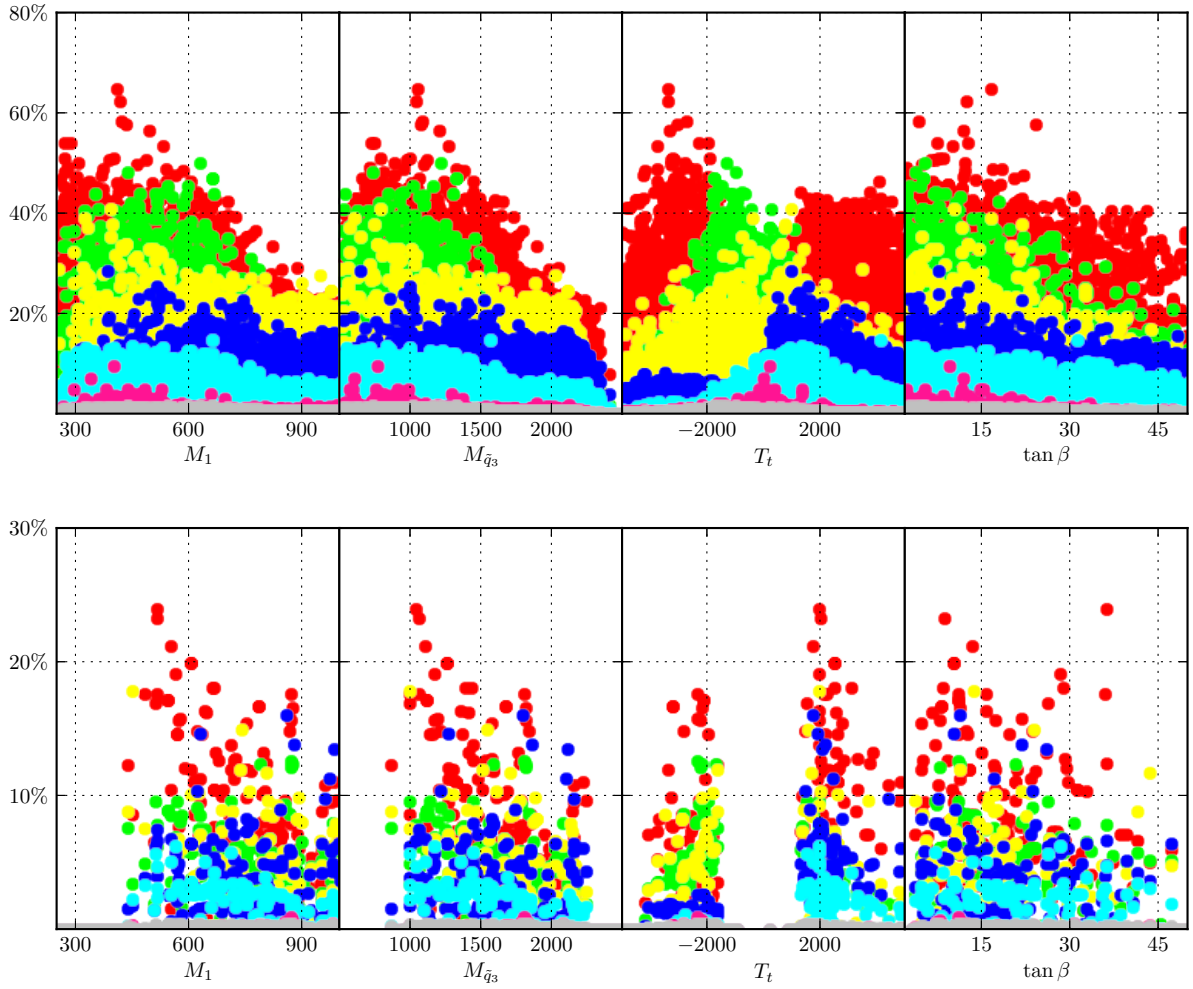

Figure 4.5.: Relative contributions of the neutralino-stop coannihilation channels for the generated parameter points as a function of the input parameters M_1, $M_{\tilde{q}_3}$, T_t, and $\tan\beta$ after applying the flavor constraints (top), and all the mentioned constraints (bottom). Shown are the contributions from th^0 (red), tg (green), tZ^0 (blue), tH^0 and tA^0 (yellow), bW^+ (cyan), bH^+ (pink), and $t\gamma$ (gray) final states. The parameters M_1, $M_{\tilde{q}_3}$, and T_t are given in GeV. The constraints are detailed in the text.

Chapter 5.

Impact of non minimal flavor violation on the relic density

5.1. Introduction

In the MSSM with the most general flavor structure, not only the different helicity of the squarks can mix, but also their different generations, and the full mixing of the up and down squarks is then parametrized by two 6×6 matrices in the generation-helicity space. Within the minimal flavor violation (MFV) framework [120–122], already mentioned at the end of Sec. 3.4.1, it is assumed that the mechanisms of flavor violation in the MSSM are the same as in the Standard Model, i.e. the rotation of the Yukawa couplings from gauge to mass eigenstates remains the only source of flavor violation, and thus all flavor-violating interactions are parameterized through the CKM matrix (and the PMNS matrix in the slepton sector). However the RGE evolution from the high to the weak scale introduces a mismatch of the quark and squark field rotations since their renormalization group equations are different. Therefore in MFV there will be off-diagonal elements[1] in the squark mixing matrices which can be deduced from the CKM matrix. In Sec. 3.5.4 we have described the squark sector of the MSSM in a framework called constrained minimal flavor violation (cMFV). Not only the soft-breaking mass and trilinear matrices were considered diagonal, but the CKM matrix effects were also neglected and there were therefore no off-diagonal elements in the full (i.e. 6×6) mixing matrices, even at the weak scale. The mixing of the squarks was then fully expressed by the 2×2 helicity mixing matrices for each generation of up and down squarks. It is crucial to keep in mind that the flavor structure of the MSSM is not known and it is possible to go beyond MFV. In the framework of non-minimal flavor violation (NMFV) new sources of flavor mixing are allowed, depending on the exact mechanism of Supersymmetry breaking. In particular these terms car arise when embedding Supersymmetry in GUTs. In NMFV, the terms originating from the additional sources are not related to the CKM and PMNS matrices, such that they are considered as additional parameters at the SUSY scale.

[1] Here off-diagonal is understood in each of the four 3×3 helicity blocks.

In recent years, supersymmetric scenarios beyond MFV have received considerable attention in the community, especially in the context of signatures at current or future colliders. Concerning (s)quark flavor violation, the production and subsequent decays of squarks and gluino at the LHC have been studied, e.g., in [123–128]. Apart from the production of superpartners at colliders, the flavor-violating terms also appear in the (co)annihilation cross section of the neutralino, which is needed in the calculation of its relic density. In this chapter we therefore investigate the possible impacts of these terms on the relic density of neutralino. Indeed, possible flavor-mixing effects in the context of dark matter relic density are generally not considered in the literature. An exception is the reference [129] where the impact of non-minimal flavor violation in the sector of sleptons on the coannihilation of a neutralino with a slepton has been discussed. We study the cases of neutralino pair annihilation and neutralino-squark coannihilation in the MSSM beyond MFV. We will first introduce in Sec. 5.2 the MSSM with NMFV in the sector of squarks and discuss its parameterization, as well as the experimental constraints on the flavor violating terms. The role of generation mixing in the context of neutralino (co)annihilation will be discussed in detail in Sec. 5.3. Sec. 5.4 and 5.5 are then devoted to numerical examples in the context of neutralino (co)annihilation and its relic density, before concluding in Sec. 5.6

This chapter is based on results presented in [130]. We warn the reader that these numerical results have been obtained in supersymmetric scenarios which have been recently excluded by experimental results. A few numerical results will be nevertheless shown for the sake of illustration. The qualitative discussion reproduced here is however still valid.

5.2. Non minimal flavor violation in the squark sector of the MSSM

Taking into account generation mixing, the 2×2 squarks helicity mixing matrices given in Eq. (3.47) can be generalized to 6×6 mixing matrices:

$$\mathcal{M}^2_{\tilde{q}} = \begin{pmatrix} \mathcal{M}^2_{\tilde{q},\mathrm{LL}} & \mathcal{M}^2_{\tilde{q},\mathrm{LR}} \\ \mathcal{M}^2_{\tilde{q},\mathrm{RL}} & \mathcal{M}^2_{\tilde{q},\mathrm{RR}} \end{pmatrix} \tag{5.1}$$

for $q = u, d$. The diagonal and off-diagonal blocks are given by

$$\begin{aligned}
\mathcal{M}^2_{\tilde{d},\mathrm{RR}} &= M^2_{\tilde{D}} + m^2_d + e_d m^2_Z \sin^2\theta_W \cos 2\beta, \\
\mathcal{M}^2_{\tilde{d},\mathrm{LL}} &= M^2_{\tilde{Q}} + m^2_d + m^2_Z \cos 2\beta (I_d - e_d \sin^2\theta_W), \\
\mathcal{M}^2_{\tilde{u},\mathrm{RR}} &= M^2_{\tilde{U}} + m^2_u + e_u m^2_Z \sin^2\theta_W \cos 2\beta, \\
\mathcal{M}^2_{\tilde{u},\mathrm{LL}} &= V_{\mathrm{CKM}} M^2_{\tilde{Q}} V^\dagger_{\mathrm{CKM}} + m^2_u + m^2_Z \cos 2\beta (I_u - e_u \sin^2\theta_W), \\
\mathcal{M}^2_{\tilde{u},\mathrm{RL}} = \left(\mathcal{M}^2_{\tilde{u},\mathrm{LR}}\right)^\dagger &= \frac{v_u}{\sqrt{2}} T_U - \mu^* m_u \cot\beta, \\
\mathcal{M}^2_{\tilde{d},\mathrm{RL}} = \left(\mathcal{M}^2_{\tilde{d},\mathrm{LR}}\right)^\dagger &= \frac{v_d}{\sqrt{2}} T_D - \mu^* m_d \tan\beta.
\end{aligned} \tag{5.2}$$

Here $M_{\tilde{Q}}$, $M_{\tilde{U}}$, and $M_{\tilde{D}}$ are the 3×3 (non-diagonal) soft-breaking mass matrices of the squarks. T_U, T_D are the 3×3 (non-diagonal) trilinear matrices related to the soft-breaking matrices $A_{u,d}$ and the respective Yukawa matrices $Y_{u,d}$ through $(T_{U,D})_{ij} = (A_{u,d})_{ij}\,(Y_{u,d})_{ij}$. The 3×3 diagonal mass matrices of up- and down-type quarks are denoted m_u and m_d. Due to the SU(2) symmetry, the left-left entries are related through the CKM-matrix V_{CKM}. The above expressions also involve several quantities which have already been defined after Eq. (3.47). All parameters appearing in Eqs. (5.2) are understood to be in the so-called super-CKM basis [131, 132], in which the mass matrices of the quark fields are diagonalized by rotating the superfields. The quark (but not the squark) fields are then in the mass eigenstate basis. The off diagonal elements of $M_{\tilde{Q}}$, $M_{\tilde{U}}$, $M_{\tilde{D}}$, T_U and T_D lead to flavor-changing neutral currents related to the gaugino-quark-squark and higgsino-quark-squark couplings.

In order to have a scenario-independent and dimensionless parameterization of flavor-mixing, the off-diagonal entries are usually normalized to the diagonal ones according to

$$\delta^{\mathrm{LL}}_{ij} = \left(M^2_{\tilde{Q}}\right)_{ij} / \sqrt{\left(M^2_{\tilde{Q}}\right)_{ii}\left(M^2_{\tilde{Q}}\right)_{jj}}, \tag{5.3}$$

$$\delta^{u,\mathrm{RR}}_{ij} = \left(M^2_{\tilde{U}}\right)_{ij} / \sqrt{\left(M^2_{\tilde{U}}\right)_{ii}\left(M^2_{\tilde{U}}\right)_{jj}}, \tag{5.4}$$

$$\delta^{d,\mathrm{RR}}_{ij} = \left(M^2_{\tilde{D}}\right)_{ij} / \sqrt{\left(M^2_{\tilde{D}}\right)_{ii}\left(M^2_{\tilde{D}}\right)_{jj}}, \tag{5.5}$$

$$\delta^{u,\mathrm{RL}}_{ij} = \frac{v_u}{\sqrt{2}}\left(T_U\right)_{ij} / \sqrt{\left(M^2_{\tilde{Q}}\right)_{ii}\left(M^2_{\tilde{U}}\right)_{jj}}, \tag{5.6}$$

$$\delta^{d,\mathrm{RL}}_{ij} = \frac{v_d}{\sqrt{2}}\left(T_D\right)_{ij} / \sqrt{\left(M^2_{\tilde{Q}}\right)_{ii}\left(M^2_{\tilde{D}}\right)_{jj}}, \tag{5.7}$$

$$\delta^{u,\mathrm{LR}}_{ij} = \frac{v_u}{\sqrt{2}}\left(T^\dagger_U\right)_{ij} / \sqrt{\left(M^2_{\tilde{U}}\right)_{ii}\left(M^2_{\tilde{Q}}\right)_{jj}}, \tag{5.8}$$

$$\delta^{d,\mathrm{LR}}_{ij} = \frac{v_d}{\sqrt{2}}\left(T^\dagger_D\right)_{ij} / \sqrt{\left(M^2_{\tilde{D}}\right)_{ii}\left(M^2_{\tilde{Q}}\right)_{jj}}. \tag{5.9}$$

The normalization factor is defined in terms of the corresponding diagonal elements of the soft-breaking matrices. We emphasize that the following analysis is based on the diagonalization of

the full 6×6 mass matrices. This is realized by introducing two rotation matrices, such that

$$\mathcal{R}_{\tilde{q}} \mathcal{M}^2_{\tilde{q}} \mathcal{R}^\dagger_{\tilde{q}} \;=\; \mathrm{diag}\left(m^2_{\tilde{q}_1}, \ldots, m^2_{\tilde{q}_6}\right) \tag{5.10}$$

with the mass order $m_{\tilde{q}_1} \leq \cdots \leq m_{\tilde{q}_6}$ for $q = u, d$, respectively. The rotation matrices appear in the couplings of squarks with other particles, and, in consequence, the flavor-violating elements will influence observables like decay widths or production and annihilation cross sections. Analytical expressions for couplings including squark generation mixing can, e.g., be found in [123, 124, 127]. We shall discuss the relevant couplings for our analysis in more detail in Sec. 5.3.

The flavor-violating elements in the mass matrices are constrained by precision measurements in the sector of D-, B-, and K-mesons. Flavor mixing involving the first generation of squarks is severely limited [131–133]. Mixing with third generation squarks is however less constrained, in particular in the up sector [134]. In addition it has been shown in [135] that a large mixing between right-handed charm and top quarks leads to a reduction of the fine-tuning, among other advantages. We therefore first focus on flavor mixing between the second and third generation up squarks where sizable effects can still be present, and then consider the case of the down squark sector.

5.3. Impact on the relic density

In wide regions of the MSSM parameter space, the pair annihilation of two neutralinos into Standard Model particles is the dominant process. The diagrams for annihilation into quarks, i.e. where flavor violation in the (s)quark sector can become relevant, are shown in Fig. 5.1. At the tree-level, squarks can then appear only in internal propagators in case of annihilation into quark-antiquark pairs, i.e. $\tilde{\chi}^0_1 \tilde{\chi}^0_1 \to q\bar{q}$ through the exchange of a squark in the t- or u-channel [136, 137]. Going beyond minimal flavor violation, the mass splitting of the involved squarks is increased due to the additional off-diagonal elements in the mass matrix. In particular, the lightest squark mass eigenstate (purely stop-like in the cMSSM with MFV) becomes lighter with increasing flavor mixing. Its contributions to neutralino pair annihilation through t- or u-channel exchange are therefore enhanced. Apart from the impact on the squark mass eigenvalues, the flavor-violating terms discussed in Sec. 5.2 directly affect the neutralino-squark-quark coupling, which is present in the t- or u-channel diagram. The analytical expressions for

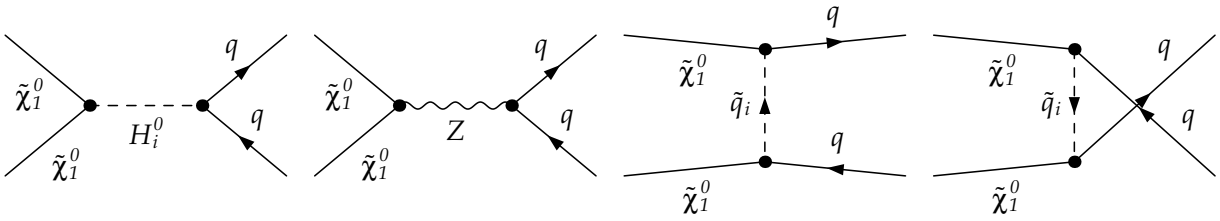

Figure 5.1.: Feynman diagrams for the annihilation of neutralinos into quark pairs through the exchange of a neutral Higgs boson $H_i^0 = h^0, H^0, A^0$ (left), a Z^0-boson (center left), or a squark (right and center right).

the left- and right-handed parts of this coupling are given by [123]

$$\begin{aligned}
L_{\tilde{\chi}_i^0 \tilde{u}_j u_k} &= \Big[(e_u - T_u) \sin\theta_W \mathcal{N}_{i1} + T_u \cos\theta_W \mathcal{N}_{i2} \Big] \mathcal{R}^{\tilde{u}*}_{jk} + \frac{m_{u_k} \cos\theta_W}{2 m_W \cos\beta} \mathcal{N}_{i4} \mathcal{R}^{\tilde{u}*}_{j(k+3)}, \\
L_{\tilde{\chi}_i^0 \tilde{d}_j d_k} &= \Big[(e_d - T_d) \sin\theta_W \mathcal{N}_{i1} + T_d \cos\theta_W \mathcal{N}_{i2} \Big] \mathcal{R}^{\tilde{d}*}_{jk} + \frac{m_{d_k} \cos\theta_W}{2 m_W \sin\beta} \mathcal{N}_{i3} \mathcal{R}^{\tilde{d}*}_{j(k+3)}, \\
-R^*_{\tilde{\chi}_i^0 \tilde{u}_j u_k} &= e_u \sin\theta_W \mathcal{N}_{i1} \mathcal{R}^{\tilde{u}}_{jk} + \frac{m_{u_k} \cos\theta_W}{2 m_W \cos\beta} \mathcal{N}_{i4} \mathcal{R}^{\tilde{u}}_{j(k+3)}, \\
-R^*_{\tilde{\chi}_i^0 \tilde{d}_j d_k} &= e_d \sin\theta_W \mathcal{N}_{i1} \mathcal{R}^{\tilde{d}}_{jk} + \frac{m_{d_k} \cos\theta_W}{2 m_W \sin\beta} \mathcal{N}_{i3} \mathcal{R}^{\tilde{d}}_{j(k+3)}.
\end{aligned} \tag{5.11}$$

Flavor mixing effects arise through the squark rotation matrices $\mathcal{R}^{\tilde{q}}$ ($q = u, d$). This can allow for new annihilation channels, that are closed in the case of minimal flavor violation. Such channels can, e.g., be $\tilde{\chi}\tilde{\chi} \to c\bar{c}$ through exchange of a squark $\tilde{u}_1$ which is now a mixture of $\tilde{c}$ and $\tilde{t}$. In the case of MFV, this final state is only possible through exchange of a heavier $\tilde{c}$ and therefore suppressed. Another example is annihilation into a mixed final state, $\tilde{\chi}\tilde{\chi} \to c\bar{t}$, which is forbidden in MFV. The discussed enhancements and new channels increase the total annihilation cross section, which in turn decreases the predicted relic density of the neutralino. The diagrams with s-channel exchange of a Higgs or gauge boson remain insensitive to squark flavor mixing.

Let us now turn to the case of neutralino-squark coannihilation. The possible final states are a quark together with a Higgs or a gauge boson. The relevant Feynman diagrams at the tree-level were depicted in Fig. 4.3. The main impact from non-minimal flavor violation will be through the modified squark mass spectrum. As already stated in the previous chapters (in particular in Sec. 1.2.3 and 4.2.1), the mass difference between neutralino and the lightest squark enters the calculation of the corresponding thermally averaged coannihilation cross section exponentially. When the squark mass approaches the neutralino mass due to increasing flavor mixing, this can significantly enhance the contribution from the corresponding coanni-

hilation with respect to the case of minimal flavor violation. Again, also the flavor-violating couplings can have subdominant effects on the coannihilation processes. Each of the diagrams depicted in Fig. 4.3 contains the squark-quark-neutralino coupling already discussed above. Moreover, the couplings of squarks to Higgs- and massive gauge bosons are sensitive to flavor-violating effects. In the mass eigenstate basis, the couplings of squarks to a Z^0-boson are given by [127]

$$C_{Z^0\tilde{q}_j\tilde{q}_k} = -i\frac{g_2}{\cos\theta_W}(p_j+p_k)_\mu\left[\sum_{i=1}^{3} I_q \mathcal{R}^{\tilde{q}*}_{ij}\mathcal{R}^{\tilde{q}}_{ik} - e_q \sin^2\theta_W \delta_{jk}\right] \tag{5.12}$$

for $q = u, d$. Here, p_j and p_k denote the momentum of $\tilde{q}_j$ and $\tilde{q}_k$, respectively. The interactions of squarks with a photon or a gluon are flavor-diagonal and are therefore not discussed in detail here. The couplings of two up-type squarks with the light scalar Higgs boson are given by [127]

$$\begin{aligned} C_{h^0\tilde{u}_j\tilde{u}_k} = & -\frac{g_2}{2m_W}\sum_{i=1}^{3}\Big[m_W^2\sin(\alpha+\beta)\Big[(1-\frac{1}{3}\tan^2\theta_W)\mathcal{R}^{\tilde{u}}_{ji}\mathcal{R}^{\tilde{u}*}_{ki} + \frac{4}{3}\tan^2\theta_W\mathcal{R}^{\tilde{u}}_{j(i+3)}\mathcal{R}^{\tilde{u}*}_{k(i+3)}\Big] \\ & +2\frac{\cos\alpha}{\sin\beta}\Big[\mathcal{R}^{\tilde{u}}_{ji}\, m^2_{u_i}\mathcal{R}^{\tilde{u}*}_{ki} + \mathcal{R}^{\tilde{u}}_{j(i+3)}m^2_{u_i}\mathcal{R}^{\tilde{u}*}_{k(i+3)}\Big] + \frac{\sin\alpha}{\sin\beta}\Big[\mu^*\mathcal{R}^{\tilde{u}}_{j(i+3)}m_{u_i}\mathcal{R}^{\tilde{u}*}_{ki} + \mu\mathcal{R}^{\tilde{u}}_{ji}m_{u_i}\mathcal{R}^{\tilde{u}*}_{k(i+3)}\Big] \\ & +\frac{\cos\alpha}{\sin\beta}\frac{v_u}{\sqrt{2}}\sum_{l=1}^{3}\Big[\mathcal{R}^{\tilde{u}}_{j(i+3)}\,(T_U)_{il}\,\mathcal{R}^{\tilde{u}*}_{kl} + \mathcal{R}^{\tilde{u}}_{ji}\,(T_U^\dagger)_{il}\,\mathcal{R}^{\tilde{u}*}_{k(l+3)}\Big]\Big]. \end{aligned} \tag{5.13}$$

From this expression, the coupling to the heavy scalar Higgs is obtained through the replacements $h^0 \to H^0$ and $\alpha \to \alpha + \pi/2$. Moreover, couplings of down-type squarks to the neutral scalar Higgses are obtained by replacing $\tilde{u}_i \to \tilde{d}_i$ and $\sin\beta \to \cos\beta$. Finally, the couplings of up-type squarks to a pseudoscalar Higgs-boson are given by [127]

$$C_{A^0\tilde{u}_j\tilde{u}_k} = -i\frac{g_2}{2m_W}\sum_{i=1}^{3}\Big[\mu^*\mathcal{R}^{\tilde{u}}_{j(i+3)}m_{u_i}\mathcal{R}^{\tilde{u}*}_{ki} + \cot\beta\frac{v_u}{\sqrt{2}}\sum_{l=1}^{3}\mathcal{R}^{\tilde{u}}_{j(i+3)}(T_U)_{il}\mathcal{R}^{\tilde{u}*}_{kl} + \text{h.c}\Big]. \tag{5.14}$$

Again, the expressions for down-type squarks can easily be obtained through $\tilde{u}_i \to \tilde{d}_i$ and $\cot\beta \to \tan\beta$.

The effects of the modified mass eigenvalues and the modified couplings are superimposed. Since the two effects are linked together through their same origin (see Eq. (5.10)), their separate impacts on the (co)annihilation cross section (and the neutralino relic density) cannot be disentangled. However, some general features can be expected. The effect of the modified squark mass eigenvalues on coannihilation is expected to be stronger than in the case of neutralino pair annihilation due to the exponential factor already mentioned above. Moreover, the squark is here an external particle, and the impact of its mass on the phase space is more important than the mass in the t- or u-channel propagator. The impact of the modified flavor contents of the involved squarks, i.e. the effect of the rotation matrix in the coupling,

is expected to be smaller than the mass effect. This is again due to the exponential factor in the thermally averaged cross section. Note also that, the mixing being unitary, the newly opened channels can be (partially) compensated by the simultaneous diminution of other contributions. The compensating contribution can, however, turn out to be forbidden in specific kinematic configurations and the impact of the new contributions can be significant. This is in particular the case when the neutralino is too light to annihilate into top-quark pairs, i.e. for $m_{\tilde{\chi}_1^0} < m_t$. The flavor violating elements lead then to a $\tilde{c}$ admixture in the lightest squark, which then allows for neutralino pair annihilation into top and charm quarks.

Note that there can also be coannihilation of a neutralino with an up-(down-)type squark into a charged Higgs boson $H^\pm$ or a W-boson together with a down-(up-)type quark. In this case, the u-channel diagram includes a chargino propagator and in consequence the corresponding chargino-squark-quark coupling, while the s- and t-channel diagrams involve couplings of up- and down-type squarks to the charged Higgs or W-boson. Analytical expressions for these couplings can be found in [123, 127]. Since they are rather similar (with obvious replacements, e.g., concerning gaugino mixing) to the interactions given in Eq. (5.11) to (5.13), they are not displayed in detail here. Note, however, that these couplings explicitly depend on the CKM-matrix. The general argumentation given above remains unchanged.

5.4. Numerical analysis

The following numerical analyses are based on the constrained MSSM with the five parameters m_0, $m_{1/2}$, A_0, $\tan\beta$, and $\mathrm{sign}(\mu)$ (see Sec.3.4.2 for more details). Starting from the high-scale parameters, the soft-breaking terms at the scale $Q = 1$ TeV [118] are obtained through renormalization group running using `SPheno`. At the same scale, we introduce the non-diagonal entries in the squark mass matrices as discussed in Sec.5.2. The physical mass spectrum is then calculated again using `SPheno`, which takes into account the general flavor structure. The same code is also used for the evaluation of constraining observables like $\mathrm{BR}(B \to X_s\gamma)$, again taking into account squark generation mixing. The pole mass of the top-quark is taken to be $m_{\mathrm{top}} = 173.1$ GeV according to measurements from D0 and CDF [138]. The CKM-matrix is taken in the usual Wolfenstein parametrization with the values $\lambda = 0.2253$, $A = 0.808$, $\bar{\rho} = 0.132$, and $\bar{\eta} = 0.341$ [139].

Making use of the SLHA, the mass spectrum and related mixing parameters are transferred to the public program `micrOMEGAs 2.4` in order to evaluate the relic density of the neutralino. The calculation of the annihilation cross section is done by the program `CalcHEP`, where we have implemented the MSSM with squark generation mixing as discussed in Sec. 5.2. The corresponding model files have been obtained using the package `SARAH` [140, 141].

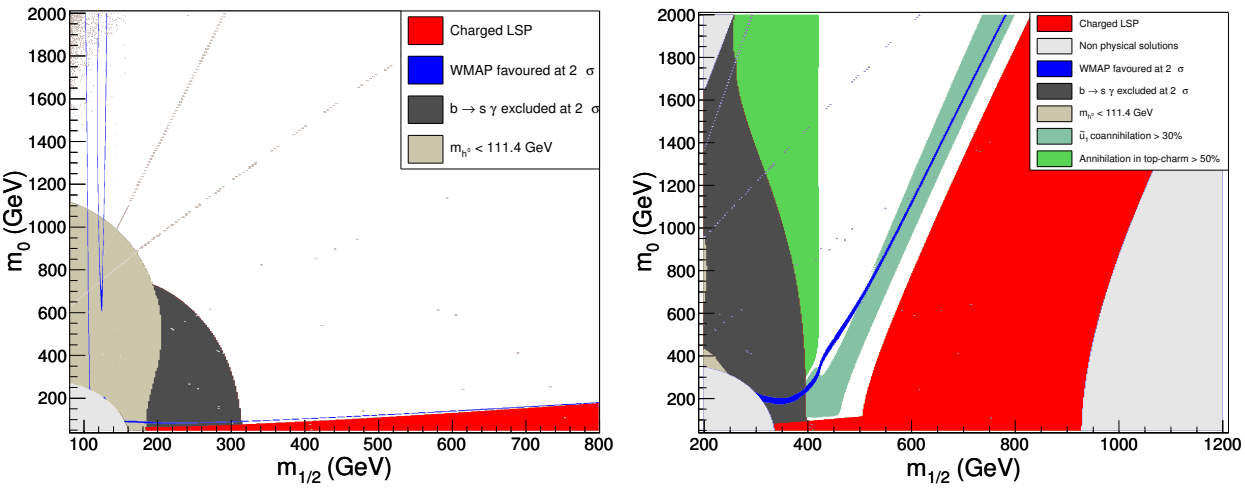

Figure 5.2.: Cosmologically favored region and related exclusion limits in the $(m_0,\, m_{1/2})$ plane of the cMSSM for $\delta_{23}^{u,\mathrm{RR}} = 0$ (left) and $\delta_{23}^{u,\mathrm{RR}} = 0.98$ (right).

In order to illustrate the numerical influence of flavor violating elements, we analyze the neutralino relic density within cMSSM, where we allow for flavor violation between the second and third generation of up-type squarks in the right-right chiral sector. In Fig. 5.2, we show typical scans of the m_0-$m_{1/2}$ plane for fixed values of $A_0 = -500$ GeV and $\tan\beta = 10$ and for positive values of μ. The cosmologically favored region of parameter space according to Eq. (1.5) together with some of the relevant constraints discussed in Sec. 4.2 are shown for the case of MFV ($\delta_{23}^{u,\mathrm{RR}} = 0$) and for the case of NMFV with important off-diagonal elements ($\delta_{23}^{u,\mathrm{RR}} = 0.98$).

In the case of MFV, the most stringent constraints on this parameter plane are due to a charged dark matter candidate (low m_0), tachyonic solutions of the renormalization group equations (high m_0 and low $m_{1/2}$) as well as the constraints from $\mathrm{BR}(B \to X_s\gamma)$ and the lightest Higgs mass (low mass region). Note that the constraint applied on the Higgs boson mass corresponds to the pre-LHC lower limit, with a 3 GeV theoretical uncertainty. As discussed in Sec. 4.1.1 the cosmologically favored region of parameter space is divided into several distinct regions: only the resonance of the light Higgs boson (low $m_{1/2}$ and moderate m_0), and the stau coannihilation region (close to the exclusion due to a charged dark matter candidate), where the neutralino mass is close to the stau mass, are visible here.

In the corresponding figure for the NMFV-case, we depict the same constraints together with the relative contribution from new (co)annihilation channels as discussed in Sec. 5.3. In this case, this involves neutralino pair annihilation into a mixed charm-top final state and coannihilation of a neutralino with the lightest squark $\tilde{u}_1$. In the latter corresponding region ($m_{1/2} \gtrsim 450$ GeV), where the relic density constraint is fulfilled, the mass difference between

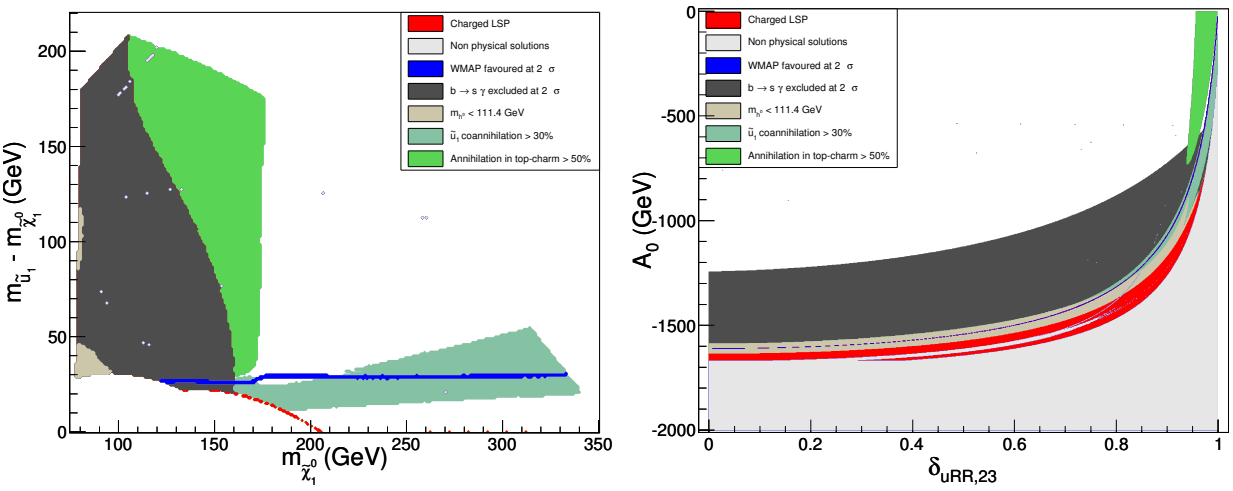

Figure 5.3.: Cosmologically favored region and related exclusion limits for $\delta_{23}^{u,\mathrm{RR}} = 0.98$ in the ($m_{\tilde{\chi}_1^0}$, $m_{\tilde{u}_1} - m_{\tilde{\chi}_1^0}$) plane for fixed $A_0 = -500$ GeV and $\tan\beta = 10$ (left) and in the ($\delta_{23}^{u,\mathrm{RR}}$, A_0) plane for fixed $m_0 = 200$ GeV and $m_{1/2} = 400$ GeV (right).

the lightest squark and the neutralino is about 30 GeV, as can be seen from the left panel of Fig. 5.3, where we show the cosmologically favored regions of parameter space in the plane of the physical masses. The dominant annihilation processes are then $\tilde{\chi}_1^0\tilde{u}_1 \to gt$ (30%) and $\tilde{u}_1\tilde{u}_1 \to gg$ (25%). Two other important processes are neutralino annihilation into pairs of top quarks (10%), and $\tilde{\chi}_1^0\tilde{u}_1 \to gc$ (15%). Note that the presence of a charm quark in the final state is a genuine effect of flavor violation. Indeed, as a consequence of the off-diagonal elements in squark mass matrices, the lightest up-type squark is here a mixing of $\tilde{t}_R$ and $\tilde{c}_R$ (with a small admixture of $\tilde{t}_L$), opening up the (co)annihilation into charm-quarks.

For lower masses (e.g. $m_0 \sim 200$ GeV and $m_{1/2} \sim 400$ GeV), coannihilation processes such as $\tilde{\chi}_1^0\tilde{u}_1 \to gt/c$ are still important (20%). However, the squark being much lighter ($m_{\tilde{u}_1} \sim 190$ GeV), the squark pair annihilation $\tilde{u}_1\tilde{u}_1 \to gg$ is now subdominant. Moreover, the neutralino mass of $m_{\tilde{\chi}_1^0} \sim 160$ GeV (see Fig. 5.3 left) forbids annihilation into top quark pairs. As a consequence, the flavor violating process $\tilde{\chi}_1^0\tilde{\chi}_1^0 \to t\bar{c}(c\bar{t})$, which is kinematically allowed and enhanced by the rather light squark in the t-channel propagator, becomes important (40%). This is represented by the green area in the left part of the plot. Notice the cut at $m_{1/2} \approx 420$ GeV, which corresponds to $m_{\tilde{\chi}_1^0} \approx m_t$. For $m_{\tilde{\chi}_1^0} > m_t$, neutralino annihilation into top quark pairs is kinematically allowed, and the $t\bar{c}(c\bar{t})$ final state is suppressed. This can also be seen in relation to the physical neutralino and squark masses in Fig. 5.3 left. For low $m_{1/2}$ but large m_0, the squark being heavier, coannihilation is not relevant and neutralino annihilation into $t\bar{c}(c\bar{t})$ is less important. Therefore, even if the relative contribution of this channel is still important, its absolute contribution is not large enough to satisfy the relic density constraint.

In the region excluded by BR($B \to X_s\gamma$) most of the deviation from the Standard Model value comes from large negative chargino contributions due to the smallness of the stop and/or chargino mass. There is, however, no significant effect coming from the flavor violating parameter $\delta_{23}^{u,\mathrm{RR}}$, since BR($B \to X_s\gamma$) constrains mainly flavor violation in the left-left sector.

Let us now discuss the interplay of helicity mixing and additional flavor mixing. The former is induced through the trilinear matrices T_U (see Eq. (5.2)) and thus the GUT-scale parameter A_0, while the latter is included at the electroweak scale through the parameter $\delta_{23}^{u,\mathrm{RR}}$. In the case of MFV, i.e. for $\delta_{23}^{u,\mathrm{RR}} = 0$, a rather large $|A_0|$ is needed in order to decrease the stop mass close to the neutralino mass, and therefore allow for efficient coannihilation. For sizable additional flavor mixing, the coannihilation is important already for lower values of A_0, since the squark mass splitting is then increased by the off-diagonal elements in the mass matrix.

This is illustrated in the right graph of Fig. 5.3, where the constraints, cosmologically favored regions, and different contributions to the annihilation cross section are shown in the (A_0,$\delta_{23}^{u,\mathrm{RR}}$) plane. The mass splitting of the squarks depends strongly on both of these parameters, which therefore have a competitive effect on the light stop mass. As a consequence, as explained above, one of these parameters has to be large in order to allow for an important coannihilation contribution. On the other hand, the flavor violating effects are only related to $\delta_{23}^{u,\mathrm{RR}}$. Therefore the flavor violating neutralino annihilation processes depend mainly on this parameter. The only possibility to satisfy simultaneously the relic density and BR($B \to X_s\gamma$) constraints is for very large $\delta_{23}^{u,\mathrm{RR}}$ and a rather low A_0. This is explained by the strong dependence of BR($B \to X_s\gamma$) on the squark mass spectrum, and therefore on A_0. Contrary, and as explained above, BR($B \to X_s\gamma$) does not depend on any flavor mixing among right up-type squarks, and the mass effects become important only for very large values of $\delta_{23}^{u,\mathrm{RR}}$.

Next, we study the possibility that not only the parameter $\delta_{23}^{u,RR}$ is large, i.e. of $\mathcal{O}(1)$, while all others are small, which might not be very natural. We therefore show in Fig. 5.4 the cosmologically favored region and related exclusion limits in the ($\delta_{23}^{u,RR}$, $\delta_{23}^{u,LR}$) plane for fixed $m_0 = 200$ GeV, $m_{1/2} = 400$ GeV, and $A_0 = -500$ GeV. We observe that the second flavor-violating parameter $\delta_{23}^{u,LR}$ can reach values up to 0.15 before being constrained by the lower Higgs mass bound of 111.4 GeV. Similarly, the RL and LL parameters (not shown) are restricted by the FCNC process $b \to s\gamma$ to values below 0.15 and 0.1, respectively, as would be the LR parameter if one applied this limit at the two (not three) sigma level.

In Fig. 5.5 we show for a given parameter point the neutralino relic density and the contributing processes as a function of the flavor-violation parameter $\delta_{23}^{u,\mathrm{RR}}$. While for the case of MFV, this scenario is cosmologically strongly disfavored with $\Omega_{\tilde{\chi}_1^0}h^2 \gtrsim 20$, the relic density decreases with increasing flavor mixing to reach the favored value of $\Omega_{\tilde{\chi}_1^0}h^2 \approx 0.11$ for $\delta_{23}^{u,\mathrm{RR}} \sim 0.98$. For low values of $\delta_{23}^{u,\mathrm{RR}}$, the annihilation is dominated by lepton final states (about 75%), which do, however, not lead to a sufficiently enhanced annihilation cross section.

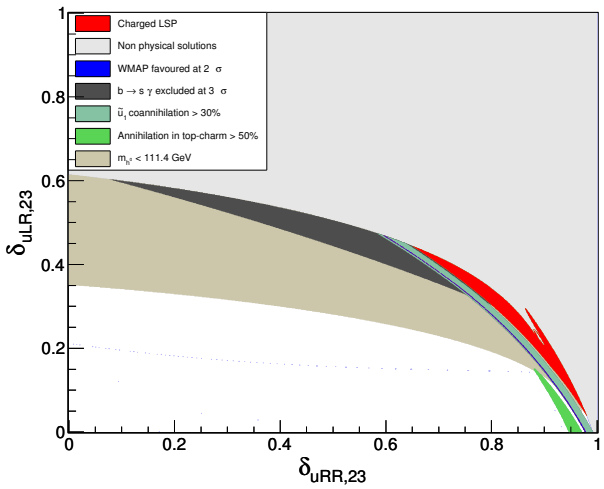

Figure 5.4.: Cosmologically favored region and related exclusion limits in the $(\delta_{23}^{u,RR}, \delta_{23}^{u,LR})$ plane for fixed $m_0 = 200$ GeV, $m_{1/2} = 400$ GeV, and $A_0 = -500$ GeV.

The subleading channel is annihilation into top-quark pairs (about 25%). For $\delta_{23}^{u,\mathrm{RR}} \gtrsim 0.2$, flavor violation effects start to manifest by opening the channel $\tilde{\chi}_1^0\tilde{\chi}_1^0 \to c\bar{t}(t\bar{c})$. The relative contribution of this process amounts to almost 40% at $\delta_{23}^{u,\mathrm{RR}} \sim 0.8$. For $\delta_{23}^{u,\mathrm{RR}} > 0.5$, the annihilation into top-quarks is significantly enhanced due to the lighter squark in the t-channel propagator, so that this channel remains more important than the newly opened annihilation into top- and charm-quarks. All contributions from neutralino pair annihilation drop at $\delta_{23}^{u,\mathrm{RR}} \sim 0.95$ when the squark $\tilde{u}_1$ becomes light enough for efficient coannihilation. The corresponding total relative contribution amounts to about 60%. When the squark becomes even lighter, also squark pair annihilation into gluon pairs plays an important role (see Sec. 4.2.1), leading to relative contributions of about 90% at most.

For this discussed scenario, the favored relic density of the neutralino is achieved through important coannihilation for rather large values of the flavor mixing parameter $\delta_{23}^{u,\mathrm{RR}}$. Note that, depending on the exact parameter point under consideration and the corresponding relic density in the MFV case, this can also happen for lower values of $\delta_{23}^{u,\mathrm{RR}}$. In the same way, the enhancement of the total cross section through the new contributions from $c\bar{t}(t\bar{c})$ final states can be sufficient to achieve $\Omega_{\tilde{\chi}_1^0}h^2 \sim 0.11$.

For completeness, we show in Fig. 5.6 the masses of the two lightest up-type squarks, the gluino, and the lightest neutralino as a function of the NMFV-parameter $\delta_{23}^{u,\mathrm{RR}}$ as well as the flavor decomposition for the same scenario as discussed above. The squark mass splitting is increased due to the additional off-diagonal entries in the mass matrix, so that the mass of $\tilde{u}_1$ decreases. For large flavor mixing, it comes close to the neutralino mass, leading to the

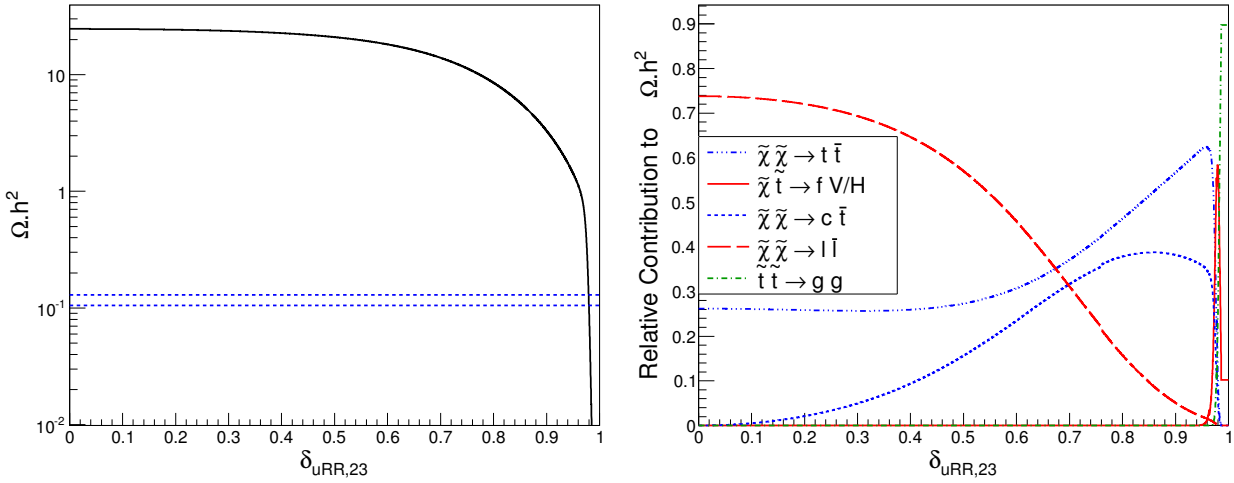

Figure 5.5.: Relic density of the neutralino (left) and contributing processes (right) as a function of $\delta_{23}^{u,\mathrm{RR}}$ for $m_0 = 1500$ GeV, $m_{1/2} = 680$ GeV, $A_0 = -500$ GeV, $\tan\beta = 10$, and $\mu > 0$.

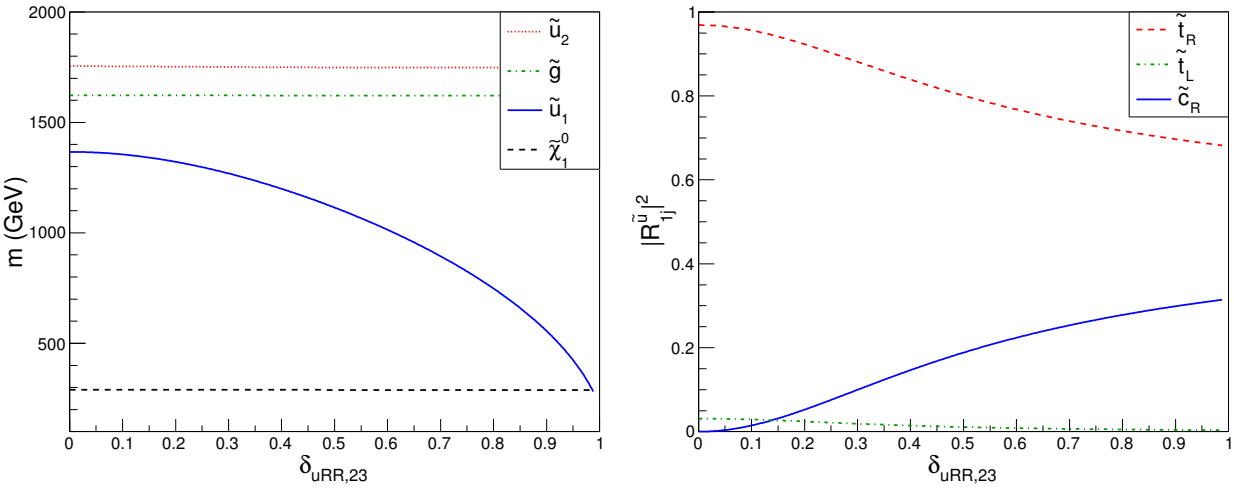

Figure 5.6.: Masses of the two lightest up-type squarks, gluino, and lightest neutralino (left) and flavor decomposition of lightest up-type squark (right) as a function of $\delta_{23}^{u,\mathrm{RR}}$ for $m_0 = 1500$ GeV, $m_{1/2} = 680$ GeV, $A_0 = -500$ GeV, $\tan\beta = 10$, and $\mu > 0$.

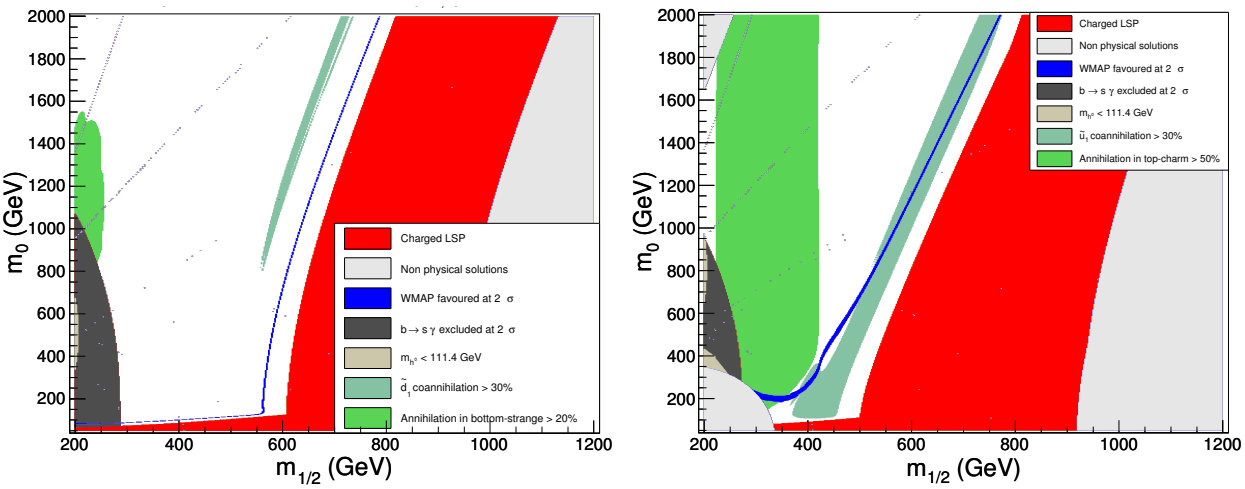

Figure 5.7.: Cosmologically favored region and related exclusion limits in the $(m_0,\, m_{1/2})$ plane of the cMSSM for $\delta_{23}^{u,\mathrm{RR}} = 0$, $\delta_{23}^{d,\mathrm{RR}} = 0.98$ (left) and $\delta_{23}^{u,\mathrm{RR}} = \delta_{23}^{d,\mathrm{RR}} = 0.98$ (right).

important coannihilation as seen in Fig. 5.3. The masses of $\tilde{u}_2$ $(= \tilde{c}_L)$, the neutralino and the gluino remain practically unaffected by the considered generation mixing.

5.5. Flavor violating down-squark and sbottom coannihilation

In this section we consider the possibility of flavor violating terms in the sector of down squarks. In Fig. 5.7 are shown scans of the m_0-$m_{1/2}$ plane for similar parameters as in the Fig. 5.2, except that there is now a large mixing between the second and third generation down squarks, still in the right-right sector ($\delta_{23}^{d,\mathrm{RR}} = 0.98$). On the left panel of Fig. 5.7, where $\delta_{23}^{u,\mathrm{RR}} = 0$ and $\delta_{23}^{d,\mathrm{RR}} = 0.98$, the relic density reaches the experimental value in two regions: the stau coannihilation region, and the down squark coannihilation region. In the latter the neutralino coannihilates with the lightest down squark $\tilde{d}_1$, which is here a mixture of $\tilde{s}$ and $\tilde{b}$. This coannihilation is possible thanks to the high value of $\delta_{23}^{d,\mathrm{RR}}$ wich decreases the lightest down squark mass. Next to the region where $\tilde{d}_1$ is the LSP, its mass can be very close to the neutralino mass, and new processes can contribute to reduce the relic density. The most important contributions come from down squark annihilation into gluons (70%), and neutralino coannihilation with down squarks into a gluon and a bottom (10%) or a strange (10%) quark. The region where coannihilation processes are important (more than 30%) is shown in light green. This region does not exactly match with the cosmological favored region because of the strong contribution from squark annihilation into gluon pairs.

It is interesting to note that neutralino-sbottom coannihilation can not occur in the cMSSM and can be achieved only within non universal models, in particular non universal sfermion

mass (NUSM) models described in Sec. 4.1.2 [69,142]. Large flavor violating terms are therefore another way of achieving efficient coannihilation between neutralino and a down squark. From this aspect, the cMSSM with NMFV is somehow similar to NUSM models: large off-diagonal elements decrease the mass of some specific squarks and therefore have a non universal effect.

On the right panel of the Fig. 5.7, where $\delta_{23}^{u,\mathrm{RR}} = \delta_{23}^{d,\mathrm{RR}} = 0.98$, coannihilation proceeds only with the up squark, and the relic density constraint is similar as in the right panel of Fig. 5.2. Indeed, because of the high top quark mass, the splitting between stop mass eigenstates is larger than for the bottom squarks. As a result, $\tilde{t}_1$ is lighter than $\tilde{b}_1$. However the constraint from $\mathrm{BR}(B \to X_s\gamma)$ is significantly weaker. Indeed, the main SUSY contributions to $\mathrm{BR}(B \to X_s\gamma)$ come here from up squark-chargino and down squark-gluino loops. The former one is negative, and its absolute value increases with $\delta_{23}^{u,\mathrm{RR}}$, while the latter one is positive and increases with $\delta_{23}^{d,\mathrm{RR}}$. The dominant contribution is however the down squark-gluino loop, which means that the low masses region is excluded here because of a too large $\mathrm{BR}(B \to X_s\gamma)$. This is in contrary to the case of the right panel of Fig. 5.2 where only the up sector was considered: $\mathrm{BR}(B \to X_s\gamma)$ was too low because of a large negative up squark-chargino loop contribution. In addition, as the Standard Model value for $\mathrm{BR}(B \to X_s\gamma)$ lies close to the lower experimental bound, the constraint is here not significantly stronger than in the case of MFV. This explains why the constraint for $\delta_{23}^{u,\mathrm{RR}} = \delta_{23}^{d,\mathrm{RR}} = 0.98$ (see right panel of Fig. 5.7) is similar as the one for $\delta_{23}^{u,\mathrm{RR}} = \delta_{23}^{d,\mathrm{RR}} = 0$ (see left panel of Fig. 5.2).

5.6. Conclusion

While the MSSM with a most general flavor structure has been extensively studied in the context of collider signatures, the possibility of squark flavor mixing has not been considered for observables related to dark matter so far. However, as the LHC is running and more precise cosmological and astrophysical experiments are taking data or being set up, it becomes more and more important to take into account such effects when studying the interplay between collider and astroparticle phenomenology.

In the case of neutralino dark matter in supersymmetric theories, flavor violating couplings can influence the (co)annihilation cross section, and in consequence the predicted relic density, in different ways. The strongest effect is due to the modified mass spectrum of squarks, the lightest squark becoming lighter with increasing flavor non-diagonal terms in the mass matrices. The exchange of squarks in neutralino pair annihilation as well as the presence of coannihilation with a squarks become then important. Another effect comes from the fact that couplings of neutralinos to squarks are not diagonal in flavor space any more. This opens new (co)annihilation channels, such as $\tilde{\chi}_1^0\tilde{\chi}_1^0 \to c\bar{t}$ or $\tilde{\chi}_1^0\tilde{u}_1 \to ch^0(cg, cZ^0)$, which can give

sizable contributions to the annihilation cross-section already for moderate flavor violation parameters.

Considering flavor mixing in the sector of right-handed up-type squarks, we have shown that the modified squark masses and flavor contents have a strong impact on the (co)annihilation modes. New annihilation channels are opened due to the presence of non-diagonal couplings in flavor space. These new contributions may become numerically important in particular regions of the parameter space. As a consequence, new regions that are compatible with the relic density constraint are opened.

In addition we have studied the impact of flavor mixing in the sector of right-handed down-type squarks. In analogy to the up-type squark sector, new (co)annihilation channels open and lead to new favored regions. In particular we observed new contributions from coannihilations between neutralinos and the lightest down squark $\tilde{d}_1$ (in our case a mixture of strange and bottom squarks), usually not possible in the cMSSM with MFV. We also noticed that the constraint from $\mathrm{BR}(B \to X_s\gamma)$ was weaker when considering flavor mixing in both the up and down squark sectors at the same time, due to a cancellation between negative and positive contributions.

Since the annihilation cross section of the neutralino also governs the particle fluxes, flavor violating couplings would also have an impact on indirect detection of dark matter. In particular, additional $\tilde{c}$–$\tilde{t}$ mixing, as discussed in this paper, would change the spectrum of photons originating from dark matter annihilation. The impact of flavor mixing is, however, expected to be very small compared to the astrophysical uncertainties in this context.

Direct dark matter detection might also be influenced by the discussed flavor mixing. Here, the scattering of a neutralino off a nucleus can proceed through squark-exchange, such that the charm-content in the nucleon becomes relevant if the lightest squark is a mixture of stop and scharm. In the same way, flavor mixing in the sector of down-type squarks would increase the importance of the strange quark in the nucleus. Detailed studies of direct or indirect detection of dark matter in the context of flavor violation are, however, beyond the scope of this work.

Chapter 6.

Impact of next-to-leading order corrections on the relic density

6.1. The DM@NLO project

6.1.1. NLO cross sections for dark matter relic density

As described in Sec. 4.2.1, one of the main sources of uncertainties in the calculation of the dark matter relic density is the precision with which the (co)annihilation cross sections entering in Eq. (1.15) are computed. The cross sections in public dark matter tools such as `DarkSUSY` [27] or `micrOMEGAs` [25,26] are implemented using only an effective tree-level calculation. `micrOMEGAs` for example includes important effects from the running strong coupling constant and running quark masses in the default implementation of the MSSM. It is, however, well known that higher-order corrections, particularly those involving the strong coupling constant, can have a sizable impact on such processes [1]. The impact of next-to-leading order corrections to neutralino annihilation and coannihilation on the neutralino relic density has been discussed in several previous analyses.

We first comment on a class of corrections called "Sommerfeld corrections" which arise from long range interactions between the neutralinos before their (co)annihilation, this interaction being mediated by the exchange of a light boson. For massless bosons these corrections diverge in the limit of vanishing relative velocity of neutralinos. When the boson mass is of the same order as the WIMP mass, it is possible to treat this so-called "Sommerfeld enhancement" pertubatively, i.e. at one loop for instance. This has been done for the annihilation and coannihilation of WIMPs in [144] and [145], and applied to the annihilation of the lightest neutralino and its coannihilation with other neutralino and chargino in the MSSM, with exchange of light Higgs or Z bosons. On the other hand, if the exchanged boson is much ligher than the WIMP, these corrections explode and have to be treated in a non-perturbative way. This has been done

[1] Note that higher-order corrections can also modify the direct detection cross sections [143].

for example in [146], [147], [148], [149] and applied to the case of (co)annihilation of heavy wino or higgsino neutralino and chargino exchanging electroweak gauge bosons. In [150] the case of scalar-fermion coannihilation was discussed together with an application to neutralino-stau and neutralino-stop coannihilations.

Let us now turn to the class of perturbative next-to-leading order corrections. Electroweak corrections to many processes of neutralino annihilation and coannihilation have been evaluated in [151–153]. In [153, 154] the authors focused on neutralino annihilation and neutralino-gaugino coannihilation into vector bosons final states, while in [152] they also considered neutralino annihilation into quark and leptons final states, and neutralino stau coannihilation processes. Other studies rely on effective coupling approaches in order to capture certain classes of corrections to neutralino pair annihilation and coannihilation with a tau slepton [154, 155]. The SUSY-QCD corrections to neutralino annihilation into b quark pairs in the A^0-funnel has been studied in [152] and [119]. In [136, 137] this latter study was extended to the general case of neutralino annihilation into massive quarks in the parameter space of minimal and non-minimal MSSM models. All these analyses show that radiative corrections are not negligible in the context of relic density calculations, the impact of the corrections being larger than the experimental uncertainty from WMAP in many regions of parameter space. With the recently released Planck satellite data providing more precise cosmological measurements, it becomes even more pressing that theoretical predictions match the experimental precision.

As SUSY-QCD corrections are relevant for colored particles like quarks and squarks, one can expect significant corrections to the cross section in the case of neutralino-stop coannihilation. The motivations for this region of the MSSM parameter space and the relevant constraints have been discussed in the last chapter. In this chapter we present the calculation of the full one-loop SUSY-QCD corrections to the neutralino-stop coannihilation cross section. This case has so far only been considered in [156]. This study concerns the very specific cases of coannihilation of a bino-like neutralino with a right-handed stop into a top quark and a gluon as well as into a bottom quark and a W-boson. However, depending on the considered region of parameter space, many other final states, including those with other electroweak gauge and Higgs bosons, can become dominant. Moreover, in realistic supersymmetric scenarios, helicity mixing in the stop sector is usually non-negligible, as is the mixing of bino, wino, and higgsino components in the lightest neutralino, which strongly influences its couplings and preferred (co)annihilation channels. Therefore, we have extended the analysis of QCD and SUSY-QCD corrections to coannihilation of a neutralino with a stop by computing the general case of neutralino-stop co annihilation into a quark and a Higgs or an electroweak vector boson, which has been presented in [157]. In this chapter, after commenting on some practical aspects of the calculation, we will review in detail the virtual and real parts of the corrections in Sec. 6.2 and 6.3. We will then show numerical results for the NLO cross sections in Sec. 6.4, and see

the numerical impact of these corrections on the relic density in Sec. 6.5. Lastly, in Sec. 6.6, we will discuss the ongoing calculation of the gluon final state, before concluding in Sec. 6.7.

6.1.2. Calculation and implementation: practical aspects

The calculation of neutralino annihilation into quarks at NLO in SUSY-QCD used in [119,136, 137] has been implemented in a Fortran code, which was the starting of point of the DM@NLO ("Dark Matter at Next-to-Leading Order") project. The generalization of this implementation to the cases of neutralino-chargino and chargino-chargino coannihilation is under work, and the calculation of stop annihilation at NLO also started (as described in Sec. 4.2.1 the latter process is relevant in the neutralino-stop coannihilation region). Our calculation of the neutralino-stop coannihilation at NLO has been implemented in the same code, the purpose being to be able to compute automatically all the processes needed for the relic density at NLO in SUSY-QCD in a single framework. We stress that our calculations and implementations are general so that they can be used for any neutralino-sfermion coannihilation process, even if we focus in this study on the case of $\tilde{\chi}_1^0\tilde{t}_1$, which is the most relevant process of this kind within the MSSM. In practice, the code can be used to compute for instance neutralino coannihilation with a bottom squark, which can appear in non universal supergravity inspired by SU(5) GUT models [69, 142, 158] or D-brane models [159] (and is of course present in pMSSM-like models [160]).

The one-loop SUSY-QCD virtual and real corrections to the neutralino-squark coannihilation involves a given set of Feynman diagrams that will be shown in the next sections when the corresponding calculation will be detailed. These one-loop amplitudes have been calculated analytically and cross-checked using hand calculations but also the publicly available tools `FeynArts` [161], `FeynCalc` [162], and `Form` [163]. As said above they have been implemented in a Fortran code similar to the one already used for the neutralino annihilation, which required some work on the generalization of the code structure and on some specific aspects like the kinematics, the two initial (and final) particles being not identical in that case. In addition, one of the final state can either be a vector or a scalar in the coannihilation case. The detailed structure of the code is shown in App. A, but we will explain briefly how it works in the following. Our program takes as input the masses and mixings of all particles (we use `SPheno` to compute the supersymmetric mass spectrum), the PDG numbers of the external particles and the center-of-mass momentum involved in the coannihilation process together with several flags (specifying if the cross section has to be calculated at tree-level or one loop and in which unit, for instance). It gives as output the corresponding numerical cross section. This code is used as an extension to the public package `micrOMEGAs`: it provides the cross section for the relevant coannihilation processes which then replace the default one calculated by `CalcHEP`. It is linked to `micrOMEGAs` in such a way that all relevant parameters, i.e. the masses and mixings of all particles, are passed between the two codes in a consistent way.

As the work has been divided within the collaboration into electroweak gauge boson final states on one hand, and Higgs boson final states on the other hand, we would like to focus on the specific features of the vector final states before going into the details of the calculation. First, the amplitudes with gauge boson final states have to be treated carefully regarding the gauge dependence. Fortunately the gauge dependence of the computed expressions is rather trivial in our case since gauge bosons appear only as external particles. The only term to be treated carefully is therefore the summation over the polarization vectors of the gauge bosons. We work in unitary gauge (see Sec. 2.5), in which they are defined as the following:

$$\sum_{\lambda} \varepsilon_{\lambda}^{\mu}(p_4)\, \varepsilon_{\lambda}^{*\nu}(p_4) \to -g^{\mu\nu} + x_v\, p_4^{\mu}\, p_4^{\nu} \tag{6.1}$$

where x_v is equal to 0 for the massless gauge bosons, $1/m_W^2$ for the W boson and $1/m_Z^2$ for the Z boson. In this way, our general amplitudes for vector boson final states (see App. A) can be used for any of the gauge bosons, depending on the value given to x_v. Another advantage of this general formulation is that we could in principle easily switch to Feynman gauge, in which case x_v would be equal to zero for the massive vector bosons. We would then need to add the amplitudes with the Goldstone boson final states. As the structure of these amplitudes is similar as the one for the Higgs boson (which is also a scalar), it should be possible to use them.

In addition, as we will discuss in Sec. 6.3.3, the W boson and photon final states involve additional sources of IR divergences which have to be removed in a consistent way. We will also see that the vector bosons are related to Feynman diagrams involving squark-squark-vector-gluon vertices giving additional contributions to the virtual and real corrections, as compared to the Higgs boson final states. Also, the photon being massless, one needs dedicated special cases for some Passarino-Veltman integrals in which the mass of the final boson appears. Lastly, due to the vector couplings the vertex and box corrections have rather complicated general structures which are given in App. A.

6.2. Virtual corrections and renormalization

6.2.1. Introduction

The tree-level Feynman diagrams for neutralino-stop coannihilation are shown in Fig. 6.1. The virtual corrections Feynman diagrams consist in two, three and four-points corrections respectively called self-energies (or "bubbles"), vertex (or "triangles") and box diagrams. They are shown in Figs. 6.2, 6.3 and 6.4.

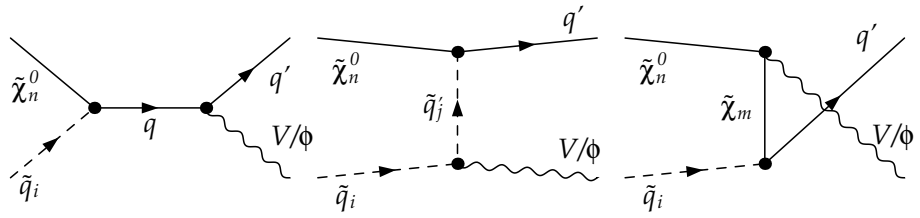

Figure 6.1.: Leading-order Feynman diagrams for neutralino-squark coannihilation into a quark and Higgs (ϕ) or electroweak gauge (V) bosons. The u-channel is absent for a photon in the final state.

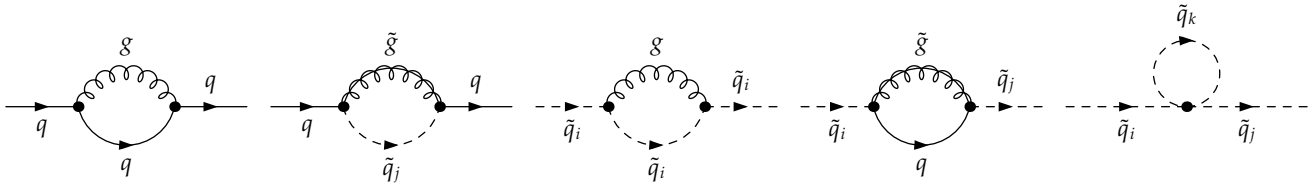

Figure 6.2.: Self-energy corrections for the quarks and squarks at one-loop level in QCD contributing to neutralino-squark coannihilation.

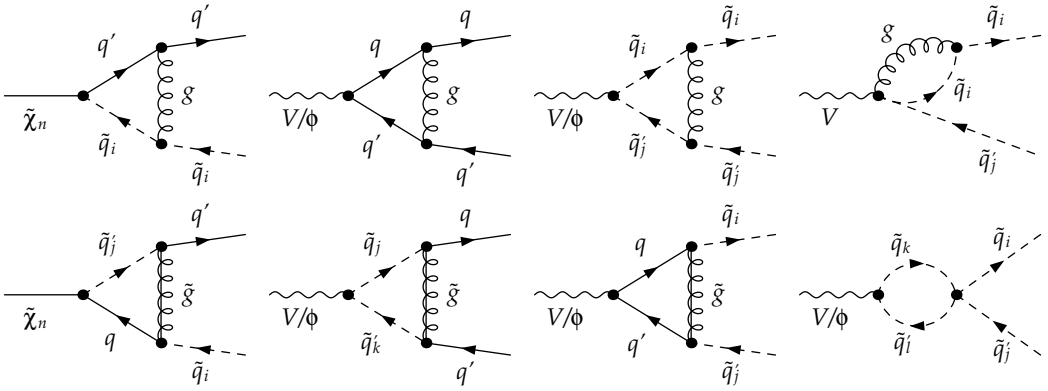

Figure 6.3.: Vertex corrections at one-loop level contributing to neutralino-squark coannihilation into quarks and Higgs (ϕ) or electroweak gauge (V) bosons. The diagram involving the $V - g - \tilde{q} - \tilde{q}$ vertex is present only for the case of a gauge boson in the final state.

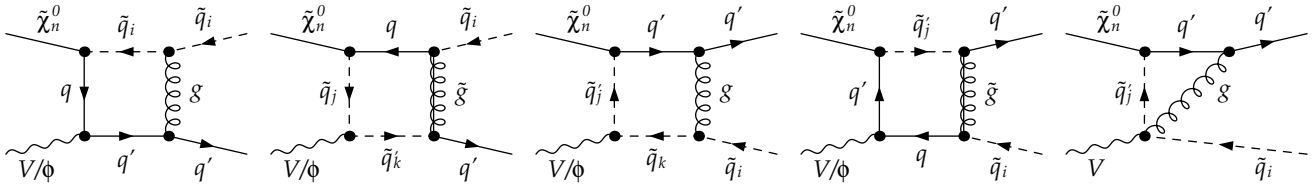

Figure 6.4.: Four-point diagrams at one-loop level contributing to neutralino-squark coannihilation into quarks and Higgs (ϕ) or electroweak gauge (V) bosons. The last diagram involving the four-vertex is absent for a scalar in the final state.

The main difficulty encountered when calculating virtual corrections come from the integration over the internal particles momenta. As we will see these integrals are not always finite and the infinities have to be subtracted by a procedure called renormalization. To be able to apply the renormalization procedure one first needs to extract the divergence analytically from the integral: this is called regularization. In this section we discuss in detail the procedures used in our calculation.

6.2.2. Regularization of UV divergences

Dimensional regularization

When calculating NLO amplitudes one has to integrate over the four-momenta of internal particles, which can lead to divergences when the energy of the particle in the loop goes to the infinity: these are UV divergences. Whether the integral will diverge or not depends on the number of four-momenta in the numerator and denominator of the integrand. The general form of one-loop integral with N propagators and M loop momentum factors in the numerator is

$$T^N_{\mu_1,\dots,\mu_M}(p_1,\dots,p_{N-1},m_0,\dots,m_{N-1}) \equiv \frac{(2\pi\mu)^{4-D}}{i\pi^2}\times \int d^Dq \frac{q_{\mu_1}\dots q_{\mu_M}}{[q^2-m_0^2+i\varepsilon][(q+p_1)^2-m_1^2+i\varepsilon]\dots[(q+p_{N-1})^2-m_{N-1}^2+i\varepsilon]}. \quad (6.2)$$

Here the parameter μ has the dimension of energy which ensures that the integral has the same dimension even when $D \neq 4$ and is called "renormalization scale". Depending on the values of N and M this integral can be divergent in the UV, i.e. when $q \to \infty$. A naive way of regularizing this integral would be to introduce a cutoff Λ on the integration, which however breaks Lorentz and gauge invariance. More complex regularization procedure are preferred, in particular dimensional regularization (or reduction). The integral (6.2) diverges if $D + M - 2N \geq 0$. If $D + M - 2N = 0$ it is a logarithmic divergence, if $D + M - 2N > 0$ it is a polynomial divergence. One notes that a divergent integral can be made convergent by lowering the number of dimensions D. This is the basis of *dimensional regularization*, in which the calculation of loop integrals is performed in a general number of dimension $D < 4$. The limit $D \to 4$ being taken only at the end one can extract the divergence as a $1/(D-4)$ pole. In dimensional regularization the space-time dimension is continued to D dimension. As a consequence all four-vectors, metric tensors and Dirac matrices are continued to D dimension, and obey specific relations which can be found in the literature. The case of the γ^5 matrix is peculiar and can lead to some issues. The generalization of vector field to D dimension is however not compatible with Supersymmetry as it introduces a mismatch between the fermionic and bosonic degrees of freedom. In Supersymmetry we therefore often

use *dimensional reduction* [164] in which the four-momenta are continued to D dimensions, while the gauge fields and Dirac matrices remain in 4 dimensions.

Passarino-Veltman integrals

We now describe a method to calculate one-loop integrals based on the work of 't Hooft and Veltman [165] and Passarino and Veltman [166]. The general integral (6.2) can be classified into several cases depending on the number of propagators in the denominator(N): $A \equiv T^1$, $B \equiv T^2$, $C \equiv T^3$, $D \equiv T^4$. Depending on the number of momenta present in the numerator these integrals will have a given number of Lorentz indices ($C_{\mu\nu}$ for instance). A particular case consists in the integrals without any momentum in the numerator, which are called scalar integrals: A_0, B_0, C_0, D_0, only the first two ones being UV divergent. These scalar integrals are of primary importance since it turns out that every integral of the kind (6.2) can be expressed in function of them. Then two steps are needed in order to calculate any one-loop integral: first, find a relation between the needed integral and the scalar integrals. Then, calculate an analytical expression of these scalar integrals in dimensional reduction. The main difficulty comes from the large number of possible combinations of arguments, with many special cases needing a dedicated derivation.

As we said all integrals (6.2) can be expressed in function of the scalar integrals thanks to a method called Passarino-Veltman tensor reduction. First, due to Lorentz invariance, it is possible to decompose any tensor integral on the metric tensor and the four-momenta appearing in its denominator. We have for instance:

$$\begin{aligned}
A^{\mu\nu} &= g^{\mu\nu}\, A_2 \\
A^{\mu\nu\rho\sigma} &= \left(g^{\mu\nu}g^{\rho\sigma} + g^{\mu\rho}g^{\nu\sigma} + g^{\mu\sigma}g^{\nu\rho}\right)\, A_4 \\
B^{\mu} &= p_1^{\mu}\, B_1 \\
B^{\mu\nu} &= g^{\mu\nu}\, B_{00} + p_1^{\mu}p_1^{\nu}\, B_{11} \\
C^{\mu} &= p_1^{\mu}\, C_1 + p_2^{\mu}\, C_2 \\
C^{\mu\nu} &= g^{\mu\nu}\, C_{00} + p_1^{\mu}p_1^{\nu}\, C_{11} + \left(p_1^{\mu}p_2^{\nu} + p_2^{\mu}p_1^{\nu}\right) C_{12} + p_2^{\mu}p_2^{\nu}\, C_{22}.
\end{aligned} \tag{6.3}$$

This decompositions contain scalar coefficients (e.g. B_1, B_{00}, B_{11}, C_1, etc.) which can then be expressed in function of the scalar integrals A_0, B_0, C_0, etc. This is done by contracting the decomposition shown above with four-momenta or metric tensor. On the left-hand side the tensor integral are reduced to integrals of lower rank, while the right-hand side lead to a combination of scalar coefficients. The latter are then expressed by solving the obtained linear

equation. We obtain for instance:

$$A_2(m^2) = \frac{m^2}{4} A_0(m^2) + \frac{m^4}{8}, \tag{6.4}$$

$$B_1(p_1^2, m_0^2, m_1^2) = \frac{1}{2p_1^2}\left[A_0(m_0^2) - A_0(m_1^2) - (p_1^2 - m_1^2 + m_0^2)\, B_0(p_1^2, m_0^2, m_1^2)\right]. \tag{6.5}$$

Among the scalar integrals only A_0 and B_0 are UV divergent and their expressions in $D = 4-2\varepsilon$ dimensions exhibit poles for $\varepsilon \to 0$:

$$A_0(m^2) = m^2 \left(\Delta - \ln\left(\frac{m^2 - i\varepsilon}{\mu^2}\right) + 1 + \mathcal{O}(\varepsilon)\right) \tag{6.6}$$

$$B_0(p_1^2, m_0^2, m_1^2) = \Delta - \ln\left(\frac{m_0 m_1}{\mu^2}\right) + 2 + \frac{m_0^2 - m_1^2}{p_1^2} \ln\frac{m_1}{m_0} \times \frac{\sqrt{\lambda(p_1^2, m_0^2, m_1^2) + 4ip_1^2\varepsilon}}{2p_1^2}\left[\ln\left(1 - \frac{1}{x_1}\right) - \ln\left(1 - \frac{1}{x_2}\right)\right] \tag{6.7}$$

with

$$x_{1,2} = \frac{1}{2\,p_1^2}\left(p_1^2 - m_1^2 + m_0^2 \pm \sqrt{(p_1^2 - m_1^2 - m_0^2)^2 - 4\,m_0^2 m_1^2 + 4ip_1^2\varepsilon}\right) \tag{6.8}$$

and

$$\Delta = \frac{1}{\varepsilon} - \gamma_E + \ln 4\pi. \tag{6.9}$$

The derivation of these formulas is quite lengthy and will therefore not be detailed here. In addition, the procedure has to be redone for all needed special kinematic cases (i.e. when some masses are equal to zero, or when two masses are equal, etc.).

In our calculation all tensor loop integrals are reduced using this Passarino-Veltman reduction and the resulting scalar integrals are evaluated using the known results in, e.g., [167, 168]. We have checked that all needed integrals agree with `LoopTools` [169]. Note that the conventions used in `LoopTools` and in the mentioned references are different so that one has to include an additional factor

$$\frac{1 + \pi^2\varepsilon^2/6}{\Gamma(1+\varepsilon)(4\pi)^\varepsilon} \tag{6.10}$$

when comparing both. The term in ε^2 has no impact excepted when dealing with soft-collinear divergences, as will be the case when considering the gluon final state in Sec. 6.6. In this case this term multiplies the double pole $1/\varepsilon^2$ to give an additional finite part to the integral.

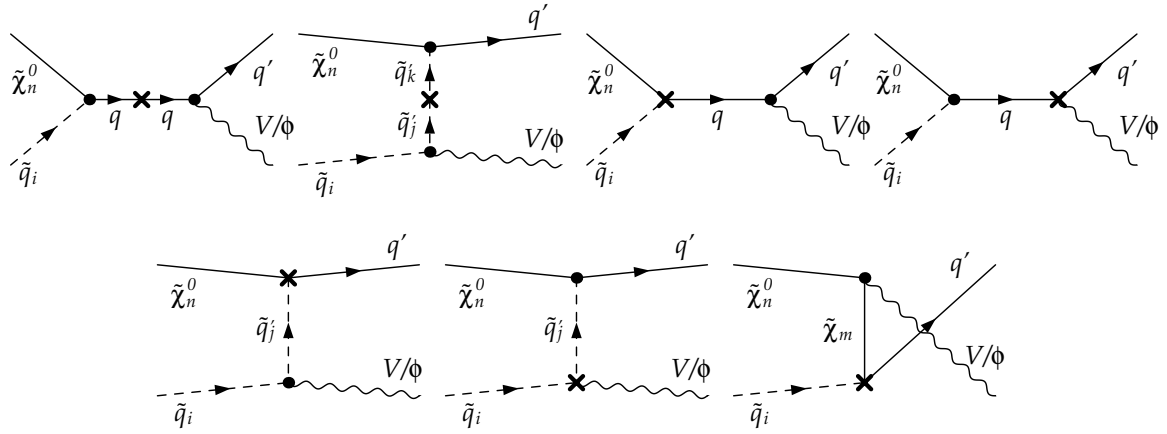

Figure 6.5.: Counterterms diagrams for the quarks and squarks propagators, the $\tilde{\chi}-\tilde{q}-q$, $q-q-V/\phi$ and $\tilde{q}-\tilde{q}-V/\phi$ vertices contributing to neutralino-squark coannihilation into quarks and Higgs (ϕ) or electroweak gauge (V) bosons. Again, the last diagram is absent in the case of photon final state.

6.2.3. QCD renormalization of the MSSM

Once the UV divergences have been extracted in an analytical form on has to absorb them by redefining the parameters (masses, couplings and fields) in the Lagrangian. This procedure called renormalization can be done by introducing new terms called counterterms, containing divergences opposite in sign as compared to the one present in the virtual corrections. A theory is called renormalizable if only a finite number of independent counterterms is needed. In multiplicative renormalization each parameters is multiplied by a renormalization constant of the form $Z = 1+\delta Z$ at the one-loop order. The Lagrangian parameters are therefore expressed as a sum of a renormalized (finite) parameter and a renormalization constant (counterterm). By expanding the Lagrangian and keeping only the terms of up to one-loop order, one ends up with a sum of a renormalized Lagrangian and a counterterm Lagrangian. The latter is associated with counterterms Feynman diagrams, shown in Fig. 6.5, which cancel the divergences of the one-loop virtual corrections diagrams. The propagator and vertex counterterms respectively cancel with the propagator and vertex virtual corrections, while there are no counterterm corresponding to the boxes diagrams which are UV finite. These counterterms are determined from a set of conditions called renormalization scheme, and physical quantities predicted from different renormalization schemes differ only up to higher orders.

When considering the QCD renormalization of the MSSM, a consistent treatment of all parameters in the quark and squark sectors is essential. In this section we will present different renormalization schemes (namely the $\overline{\text{MS}}$, $\overline{\text{DR}}$ and on-shell schemes). We will introduce then a hybrid on-shell/$\overline{\text{DR}}$ renormalization scheme for the quarks and squarks which is set up in such a way that it minimizes potential problems connected to sensitive parameters (e.g. the

bottom trilinear coupling A_b) and is valid in a large region of MSSM parameter space. Similar renormalization schemes for the quark and squark sectors of the MSSM were already introduced and studied in [170,171]. Compared to those analyses, our approach differs significantly in the treatment of the squark mixing angles θ_b and θ_t, but shares some important features with the RS2 scheme introduced in [171].

Renormalization schemes

The "Minimal Substraction" (MS) prescription is simply to remove (after dimensional regularization) only the $1/\varepsilon$ poles. Thus in that scheme the counterterms have no finite parts and depend on a renormalization scale μ. As singular terms are often accompanied by (potentially large) finite terms it is convenient to subtract them as well. In the "modified Minimal Substraction" ($\overline{\text{MS}}$) we therefore have:

$$\frac{1}{\varepsilon} - \gamma_E + \ln(4\pi) - \ln(m^2) \to -\ln(m^2/\mu^2). \tag{6.11}$$

As we have seen in Sec. 6.2.2, in Supersymmetry dimensional reduction must be used. The corresponding modified minimal subtraction scheme is called $\overline{\text{DR}}$. In this way expressions are simplified, however measured quantities are not easily expressed in that scheme.

The on-shell renormalization scheme (OS) requires that the renormalized mass parameter is the physical mass (i.e. the real part of the propagators pole). In addition, it is required that the renormalized field does not mix with others and that the propagator has a unit residue. Coupling constants are then unchanged when all interacting particles are on-shell. In that scheme there is no dependence on the renormalization scale.

Quark sector

The process of neutralino-stop coannihilation considered here involves only quarks and squarks of the third generation. We will therefore discuss only the case of massive quarks. The parameters to be renormalized are the quark fields (wave-functions) and masses. The counterterms for these parameters are obtained by applying specific renormalization conditions to the renormalized two-point Green's functions of the quarks, and will be therefore expressed in function of them. These conditions are given by the chosen renormalization schemes which will be described. We perform the wave-function renormalization by introducing counterterms $\delta Z_{L,R}$ for each chirality of the third-generation quarks

$$\begin{pmatrix} q_L \\ q_R \end{pmatrix} \to \begin{pmatrix} 1 + \frac{1}{2}\delta Z_L & 0 \\ 0 & 1 + \frac{1}{2}\delta Z_R \end{pmatrix} \begin{pmatrix} q_L \\ q_R \end{pmatrix}. \tag{6.12}$$

The wave-function renormalization constants are fixed by the on-shell scheme conditions, i.e. by requiring the external quark propagators to have unit residue even at one-loop order. This leads to the following expression for the massive quarks ($q = t, b$)

$$\begin{aligned}\delta Z_L &= \Re\Big\{ -\Pi_L(m_q^2) - m_q^2\Big[\dot{\Pi}_L(m_q^2) + \dot{\Pi}_R(m_q^2)\Big] \\ &\quad + \frac{1}{2m_q}\Big[\Pi_{SL}(m_q^2) - \Pi_{SR}(m_q^2)\Big] - m_q\Big[\dot{\Pi}_{SL}(m_q^2) + \dot{\Pi}_{SR}(m_q^2)\Big]\Big\}\,, \qquad (6.13)\\ \delta Z_R &= \delta Z_L(L \leftrightarrow R)\,, \qquad (6.14)\end{aligned}$$

where $\Pi_{L,R}(k^2)$ and $\Pi_{SL,SR}(k^2)$ stand for the vector and the scalar parts of the two-point Green's function as defined in [172] and $\dot{\Pi}(m^2) = \left[\frac{\partial}{\partial k^2}\Pi(k^2)\right]_{k^2=m^2}$.

After the wave-function renormalization has been performed, we still have to renormalize the masses of the quarks. Although both the top and bottom quark are heavy, their properties are very different, and so is our treatment of their masses. On the one hand, the top quark does not form bound states and its physical mass is directly measurable. Therefore in our calculation, we use the physical (on-shell) top quark mass $m_t = 173.1$ GeV. This implies using the on-shell mass counterterm for the top quark defined as

$$\delta m_t = \frac{1}{2}\,\Re\Big\{m_t\Big[\Pi_L(m_t^2) + \Pi_R(m_t^2)\Big] + \Pi_{SL}(m_t^2) + \Pi_{SR}(m_t^2)\Big\}\,. \qquad (6.15)$$

On the other hand, the bottom quark forms hadrons and its mass cannot be directly measured. Conventionally a mass parameter $m_b(m_b)$ is extracted in the $\overline{\mathtt{MS}}$ renormalization scheme from the Standard Model analysis of Υ sum rules [173–176]. In order to obtain the appropriate bottom quark mass in the $\overline{\mathtt{DR}}$ renormalization scheme within the MSSM, we first use the Standard Model next-to-next-to-leading order (NNLO) renormalization group evolution to obtain the mass of the bottom quark at a scale Q [177]. We then convert the $\overline{\mathtt{MS}}$ mass $m_b^{\overline{\mathtt{MS}},\,\mathtt{SM}}(Q)$ to a mass in the $\overline{\mathtt{DR}}$ renormalization scheme $m_b^{\overline{\mathtt{DR}},\,\mathtt{SM}}(Q)$ while still in the Standard Model [177]. Finally we apply the threshold corrections including also contributions from SUSY particles in the loop (denoted by Δm_b)

$$m_b^{\overline{\mathtt{DR}},\,\mathtt{MSSM}}(Q) \;=\; m_b^{\overline{\mathtt{DR}},\,\mathtt{SM}}(Q) - \Delta m_b\,. \qquad (6.16)$$

The corresponding counterterm contains the pole in ε and can be written as

$$\frac{\delta m_b^{\overline{\mathtt{DR}}}}{m_b} = (-2)\frac{\alpha_s C_F}{4\pi}\,\frac{c_\varepsilon}{\varepsilon}\,, \qquad (6.17)$$

where we factored out the constant $c_\varepsilon = \Gamma(1+\varepsilon)(4\pi)^\varepsilon$. One prominent place where the quark masses enter the calculation is through the Yukawa couplings of the Higgs bosons to the quarks. Especially the Yukawa couplings of the bottom quark were extensively studied in the decays

of Higgs bosons in the Standard Model. Important QCD and top-quark induced corrections to the coupling of Higgs bosons to bottom quarks were calculated up to $\mathcal{O}(\alpha_s^4)$ [178–180] and can be used to define an effective Yukawa coupling which includes these corrections as

$$\left[\left(h_b^{\overline{\text{MS}},\text{QCD},\Phi}\right)(Q)\right]^2 = \left[\left(h_b^{\overline{\text{MS}},\Phi}\right)(Q)\right]^2 \left[1 + \Delta_{\text{QCD}} + \Delta_t^\Phi\right], \tag{6.18}$$

for each Higgs boson $\Phi = h^0, H^0, A^0$. The QCD corrections Δ_{QCD} are explicitly given by

$$\begin{aligned}\Delta_{\text{QCD}} &= \frac{\alpha_s(Q)}{\pi} C_F \frac{17}{4} + \frac{\alpha_s^2(Q)}{\pi^2}\left[35.94 - 1.359\, n_f\right] \\ &+ \frac{\alpha_s^3(Q)}{\pi^3}\left[164.14 - 25.77\, n_f + 0.259\, n_f^2\right] \\ &+ \frac{\alpha_s^4(Q)}{\pi^4}\left[39.34 - 220.9\, n_f + 9.685\, n_f^2 - 0.0205\, n_f^3\right],\end{aligned} \tag{6.19}$$

and the top-quark induced corrections Δ_t^Φ for each Higgs boson Φ read

$$\Delta_t^h = c_h(Q)\left[1.57 - \frac{2}{3}\log\frac{Q^2}{m_t^2} + \frac{1}{9}\log^2\frac{m_b^2(Q)}{Q^2}\right], \tag{6.20}$$

$$\Delta_t^H = c_H(Q)\left[1.57 - \frac{2}{3}\log\frac{Q^2}{m_t^2} + \frac{1}{9}\log^2\frac{m_b^2(Q)}{Q^2}\right], \tag{6.21}$$

$$\Delta_t^A = c_A(Q)\left[\frac{23}{6} - \log\frac{Q^2}{m_t^2} + \frac{1}{6}\log^2\frac{m_b^2(Q)}{Q^2}\right], \tag{6.22}$$

with

$$\left\{c_h(Q), c_H(Q), c_A(Q)\right\} = \frac{\alpha_s^2(Q)}{\pi^2}\left\{\frac{1}{\tan\alpha\tan\beta}, \frac{\tan\alpha}{\tan\beta}, \frac{1}{\tan^2\beta}\right\}. \tag{6.23}$$

We take into account these corrections excluding the one-loop part as it is provided consistently through our own calculation.

In the MSSM, the Yukawa coupling to bottom quarks can receive large corrections for large $\tan\beta$ or large A_b, even beyond the next-to-leading order, which can affect our analysis. Therefore, in addition, we include these corrections that can be resummed to all orders in perturbation theory [181, 182]. Denoting the resummable part by Δ_b we redefine the bottom

quark Yukawa couplings as

$$h_b^{\texttt{MSSM},h}(Q) = \frac{h_b^{\overline{\texttt{MS}},\texttt{QCD},h}(Q)}{1+\Delta_b}\left[1-\frac{\Delta_b}{\tan\alpha\tan\beta}\right], \tag{6.24}$$

$$h_b^{\texttt{MSSM},H}(Q) = \frac{h_b^{\overline{\texttt{MS}},\texttt{QCD},H}(Q)}{1+\Delta_b}\left[1+\Delta_b\frac{\tan\alpha}{\tan\beta}\right], \tag{6.25}$$

$$h_b^{\texttt{MSSM},A}(Q) = \frac{h_b^{\overline{\texttt{MS}},\texttt{QCD},A}(Q)}{1+\Delta_b}\left[1-\frac{\Delta_b}{\tan^2\beta}\right]. \tag{6.26}$$

In the same way as for the QCD corrections, we exclude the one-loop part of these SUSY-QCD corrections and include only the resummed remainder, since the one-loop part is already present in our calculation.

Squark sector

As in the above discussion for quarks, we will address here only the squarks of the third generation, i.e. stops and sbottoms. We work in the mass eigenstate basis and introduce the wave-function renormalization counterterms δZ_{ij} through

$$\tilde{q}_i \to \left(\delta_{ij}+\frac{1}{2}\delta Z_{ij}\right)\tilde{q}_j\,, \tag{6.27}$$

where in contrast to the case of quarks the δZ_{ij} include also off-diagonal terms. The wave-function renormalization counterterms are again fixed by requiring that the squark propagators have unit residue also at one-loop level. In addition we require that mixing for on-shell squarks is absent. These conditions lead to the counterterms

$$\delta Z_{ii} = -\Re\left[\dot{\Pi}^{\tilde{q}}_{ii}(m^2_{\tilde{q}_i})\right], \tag{6.28}$$

$$\delta Z_{ij} = \frac{2\,\Re\left[\Pi^{\tilde{q}}_{ij}(m^2_{\tilde{q}_j})\right]}{m^2_{\tilde{q}_i}-m^2_{\tilde{q}_j}}, \qquad \text{for} \quad i\neq j\,, \tag{6.29}$$

where $\Pi^{\tilde{q}}_{ij}(k^2)$ are again the two-point Green's functions, this time for squarks.

The renormalization of the squark masses is complicated due to the mixing of squarks of the third generation. Therefore, it has to be discussed in conjunction with the renormalization of all other parameters in the squark sector appearing in the mass matrix. At tree-level, the

masses $m^2_{\tilde{q}_i}$ for stops and sbottoms are obtained by diagonalization of the mass matrix

$$U^{\tilde{q}} \begin{pmatrix} M^2_{\tilde{Q}} + (I^{3L}_q - e_q\, s^2_W)\cos 2\beta\, m^2_Z + m^2_q & m_q\big(A_q - \mu\,(\tan\beta)^{-2I^{3L}_q}\big) \\ m_q\big(A_q - \mu\,(\tan\beta)^{-2I^{3L}_q}\big) & M^2_{\{\tilde{U},\,\tilde{D}\}} + e_q\, s^2_W \cos 2\beta\, m^2_Z + m^2_q \end{pmatrix} (U^{\tilde{q}})^\dagger = \begin{pmatrix} m^2_{\tilde{q}_1} & 0 \\ 0 & m^2_{\tilde{q}_2} \end{pmatrix}, \tag{6.30}$$

where e_q is the fractional charge of the squark in units of e, s_W is the sine of weak mixing angle, I^{3L}_q is the weak isospin of the squark, and $U^{\tilde{q}}$ are the squark mixing matrices. The generation indices have been suppressed since only the third generation squarks are considered here. As it is well known, we have to consider both the stop and the sbottom sector at the same time, since due to $SU(2)$ symmetry the mass matrices share a common soft breaking parameter $M^2_{\tilde{Q}}$ connecting the two sectors. In fact, out of the total set of eleven parameters $M^2_{\tilde{Q}}, M^2_{\tilde{U}}, M^2_{\tilde{D}}, A_t, A_b, \theta_{\tilde{t}}, \theta_{\tilde{b}}, m^2_{\tilde{t}_1}, m^2_{\tilde{t}_2}, m^2_{\tilde{b}_1}$, and $m^2_{\tilde{b}_2}$, only five are completely independent and can be considered as input parameters. Their counterterms can then be freely chosen. The remaining parameters are derived by requiring that Eq. (6.30) is valid even at one-loop order.

Here, we adopt a hybrid on-shell/$\overline{\text{DR}}$ renormalization scheme choosing as input the parameters $A_t, A_b, m^2_{\tilde{t}_1}, m^2_{\tilde{b}_1}$, and $m^2_{\tilde{b}_2}$, where the trilinear couplings A_t, A_b are defined in the $\overline{\text{DR}}$ renormalization scheme and all input masses are defined on-shell. This choice is motivated by the fact that we want to obtain a renormalization scheme which is applicable for all annihilation and coannihilation processes, where squarks play an important role. For example, as the coannihilation processes are extremely sensitive to the mass of the lightest stop and as this mass also plays an important role in the t-channel exchange of neutralino annihilations [137], we choose to include its mass in the input parameters. It is then crucial to take its physical/on-shell definition. Moreover, due to the appearance of the trilinear parameters A_t, A_b in the important Higgs-squark-squark coupling in the coannihilation processes, it is a natural choice to include them in our input set as well. Given the possible problems with the one-loop definition of the A_b parameter widely discussed in the literature [171, 183, 184], we choose to define both trilinear parameters in the $\overline{\text{DR}}$ scheme. A different approach would be to define these parameters in the on-shell scheme, e.g. through the decay process of a squark into a squark and a Higgs boson [170]. This, however, would require a dedicated treatment of the infrared divergences arising in such a calculation.

Having explained above our choice of renormalization scheme, we must now specify the counterterms for the input parameters depending on their definition. The counterterms for the on-shell masses $m^2_{\tilde{t}_1}, m^2_{\tilde{b}_1}$, and $m^2_{\tilde{b}_2}$ are defined in the usual way as

$$\delta m^2_{\tilde{q}_i} = \Re\left[\Pi^{\tilde{q}}_{ii}(m^2_{\tilde{q}_i})\right]. \tag{6.31}$$

The $\overline{\text{DR}}$ counterterms of the trilinear parameters contain only the UV poles and can be given in terms of other $\overline{\text{DR}}$ counterterms as

$$\begin{aligned}\delta A_{\tilde{q}}^{\overline{\text{DR}}} &= \frac{1}{m_q}\Bigg[U_{11}^{\tilde{q}}U_{12}^{\tilde{q}}(\delta m_{\tilde{q}_1}^2)^{\overline{\text{DR}}} + U_{21}^{\tilde{q}}U_{22}^{\tilde{q}}(\delta m_{\tilde{q}_2}^2)^{\overline{\text{DR}}} + \left(U_{21}^{\tilde{q}}U_{12}^{\tilde{q}} + U_{11}^{\tilde{q}}U_{22}^{\tilde{q}}\right)\left(m_{\tilde{q}_1}^2 - m_{\tilde{q}_2}^2\right)\delta\theta_{\tilde{q}}^{\overline{\text{DR}}} \\ &\quad - \frac{\delta m_q^{\overline{\text{DR}}}}{m_q}\left(U_{11}^{\tilde{q}}U_{12}^{\tilde{q}}m_{\tilde{q}_1}^2 + U_{21}^{\tilde{q}}U_{22}^{\tilde{q}}m_{\tilde{q}_2}^2\right)\Bigg]. \end{aligned} \tag{6.32}$$

The remaining $\overline{\text{DR}}$ counterterms for squark masses and their mixing angle are given as (for $j \neq i$; for the quark mass counterterm see Eq. (6.17))

$$\begin{aligned}(\delta m_{\tilde{q}_i}^2)^{\overline{\text{DR}}} &= \frac{\alpha_s C_F}{4\pi}\frac{c_\varepsilon}{\varepsilon}\Bigg[\left((U_{i1}^{\tilde{q}})^2 - (U_{i2}^{\tilde{q}})^2\right)^2 m_{\tilde{q}_i}^2 - m_{\tilde{q}_i}^2 + \left(U_{21}^{\tilde{q}}U_{11}^{\tilde{q}} - U_{22}^{\tilde{q}}U_{12}^{\tilde{q}}\right)^2 m_{\tilde{q}_j}^2 \\ &\quad + 8m_q m_{\tilde{g}}\, U_{i1}^{\tilde{q}}U_{i2}^{\tilde{q}} - 4m_{\tilde{g}}^2 - 4m_q^2\Bigg], \\ \delta\theta_{\tilde{q}}^{\overline{\text{DR}}} &= \frac{\alpha_s C_F}{4\pi}\frac{c_\varepsilon}{\varepsilon}\frac{1}{(m_{\tilde{q}_1}^2 - m_{\tilde{q}_2}^2)}\Bigg[\left(U_{21}^{\tilde{q}}U_{11}^{\tilde{q}} - U_{22}^{\tilde{q}}U_{12}^{\tilde{q}}\right)\Big(\left((U_{11}^{\tilde{q}})^2 - (U_{12}^{\tilde{q}})^2\right)^2 m_{\tilde{q}_1}^2 \\ &\quad + \left((U_{21}^{\tilde{q}})^2 - (U_{22}^{\tilde{q}})^2\right)^2 m_{\tilde{q}_2}^2\Big) + 4m_{\tilde{g}}m_q\left(U_{11}^{\tilde{q}}U_{22}^{\tilde{q}} + U_{12}^{\tilde{q}}U_{21}^{\tilde{q}}\right)\Bigg]. \end{aligned} \tag{6.33}$$

The values of the dependent parameters $M_{\tilde{Q}}^2, M_{\tilde{U}}^2, M_{\tilde{D}}^2, m_{\tilde{t}_2}^2, \theta_{\tilde{t}}$, and $\theta_{\tilde{b}}$ are determined using Eq. (6.30). For example, by taking a trace and a determinant of both sides of Eq. (6.30) for stops and sbottoms, we can relate the four parameters $M_{\tilde{Q}}^2, M_{\tilde{U}}^2, M_{\tilde{D}}^2$, and $m_{\tilde{t}_2}^2$ to the on-shell sfermion masses and the other parameters of the mass matrix such as μ or $\tan\beta$, which do not receive any QCD corrections and hence do not require renormalization. Having determined all mass parameters, we diagonalize the stop and sbottom mass matrices leading to the values of both mixing matrices. The eigenvalues are then the chosen on-shell masses and by construction the dependent mass $m_{\tilde{t}_2}^2$.

The counterterms of the dependent parameters are derived also from the defining Eq. (6.30). We do not give counterterms for $M_{\tilde{Q}}^2, M_{\tilde{U}}^2, M_{\tilde{D}}^2$ as they never appear in any vertex. Unlike in other analyses where the mixing angles are the input parameters and their counterterms are, e.g., given as a combination of wave-function renormalization constants [172], here both mixing angles $\theta_{\tilde{t}}$ and $\theta_{\tilde{b}}$ are dependent and have the counterterms

$$\begin{aligned}\delta\theta_{\tilde{q}} = \frac{1}{\left(U_{21}^{\tilde{q}}U_{12}^{\tilde{q}} + U_{11}^{\tilde{q}}U_{22}^{\tilde{q}}\right)\left(m_{\tilde{q}_1}^2 - m_{\tilde{q}_2}^2\right)}\times \\ \Big(\delta m_q\left(A_q - \mu\,(\tan\beta)^{-2I_q^{3L}}\right) + m_q\,\delta A_q - U_{11}^{\tilde{q}}U_{12}^{\tilde{q}}\left(\delta m_{\tilde{q}_1}^2 - \delta m_{\tilde{q}_2}^2\right)\Big).\end{aligned}$$

In the case of the stop mixing matrix this counterterm includes the last remaining undetermined counterterm of the mass of the heavy stop quark

$$\delta m^2_{\tilde{t}_2} = \frac{1}{U^{\tilde{t}}_{21}U^{\tilde{t}}_{12}} \quad \Bigg[\left(U^{\tilde{t}}_{21}U^{\tilde{t}}_{12} + U^{\tilde{t}}_{11}U^{\tilde{t}}_{22}\right)\Big((U^{\tilde{b}}_{11})^2\delta m^2_{\tilde{b}_1} + (U^{\tilde{b}}_{21})^2\delta m^2_{\tilde{b}_2} + 2U^{\tilde{b}}_{11}U^{\tilde{b}}_{21}\big(m^2_{\tilde{b}_1} - m^2_{\tilde{b}_2}\big)\delta\theta_{\tilde{b}} - 2m_b\delta m_b - (U^{\tilde{t}}_{11})^2\delta m^2_{\tilde{t}_1} + 2m_t\delta m_t\Big) - 2U^{\tilde{t}}_{11}U^{\tilde{t}}_{21}\Big(\delta m_t\big(A_t - \mu/\tan\beta\big) + m_t\,\delta A_t - U^{\tilde{t}}_{11}U^{\tilde{t}}_{12}\delta m^2_{\tilde{t}_1}\Big)\Bigg]. \tag{6.34}$$

This concludes the discussion of our renormalization scheme. We have discussed in detail the definition and renormalization of every relevant parameter in the quark and squark sector. A clever choice of parameters allows to obtain a renormalization scheme which works in large parts of the relevant parameter space of the MSSM for all annihilation and coannihilation processes where quarks and squarks play an crucial role.

6.3. Real corrections and infrared treatment

6.3.1. Introduction

Including only the virtual corrections with the renormalization constants does not lead to a finite result as some diagrams where a gluon is exchanged lead to a different type of divergence - the infrared (IR) divergence - which appear when the gluon become soft, i.e. when its energy goes to zero. These divergences appear in some of the involved Passarino-Veltman integrals and cancel against similar divergences that come from the real radiation corrections. These real correction Feynman diagrams correspond to diagrams where a real massless particle is emitted from one of the particles present at tree-level (a gluon in our case). A real gluon can therefore be emitted by a (internal or external) quark or squark, but also from a four-vertex involving squarks and a vector boson, as can be seen in Fig. 6.6. The cancellation of these divergences is not as straightforward as in the case of ultraviolet divergences discussed above. It is because the IR divergence in the virtual diagrams can be explicitly isolated again by working in a general dimension D, whereas the divergence in the real corrections comes from the numerical phase-space integration over the gluon phase-space. In this section we will detail the procedure used to extract and cancel these kind of divergences, as well as other kind of IR divergences, appearing when an internal particle become on its mass shell for example.

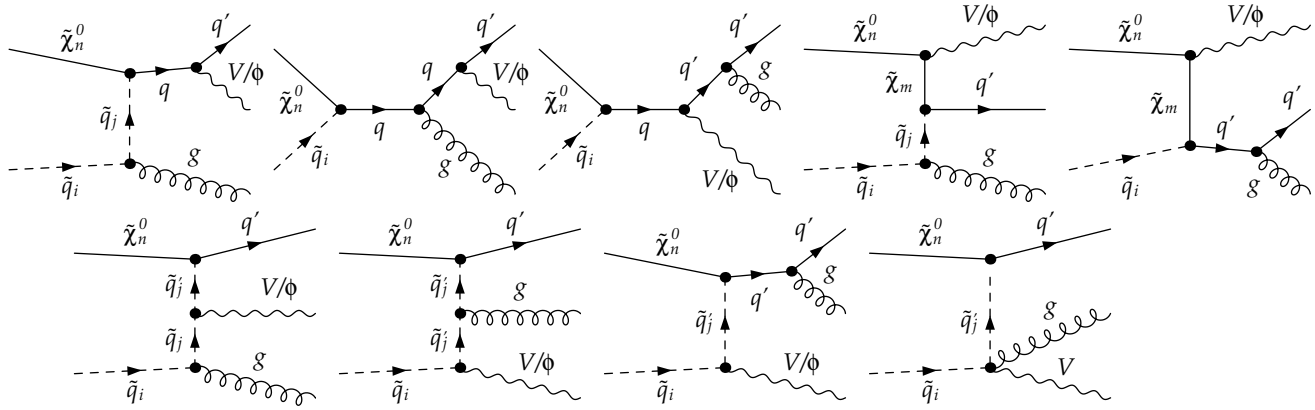

Figure 6.6.: Real gluon emission diagrams at one-loop level contributing to neutralino-squark coannihilation into quarks and Higgs (ϕ) or electroweak gauge (V) bosons. The last diagram involving the four-vertex is absent for a scalar in the final state.

6.3.2. Cancellation of soft divergences

Several approaches exist in order to cancel these divergences, most notably the so-called phase-space slicing method [185–187] or the dipole subtraction method [188] (see App. B). Here we use the phase-space slicing method which uses a lower cut on the gluon energy ΔE in the phase-space integration to split the real gluon radiation cross section is split into two parts:

$$\sigma_{2\to3}(\Delta E) = \sigma_{\text{soft}}(\Delta E, D) + \sigma_{\text{hard}}(\Delta E). \tag{6.35}$$

The cutoff ΔE render the hard gluon radiation finite after numerical integration, while the missing divergent piece of the phase-space integral can be performed analytically in the limit of small energy of the gluon - the so-called soft-gluon approximation. In dimensional reduction the divergences obtained in the soft-gluon approximation appears as $1/(D-4)$ poles and then cancel analytically with those coming from the virtual corrections. In the soft-gluon approximation the phase-space factorizes with the two final state phase space, and the squared amplitudes factorizes with the tree-level one, which allows to factorize the cross section with the tree-level cross section.

First, the three-body phase space element in D dimensions is given by

$$d\Gamma_3 = \frac{d^{D-1}p_3}{2p_3^0(2\pi)^{D-1}} \frac{d^{D-1}p_4}{2p_4^0(2\pi)^{D-1}} \frac{d^{D-1}p_5}{2p_5^0(2\pi)^{D-1}} (2\pi)^D \delta^D(p_1 + p_2 - p_3 - p_4 - p_5)\,. \tag{6.36}$$

Using the soft gluon approximation (i.e. setting $p_5 = 0$ in the delta function, where p_5 is the four-momentum of the gluon), it can be factorized into

$$d\Gamma_3^{\text{soft}} = d\Gamma_2 \frac{1}{(2\pi)^3} \frac{d^{D-1}p_5}{(2\pi)^{D-4}} \frac{1}{2E_5} \tag{6.37}$$

where $d\Gamma_2$ is the two-body phase space element

$$d\Gamma_2 = \frac{d^{D-1}p_3}{2p_3^0(2\pi)^{D-1}} \frac{d^{D-1}p_4}{2p_4^0(2\pi)^{D-1}} (2\pi)^D \delta^D(p_1 + p_2 - p_3 - p_4)\,. \tag{6.38}$$

Since the soft gluon approximation which has been used is valid only for very small energy one can use this phase-space factorization only when the energy of the gluon is smaller than a chosen cutoff: $E_5 \leq \Delta E$. The soft gluon approximation can be also used in the calculation of the amplitudes to factorize it:

$$|M_3^{\text{soft}}|^2 \simeq -g_s^2\, \mu^{4-D} \sum_{f,f'=2,3} \frac{p_f \cdot p_{f'}}{(p_f \cdot p_5)\ (p_{f'} \cdot p_5)} |M^{\text{tree}}|^2 \tag{6.39}$$

where $|M^{\text{tree}}|^2$ is the squared tree-level amplitude, and μ is here to preserve the dimension of the strong coupling and is called factorization scale. It can be identified with the renormalization scale which has been discussed in Sec. 6.2.2, and we set both scales to the center-of-mass energy $\sqrt{s}$. f and f' are summed over the two external particles emitting a gluon: the initial squark (p_2) and the final quark (p_3). Putting everything together one obtains the differential cross section which factorizes as the following:

$$d\sigma^{\text{soft}} = -d\sigma^{\text{tree}} \frac{\alpha_s}{(2\pi)^2} \sum_{f,f'=2,3} I_{ff'} \tag{6.40}$$

where $d\sigma^{\text{tree}}$ is the tree-level differential cross section and $I_{ff'}$ are soft integrals defined as

$$I_{ff'} = \mu^{4-D} \int_{E_5 \leq \Delta E} \frac{d^{D-1}p_5}{(2\pi)^{D-4}} \frac{1}{E_5} \frac{p_f \cdot p_{f'}}{(p_f \cdot p_5)\ (p_{f'} \cdot p_5)}. \tag{6.41}$$

These integrals contain the integration over the phase-space of the (soft) gluon and therefore also the divergence. They are given in [187,189]. In our case we use dimensional regularization to obtain an explicit form of the divergence:

$$I_{ff'} = \frac{4\pi\alpha\,(p_f \cdot p_{f'})}{(\alpha\, p_f)^2 - p_{f'}^2} \left\{ \frac{1}{2} \left(\log\left(\frac{4\Delta E^2}{\mu^2} \right) + \Delta_{\text{IR}} \right) \log\left(\frac{(\alpha\, p_f)^2}{p_{f'}^2} \right) + \right.$$
$$\left. \left[\frac{1}{4} \log^2\left(\frac{P^0 - |\vec{P}|}{P^0 + |\vec{P}|} \right) + \text{Li}_2\left(1 - \frac{P^0 - |\vec{P}|}{v} \right) + \text{Li}_2\left(1 - \frac{P^0 + |\vec{P}|}{v} \right) \right]_{P=p_{f'}}^{P=\alpha\, p_f} \right\}. \tag{6.42}$$

Here $\Delta_{\rm IR} = 1/\varepsilon + \log 4\pi - \gamma_E$, α is defined by $(\alpha\, p_f - p_{f'})^2 = 0$ and v by

$$v = \frac{(\alpha\, p_f)^2 - p_{f'}^2}{2(\alpha\, p_f^0 - p_{f'}^0)}. \tag{6.43}$$

The divergences contained in $d\sigma^{\rm soft}$ then cancel with the one appearing in the virtual and counterterms cross section. By looking at which particle is emitting the soft gluon it is possible to identify which real correction diagram is needed to cancel the divergence, and therefore which integral will be involved:

- The propagator and vertex counterterms diagrams have to be summed because they both involve quarks and squarks wave function renormalization constants. They then cancel with the integrals I_{22} and I_{33} in the s-, t- and u-channels diagrams.
- The boxes diagrams cancel with the integrals I_{23} and I_{32} in the s- and t-channels diagrams.
- The u-channel neutralino-squark-quark vertex correction diagram cancel with the integrals I_{23} and I_{32} in the u-channel diagrams.
- All the other virtual corrections diagrams are IR finite. In particular the s- and t-channels vertex correction diagrams are IR finite since the gluon is exchanged between external and internal particles. The virtual correction diagrams involving gluinos are also IR finite due to the non zero mass of the gluino.

As we have seen the phase-space slicing method introduces a cutoff ΔE to separate the divergent part of the phase-space from the regular one. It appears in the original real corrections as a lower limit on the integration over the energy of the gluon and also explicitly in the cross section (6.40) calculated in the soft-gluon approximation. In principle the dependence on this cutoff should completely vanish, but in practice the cancellation is limited by the stability of numerical integration of the real corrections on one hand, and by the validity of the soft gluon approximation on the other hand. For practical purposes one has to choose a value for the cutoff such that it is small enough for the soft-gluon approximation to be valid in the region of phase-space given by $E_5 \leq \Delta E$, but at the same time large enough for the numerical integration of the real correction to be still possible. In Fig. 6.7 we show the dependence of a given real radiation cross section to the value of this cutoff. On the left side of Fig. 6.7 are shown the soft and hard gluon cross sections, together with their sum, in function of the soft cutoff. it is clear that when choosing a larger cutoff, the volume of the hard gluon phase space will be reduced, and the corresponding hard radiation cross section will therefore decrease. To the contrary, the soft radiation cross section will increase, such that for different values of the cutoff the total radiation cross section (for soft and hard gluons) should be identical. For reasons discussed above the cross section will remain stable only in a given cutoff range, while it will not be the case for more extreme values. On this plot one can see that for cutoff larger

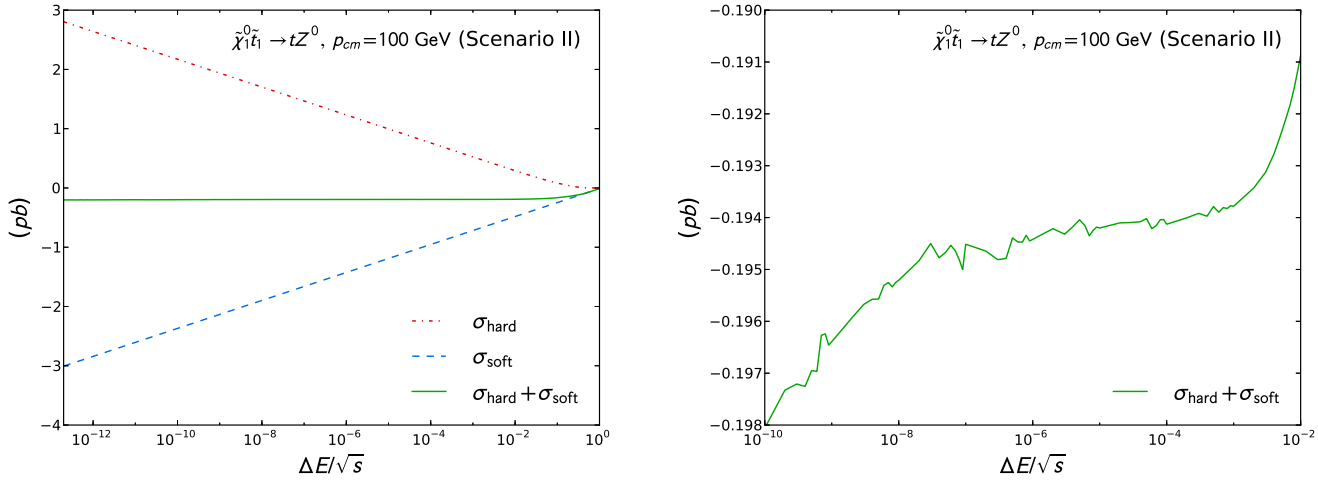

Figure 6.7.: Soft and hard gluon radiation cross sections and their sum (left plot) in function of the soft cutoff for the process $\tilde{\chi}_1^0\ \tilde{t}_1 \to t\ Z^0$ with $p_{cm} = 100$ GeV. On the right plot is shown only the sum of soft and hard cross sections on a smaller scale. The spectrum corresponds to the pMSSM scenario II introduced later in Sec. 6.4.1.

than $\sqrt{s}/10$ the total cross section clearly starts increasing with the cutoff. In the right plot of Fig. 6.7 this cross section is shown for cutoffs between 10^{-10} and 10^{-2}. It is clear that for $10^{-6} \leq \Delta E/\sqrt{s} \leq 10^{-3}$ the cross section depends only very slightly on the cutoff value. We have therefore chosen the value $\Delta E = 10^{-3}\sqrt{s}$ which allows for a faster numerical integration and verified that in our calculation all cross sections are insensitive to the choice of this cutoff.

6.3.3. Additional sources of infrared divergences

While including next-to-leading order corrections to the studied neutralino coannihilation processes, we have to take care of a few subtleties. Some processes, although well defined and separate at tree-level, cannot be unambiguously defined and separated when NLO corrections are considered. One such example is the process $\tilde{\chi}_1^0\tilde{t}_1 \to bW$. Here, additional gluon radiation can be taken to be a real correction to the Wb process. However, it can equally well be considered to be neutralino-stop coannihilation with a gluon and a top quark in the final state where the top decays into a W-boson and a bottom quark. Despite the fact that these processes cannot be separated at NLO and one should strictly speaking include also their interference, for practical purposes it is desirable to find a way how to separate them. Due to the above mentioned complication, one has to treat the process $\tilde{\chi}_1^0\tilde{t}_1 \to bWg$ with care as it contains a top quark propagator which can become on-shell. At tree-level the large masses of the neutralino and the scalar top quark prevent the internal top quark to be on-shell. In contrast, when an additional gluon is radiated either from the initial stop or the internal top-

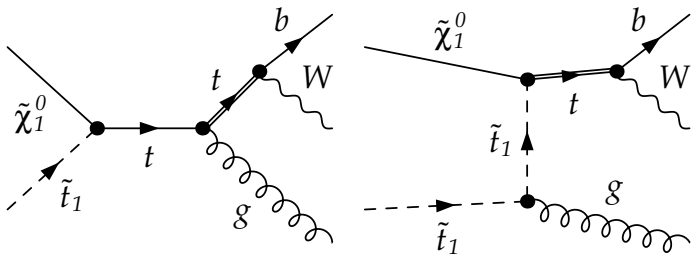

Figure 6.8.: Real gluon emission diagrams with a Wb final state where an internal top quark can become on-shell, as indicated by a double line.

quark propagator, the gluon can carry away enough energy for the top propagator to become on-shell. The relevant diagrams where this can occur are shown in Fig. 6.8.

We regularize the appearing divergence from the on-shell propagator by introducing a width Γ_t for the top quark in the problematic propagators, leading to a finite result for the integrated matrix elements for the real gluon emission. The matrix element when integrated over the whole phase-space is very large as it includes also the leading order coannihilation process $\tilde{\chi}_1^0\tilde{t}_1 \to tg$ with the top quark decaying into W^+b. This process is, however, already accounted for in the calculation of the neutralino relic density. To avoid double-counting, we need to separate the two processes. In order to treat the double-counting in the real correction contribution, we use a local on-shell subtraction scheme [190–192], in which a locally gauge invariant term is subtracted from the original cross section that has been regularized as discussed above. The subtraction term is defined as the squared resonant amplitude with the top quark being on-shell, except for the propagator denominator, which is kept as a general Breit-Wigner function

$$\left|\mathcal{M}_{2\to3}^{\texttt{sub}}\right|^2 = \frac{m_t^2\Gamma_t^2}{(p_t^2 - m_t^2)^2 + m_t^2\Gamma_t^2} \left|\mathcal{M}_{2\to3}^{\texttt{res}}\right|^2_{p_t^2=m_t^2} . \tag{6.44}$$

When the top quark is exactly on-shell, the subtraction term is equal to the full $2 \to 3$ matrix element, while it decreases as a Breit-Wigner distribution when the top quark moves away from its pole. This method has the advantage that the resulting cross section retains the non-resonant interferences of the two processes. We have checked that the total cross section after subtraction is independent of the top quark width. Other diagrams with different final states can also include on-shell propagators but for most of them only in very specific configurations, e.g., mass degeneracy between $\tilde{t}_1$ and $\tilde{t}_2$ or between $\tilde{t}_1$ and $\tilde{b}_1$. Those cases are not relevant for our study of $\tilde{\chi}_1^0\tilde{t}_1$ coannihilation.

Another numerical instability arises from the fact that, in case of coannihilation into quark and photon, also the external photon of the real emission subprocess $\tilde{\chi}_n^0\tilde{q}_i \to qg\gamma$ may become soft in certain regions of phase space, rendering the numerical integration unreliable. This issue can be addressed by introducing a cut-off on the photon energy and extracting the soft

	M_1	$M_{\tilde{q}_{1,2}}$	$M_{\tilde{q}_3}$	$M_{\tilde{\ell}}$	T_t	m_A	μ	$\tan\beta$	$m_{\tilde{\chi}_1^0}$	$m_{\tilde{t}_1}$	m_{h^0}	m_{H^0}
I	306.9	2037.7	709.7	1499.3	1806.5	1495.6	2616.1	9.0	307.1	350.0	124.43	1530.72
II	470.6	1261.2	905.3	1963.2	1514.8	1343.1	725.9	18.3	467.3	509.4	124.06	1342.77
III	314.4	2870.5	763.6	2417.7	1877.5	386.0	2301.5	10.3	316.5	371.9	123.43	367.45

Table 6.1.: Three characteristic scenarios chosen in the pMSSM, which will be considered in this study. Given are the input parameters as described in the text, the lightest neutralino mass $m_{\tilde{\chi}_1^0}$, the lightest stop mass $m_{\tilde{t}_1}$, and the masses of the light and heavy CP-even Higgs bosons m_{h^0} and m_{H^0}. All values except for $\tan\beta$ are given in GeV.

divergence using the soft photon approximation. This divergence would vanish when including also electroweak corrections, which is, however, beyond the scope of this work. We therefore cancel by hand the infrared pole, which is equivalent to including only the divergent part of the electroweak corrections. We have checked that the associated cut-off dependence was negligible for a cut-off equal to the one chosen for the QCD soft divergences described above. This details of this procedure are however not very crucial since, as we have seen in section 4.3, the impact of this process in the pMSSM is negligible.

6.4. Next-to-leading order cross sections: numerical results

6.4.1. pMSSM scenario and tree-level cross sections

For our numerical analysis, we have selected three characteristic scenarios[2], which we introduce and discuss in the following. They are listed in Tab. 6.1 and have been chosen in such a way that they represent qualitatively different scenarios (note, e.g., the differences in $M_{\tilde{q}_{1,2}}$, m_A, and μ) and that they lead to different dominant coannihilation final states. As expected from Sec. 4.3,

all three scenarios feature rather important trilinear coupling parameters $T_t \sim 1500-1800$ GeV. The selected values of $\tan\beta$ are moderate, so that neutralino pair annihilation into bottom quarks is not important here, and these scenario are not excluded by flavor observables. First and second generation squarks and sleptons are heavy compared to the stops in accordance with current LHC exclusion limits [84, 85]. Moreover, the mass difference of the lightest neutralino and the scalar top is about $10-15\%$ of the neutralino mass in each scenario and thus sufficiently small to enhance coannihilation, as explained in Sec. 4.2.1.

In Tab. 6.2 we list the resulting values for the neutralino relic density, together with the contributions from the neutralino-stop coannihilation modes, as obtained from `micrOMEGAs`

[2]Note that these scenario, originally presented in [157], have been obtained using `SPheno` version `3.2.1`. It has been recently noticed that the lightest Higgs boson mass obtained with this version could be affected by a bug. Thus the values of m_{h^0} given in Tab. 6.1, in particular for the scenario I and III, might not be correct. The remaining discussion is however independent of this issue.

	$\Omega_\chi h^2$	$\tilde{\chi}_1^0\tilde{t}_1 \to th^0$	$\tilde{\chi}_1^0\tilde{t}_1 \to tH^0$	$\tilde{\chi}_1^0\tilde{t}_1 \to tZ^0$	$\tilde{\chi}_1^0\tilde{t}_1 \to bW^+$	Sum
I	0.114	38.5%	–	3.4%	5.9%	47.8%
II	0.116	24.6%	–	10.7%	3.4%	38.7%
III	0.111	14.2%	20.7%	1.2%	2.1%	38.2%

Table 6.2.: Neutralino relic density and relative contributions of neutralino-stop coannihilation into a quark and a Higgs or electroweak gauge boson for the characteristic scenarios of Tab.6.1. The last column gives the sum of the listed contributions.

(version `2.4.1`). These will be crucial to estimate the impact of our calculations on the final relic density. Scenario I is characterized by the dominant coannihilation into a top quark and a light Higgs boson. Final states including a top quark and a Z-boson as well as a bottom quark and a W-boson contribute as well, but to a lesser extent. In total, neutralino-stop coannihilation with electroweak gauge and Higgs bosons final states accounts for almost half of the annihilation cross section at this example point. In order to understand which diagrams of Fig. 6.1 are most important in this context, we show in Fig. 6.9 the total tree-level cross sections of neutralino-stop coannihilation into the dominant final states for each characteristic scenario, together with the individual contributions of the different squared diagrams and interference terms. For the reasons discussed in Sec. 4.3, the exchange of a scalar top in the t-channel is the dominant mode at example point I, followed by its interference with the exchange of a top quark in the s-channel (upper left plot). The squared s-channel is rather small, and all other channels are even negligible in this parameter configuration, so that they are not shown in Fig. 6.9.

In comparison to the first parameter point, scenario II has a smaller μ-parameter, but a larger value of $\tan\beta$. Moreover, the gauginos and third-generation squarks are slightly heavier, and the trilinear coupling is slightly lower than for scenario I. As a consequence, the relative importance of the coannihilation channels is altered, as can be seen in Tab. 6.2. In particular, the coannihilation into the lightest Higgs boson contributes less, allowing the final state containing a Z-boson to become more important. In contrast to the coannihilation into a Higgs boson, the dominant diagram in this case is the exchange of a top quark in the s-channel, as can be seen in Fig. 6.9 (lower left plot). For this scenario, we also show the individual contributions of the three diagrams for coannihilation into a bottom quark and a W-boson (lower right plot). As in the previous case, the s-channel is the dominant mode. Its absolute cross section value is even larger than for tZ^0 due to the larger phase space. However, large destructive interferences of this diagram with the sub-leading t- and u-channels decrease its cross section, so that the total value is almost an order of magnitude smaller than for the Z-boson.

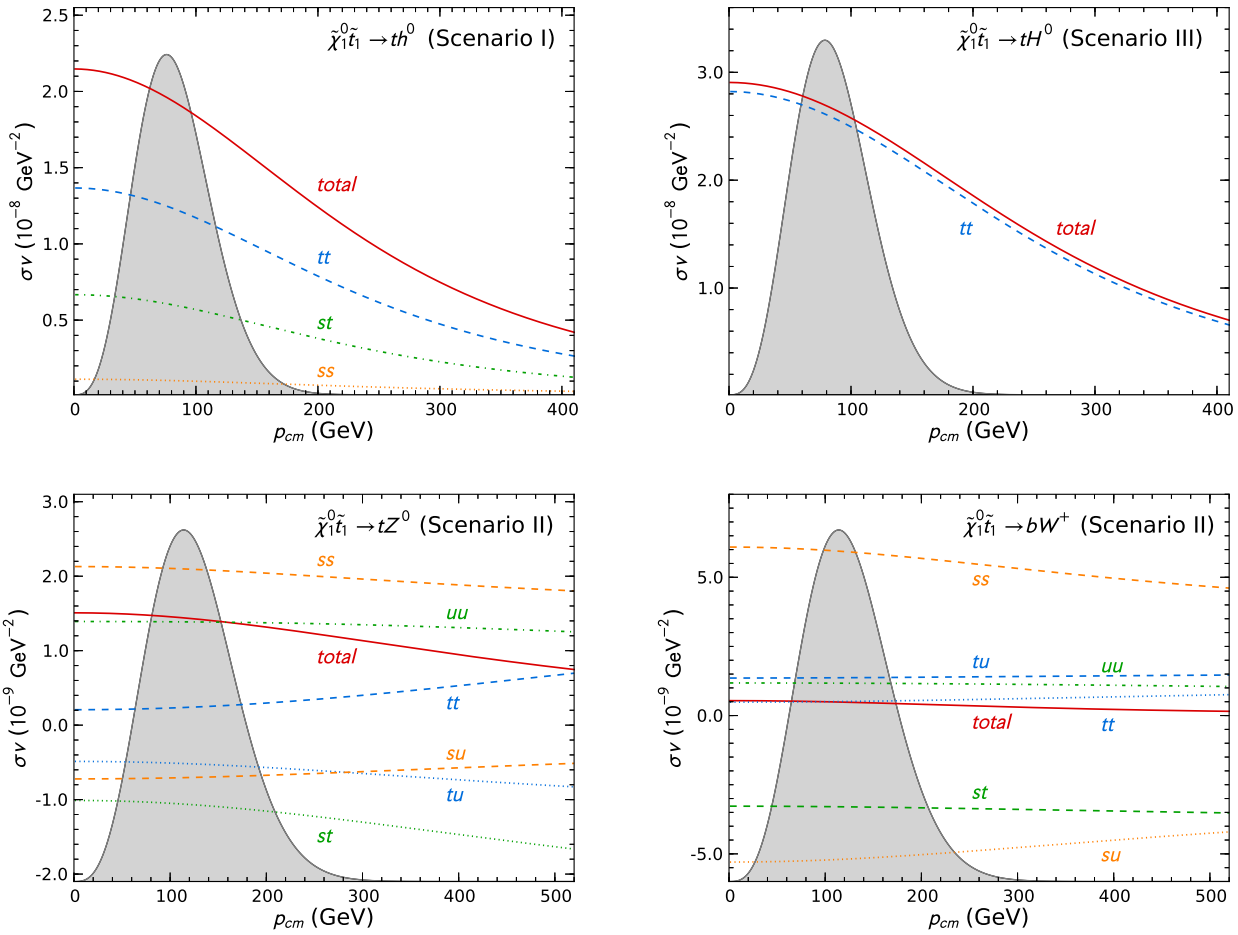

Figure 6.9.: Contribution of the different diagrams (s-, t-, and u-channels) depicted in Fig. 4.3. For the studied scenarios of Tab. 6.1 we show for selected coannihilation channels the tree-level cross section as well as the contribution of the different squared diagrams (ss, tt, uu) and the interference terms (st, su, tu).

Finally, scenario III is quite similar to scenario I with the exception of a very light pseudoscalar Higgs boson of $m_{A^0} = 386$ GeV. This leads to a similarly light heavy CP-even Higgs boson H^0 (see Tab. 6.1). As a consequence, the coannihilation into heavy CP-even Higgs bosons in association with a top quark is now open and becomes the dominant contribution to neutralino-stop coannihilation (see Tab. 6.2). The final state containing a light Higgs boson remains important, while coannihilations into Z- and W-bosons are marginal for this parameter point. As it was the case for the lightest Higgs boson, the coannihilation into tH^0 is dominated by the exchange of a scalar top in the t-channel (upper right plot of Fig. 6.9), which is again due to the enhanced trilinear coupling. The dominance is even more important here, which is explained by the modified mixing in the Higgs sector due to the smaller mass difference between h^0 and H^0.

6.4.2. Next-to-leading order cross sections

Let us now discuss in detail the numerical impact of the one-loop corrections on the coannihilation cross sections in our three scenarios of Tab. 6.1. We have calculated radiative corrections to two types of processes, one with a Higgs boson and one with a vector boson in the final state. We have seen that at tree-level the processes with the Higgs boson final state are dominated by a t-channel stop exchange, whereas the processes with a gauge vector boson are a mixture of all possible contributions (see Fig. 6.9). These different compositions of the cross sections influence also the impact of various types of loop corrections which are displayed in Fig. 6.10. This figure shows a break down of the total next-to-leading correction to the cross section σv (without the tree-level contribution) into several UV finite contributions for both types of processes, $\tilde{\chi}_1^0\tilde{t}_1 \to th^0$ (scenario I) and $\tilde{\chi}_1^0\tilde{t}_1 \to tZ^0$ (scenario II). As seen in Sec. 6.3.2, even though all contributions are UV finite, the box, vertex and real part of the correction are still IR divergent. This leads to a certain ambiguity in their exact definition. Each contribution contains an uncanceled pole along with an uncanceled logarithm of the large factorization scale (see first line of Eq. (6.42)). These large logarithms cause the box contribution to be artificially large and drive the real corrections (which in our case is a sum of the soft-gluon part and the hard radiation) to be negative.

Comparing the different loop contributions for the scalar and vector boson final states, one notices that the box and propagator corrections in the case of the Higgs boson final states are enhanced. This can be traced back to the fact that the cross section with a Higgs boson in the final state is dominated by the t-channel exchange. One of the loop corrections to the t-channel entails a correction to the stop propagator and a box diagram where a gluon is exchanged between the final state quark and the initial state squark. The enhanced box and propagator corrections lead to a large overall NLO correction in the case of the coannihilation cross section with the Higgs boson.

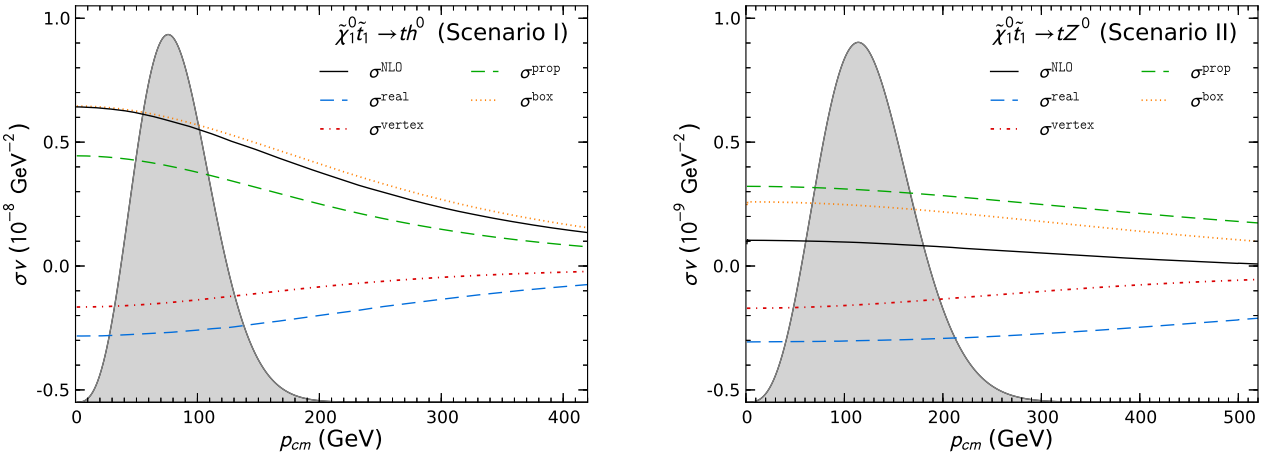

Figure 6.10.: Contribution of the different corrections to the total next-to-leading order correction for the case of coannihilation into th^0 for scenario I and into tZ^0 for scenario II. The real contribution σ^{real} is defined as the sum of the hard radiation and the soft gluon part with a cut on the gluon energy of $\Delta E = 10^{-3}\sqrt{s}$. The gray area indicates the thermal distribution (in arbitrary units).

We show the cross sections of the respectively most relevant channel in each scenario in Fig. 6.11 and compare our tree-level calculation, the effective tree-level calculation implemented in `micrOMEGAs` and our full one-loop calculation. The upper parts show the cross sections σv, while the lower panels show the ratio between the different cross sections.

For scenario I, where we show the channel $\tilde{\chi}_1^0\tilde{t}_1 \to th^0$, we have numerical agreement between our tree-level and the `micrOMEGAs` calculation. The one-loop contributions increase the cross section by about 30% caused by the large contribution from the box diagrams and propagator corrections as discussed above. We observe a similar behavior for scenario III, where the final state with a heavy Higgs boson H^0 is dominant. Here, the one-loop cross section lies about 18 – 20% above the tree-levels, which again agree well among each other.

In case of coannihilation into a quark and an electroweak gauge boson, there is a few percent difference between our tree-level and the one provided by `micrOMEGAs`. This difference stems from the fact that both tree-levels use different parameters. Our tree-level uses input parameters defined through the renormalization scheme discussed in detail in Sec. 6.2.2. It differs in several points from the parameters used by `micrOMEGAs`. More precisely, the shift between the two tree-levels is largely due to a different definition of the squark mixing angles, which enter the calculation through the different interactions between squarks and quarks, e.g., the neutralino-squark-quark vertex.

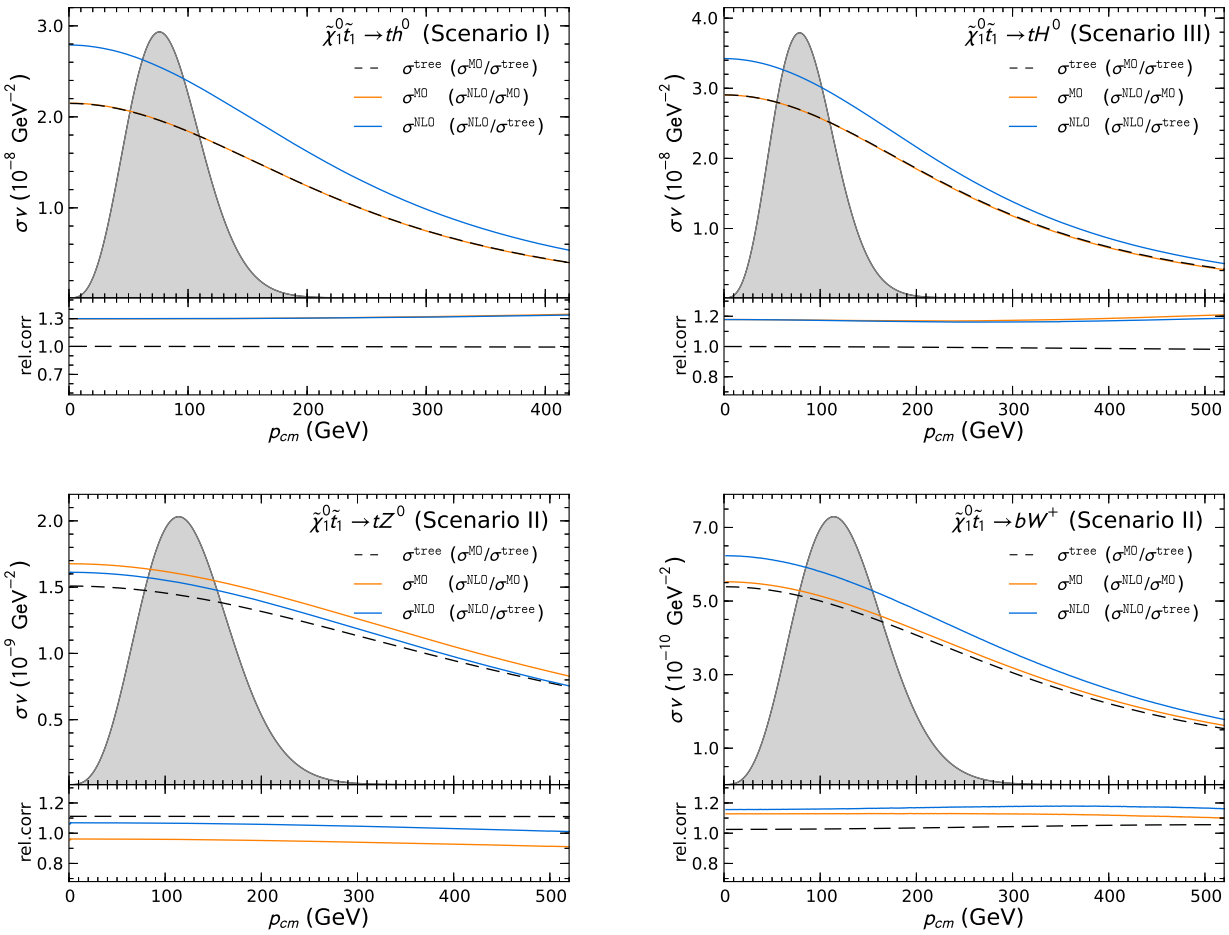

Figure 6.11.: Tree-level (black dashed line), full one-loop (blue solid line) and `micrOMEGAs` (orange solid line) cross sections for selected coannihilation channels in the scenarios of Tab. 6.1. The upper part of each plot shows the absolute value of σv together with the thermal distribution (in arbitrary units), whereas the lower part shows the corresponding relative shifts (second item in the legend).

The different influence of various definitions of the mixing angle on the two classes of processes we have calculated can be understood as follows: In the case of the Higgs boson final state, which is dominated by a squark-exchange in the t-channel, the mixing angle $\theta_{\tilde{t}}$ enters the squark-squark-Higgs and the neutralino-squark-quark vertices. The internal propagator has to be summed over the two possible squark mass eigenstates, $\tilde{t}_1$ and $\tilde{t}_2$, making the result less sensitive to the exact value of the mixing angle. For the s-channel dominated coannihilation into tZ^0 or bW^+, the situation is quite different. Here, the mixing angle appears in a single neutralino-squark-quark vertex, where the external squark is "fixed" to be $\tilde{t}_1$. The corresponding matrix element is therefore rather sensitive to changes in the mixing angle, which explains the observed difference between the two tree-level curves.

6.5. Numerical impact on the relic density

In this section we compare the neutralino relic density obtained from the three different cross section calculations: the one used by default in `micrOMEGAs`, evaluated by `CalcHEP` at tree-level, our cross section at tree-level, and our calculation including the full next-to-leading order SUSY-QCD corrections. The impact of the corrections compared to the tree-level results is studied for the three scenarios defined in Tab. 6.1.

First, we focus on scenario I. We study the change of the relic density when a single input parameter is varied around our scenario I. In Fig. 6.12, we show $\Omega_\chi h^2$ as a function of the bino mass parameter M_1 and the trilinear coupling parameter T_t, calculated on the basis of the aforementioned three calculations for the neutralino-stop coannihilation. It is clearly visible that the relic density is very sensitive to variations of the bino mass parameter. For higher values of M_1 the predicted relic density decreases rapidly due to a smaller mass splitting between the lightest neutralino and the lightest stop, which enhances the neutralino-stop coannihilation and in addition the stop-stop annihilation. In contrast, slightly lower values for the bino mass parameter increase the mass difference and suppress the contribution of coannihilation processes in favor of neutralino-neutralino annihilation. The predicted relic density is then higher due to the absence of coannihilation. Within the area which is favored by the measurements of the relic density, where the studied neutralino-stop coannihilation is dominant, a clear shift of the predicted relic density is visible when going from the default value calculated by `micrOMEGAs` to the one calculated using our full next-to-leading order result.

The impact of the presented SUSY-QCD corrections to the given neutralino-stop coannihilation processes is even better visible in the lower part of Fig. 6.12, where we show the relative correction, i.e. the ratio of the relic density calculated with our full one-loop coannihilation cross section to the one included by default in `micrOMEGAs` and our tree-level, respectively. For scenario I, our calculations result in a relative correction of about 9%. This can be ex-

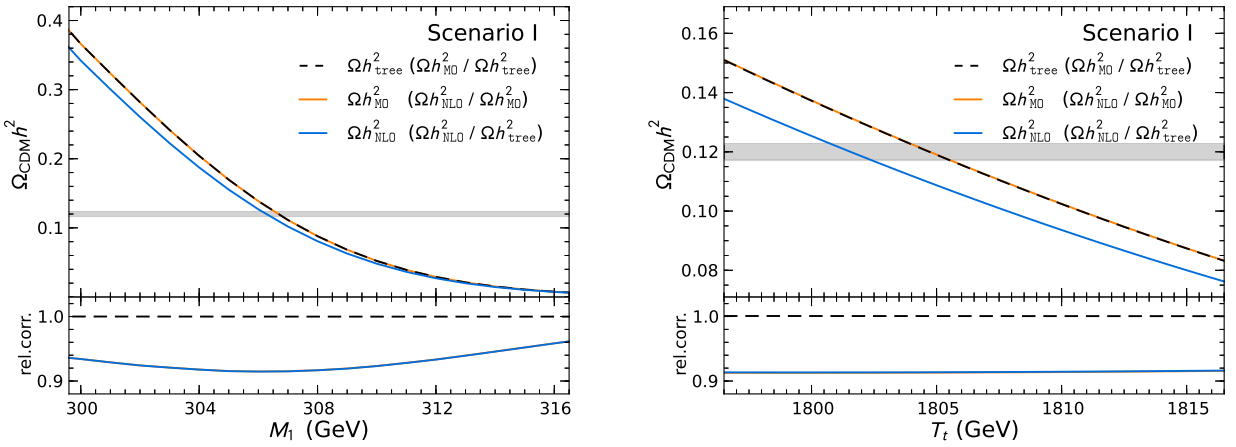

Figure 6.12.: The neutralino relic density $\Omega_\chi h^2$ as a function of M_1 (left) and T_t (right) in our scenario I calculated using different coannihilation cross sections: default `micrOMEGAs` (orange solid line), tree-level (black dashed line), and full one-loop (blue solid line). The gray band indicates the favored range according to Eq. (1.6) within 1σ. The lower part shows the relative impact of the one-loop correction on the relic-density compared to the tree-level calculation (second item in the legend).

plained by the lightest Higgs final state, which has a contribution of around 38.5% to the total (co)annihilation cross section with a corresponding correction of around 30% (see Fig. 6.11). With the current experimental uncertainty of about 2% according to Eq. (1.6), the impact of the presented corrections is significant and thus important to be taken into account.

The relic density is less sensitive to varying the trilinear coupling parameter T_t around the value in scenario I ($T_t = 1806.5$ GeV). This is depicted on the right-hand side of Fig. 6.12. Here, the difference between the uncorrected and corrected relic density in the cosmologically favored region corresponds to a difference of 3 GeV in the parameter T_t.

One can infer more about the impact of the full next-to-leading order corrections in scenario I when looking at the first row of Fig. 6.13. On the left, the Planck favored region is shown as a function of two parameters - the mass parameter of the third generation of squarks $M_{\tilde{q}_3}$ and the bino mass parameter M_1. In the same plot solid black contour lines denote the relative impact of our correction to the default `micrOMEGAs` relic density. As the coannihilation into the lightest Higgs is the dominant contribution to the total (co)annihilation cross section around the Planck-favored region in this scenario, and as it receives large corrections, a relative correction of up to 9% on the relic density is observed. The correction is larger than current experimental uncertainties, which results in two separated Planck-favored 1σ-bands corresponding to the default `micrOMEGAs` calculation (orange) and our full one-loop SUSY-QCD calculation (blue).

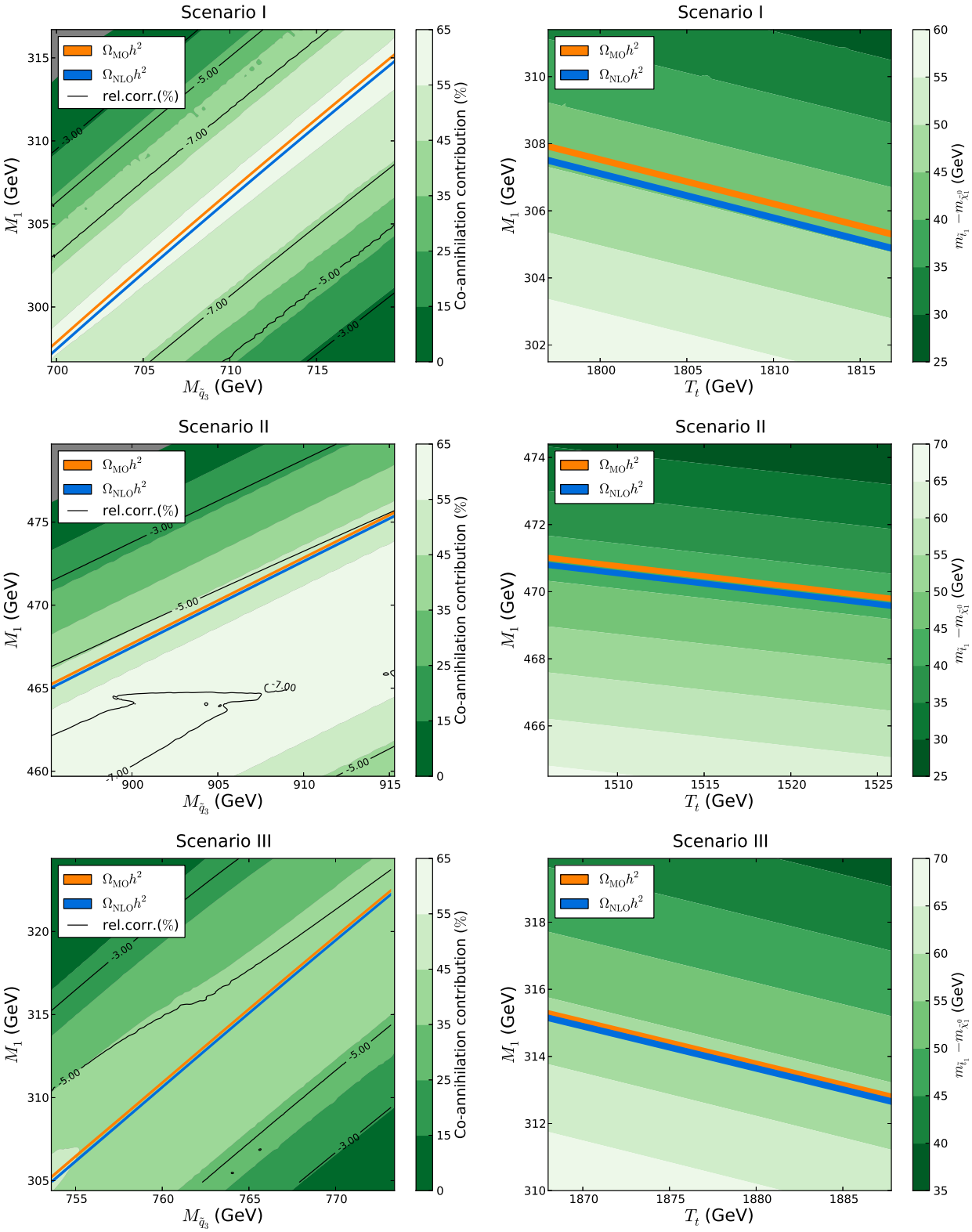

Figure 6.13.: 1σ Planck-compatible relic density bands from the default `micrOMEGAs` calculation (orange) and our one-loop calculation for coannihilation (blue) in the $(M_{\tilde{q}_3}, M_1)$ (left) and (T_t, M_1) (right) planes. In the plots on the left hand side the relative contribution of coannihilation processes is shown in green contour, and the relative impact of the one-loop corrections on the relic density in black lines. The plots on the right hand side show the LSP-NLSP mass difference in green contour.

The cosmologically allowed band follows a straight line in the M_1-$M_{\tilde{q}_3}$ plane corresponding to a constant mass difference between the lightest neutralino and the lightest stop of about 40 GeV, or 14% of the neutralino mass. Above this band where the neutralino becomes heavier and the mass difference decreases, the stop-stop annihilation becomes dominant. As it has typically a significant higher cross section than the coannihilation, it leads to a relic density which is too small. For large values of M_1 (in the gray area in the upper left corner) the stop becomes the lightest supersymmetric particle, which is disfavored as a suitable dark matter candidate both for its electric and color charge. In the opposite direction, below the allowed band, the neutralino-stop and stop-stop (co)annihilation are Boltzmann suppressed by a larger mass difference and neutralino annihilation becomes dominant. However, it has a lower cross section, such that the relic density becomes too big.

To conclude our analysis of scenario I, on the right plot in Fig. 6.13 we show Planck preferred regions in the (T_t, M_1) plane. Again, a clear separation of the two bands is visible, together with the small dependence on the trilinear coupling parameter T_t (as already discussed for Fig. 6.12). In different green colors, the mass difference between the lightest and next-to-lightest supersymmetric particle is depicted supporting the claim that the cosmologically favored region follows a contour of a constant mass difference around $10-15\%$ (see Sec. 4.2.1).

Let us now focus on scenario II, which differs in several crucial features from the previously analyzed scenario I. One example is that the total coannihilation cross section has two dominating contributions from coannihilation into the lightest Higgs and into the Z-boson. In Fig. 6.14 we show separately the effect of SUSY-QCD corrections to each of the two dominant processes as a function of the parameters $M_{\tilde{q}_3}$ and T_t. One can see distinctly different effects higher order corrections have on each process. As in scenario I, large corrections to coannihilation into the lightest Higgs bosons lead to a change of up to 6% in the relic density even though its relative importance in the total cross section dropped to 24% compared to scenario I. On the other hand corrections to coannihilation into the Z-boson are small (see Fig. 6.11) and also differ in sign. This leads to a reduction of the impact of SUSY-QCD corrections on the relic density in scenario II. The consequences can be seen in the second row of Fig. 6.13. One sees that due to the smaller correction of about $5-6\%$, the two bands corresponding to the original `micrOMEGAs` relic density (orange) and the one obtained including our SUSY-QCD corrections (blue) almost overlap.

Scenario II is different from the others also in that the preferred Planck region lies outside of the area with maximal coannihilation fraction. This is a direct consequence of the importance of the coannihilation into the Z-boson which has a smaller cross section and so in total coannihilation is not efficient enough to bring the relic density down to the level measured by Planck. The allowed region therefore lies where the mass difference is smaller (only 9% in this scenario), and receives sizable contributions from stop annihilations.

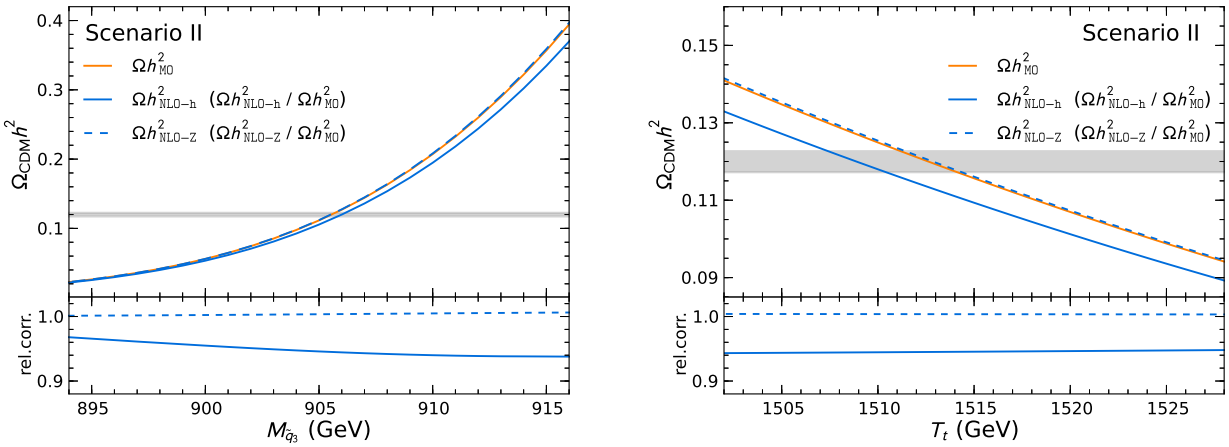

Figure 6.14.: The neutralino relic density $\Omega_\chi h^2$ as a function of $M_{\tilde{q}_3}$ (left) and T_t (right) in our scenario II calculated using different coannihilation cross sections: default `micrOMEGAs` (orange solid line), one-loop correction only for the th^0 final state (blue solid line), and one-loop correction only for the tZ^0 final state (blue dashed line). The gray band indicates the favored range according to Eq. (1.6). The lower part of the figure shows the relative impact of the one-loop correction on the relic-density compared to `micrOMEGAs` (second item in the legend).

In the third scenario, the light CP-even Higgs boson is the dominant contribution to neutralino-stop coannihilation and the characteristics of the plots in Fig. 6.13 are similar to scenario I. As the correction to the top-H^0 final states is not as large as for the top-h^0 final state in this example point (see Fig. 6.11), the overall impact on the relic density is thus smaller than for scenario I. A relative correction between 5% to 6% is reached. Nevertheless, a shift from the Planck favored region calculated by `micrOMEGAs` to the one calculated with the one-loop SUSY-QCD corrections is visible. It is interesting to note that even if the preferred region lies in the band where the mass splitting between the neutralino and stop is around 17% of the neutralino mass, stop annihilation is important here. Indeed, stop annihilation into heavy Higgs is enhanced by the small mass of H^0. As a result, the total contribution of coannihilation processes is again smaller as compared to the scenario I.

Studying the three different characteristic scenarios, we saw that the impact of the one-loop corrections on the predicted relic density of dark matter was around 5 to 9%, i.e. more important than the current experimental uncertainty of 2% by the Planck observations. Therefore it is necessary to take them into account for a theoretical prediction of the neutralino relic density.

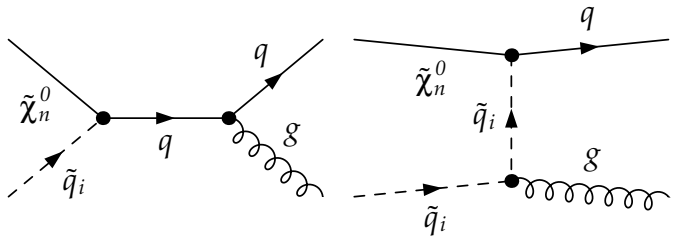

Figure 6.15.: Leading-order Feynman diagrams for neutralino-squark coannihilation into a gluon.

6.6. The gluon final state

Since we are considering QCD corrections, and as the gluon is self-interacting the case of a gluon in the final state is peculiar. As we will see in this section additional Feynman diagrams are involved and imply new treatments such as the cancellation of collinear divergences, or the renormalization of the strong coupling. At the moment the implementation of this calculation is still being cross-checked and the corresponding numerical results will be subject to a later publication.

6.6.1. Virtual corrections and renormalization

At tree-level only two Feynman diagrams are involved (see Fig. 6.15). At one-loop however, in addition to the diagrams already shown in Secs. 6.2 and 6.3 in the case of electroweak gauge bosons, there will be additional diagrams involving non-abelian interactions, i.e. $g-g-g$ or $g-\tilde{g}-\tilde{g}$ couplings. More precisely, in addition to the self-energies of the quarks and squarks shown in Fig. 6.2, we need to compute the derivatives of the gluon self-energies (see Fig. 6.16) which are involved in the vertex counterterms. Also, in addition to the diagrams shown in Fig. 6.3, the $q-q-g$ and $\tilde{q}-\tilde{q}-g$ vertices receive additional one-loop corrections shown in Fig. 6.17. Finally, new boxes diagrams shown in Fig. 6.18 have to be added to the one already shown in Fig. 6.4.

The counterterms diagrams are similar as the one shown for the electroweak gauge bosons in Fig. 6.5, excepted for the last diagram which is missing. However, the presence of a gluon at tree-level implies several complications in the calculation of the vertex counterterms. Indeed, the strong coupling constant g_s is present in the $q-q-g$ and $\tilde{q}-\tilde{q}-g$ couplings and therefore need to be renormalized by introducing a corresponding renormalization constant. The strong coupling renormalization constant can be related to the UV divergent part of the $q-q-g$ vertex correction, the quark and the gluon wave function renormalization constants. The wave

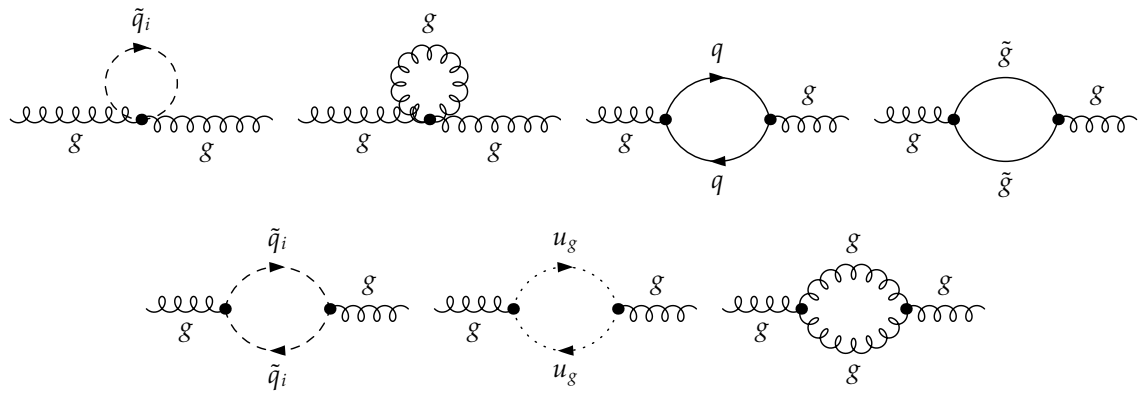

Figure 6.16.: Self-energy corrections for the gluon at one-loop level in QCD contributing to neutralino-squark coannihilation via the counterterms.

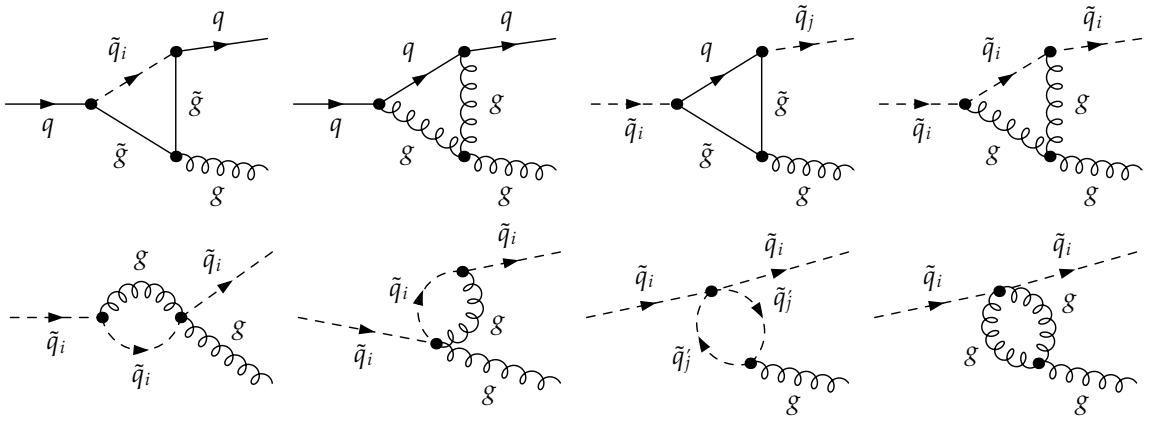

Figure 6.17.: Additional non-abelian vertex corrections at one-loop level contributing to neutralino-squark coannihilation into quarks and gluon. The lower right diagram does not contribute because of a zero color factor.

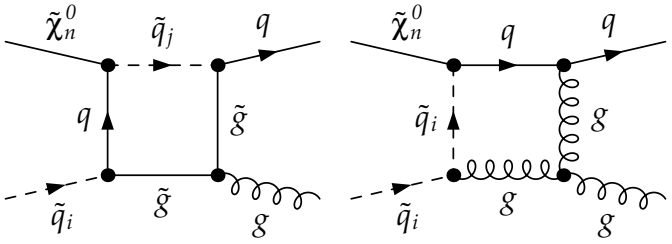

Figure 6.18.: Additional non-abelian four-point diagrams at one-loop level contributing to neutralino-squark coannihilation into quarks and gluon.

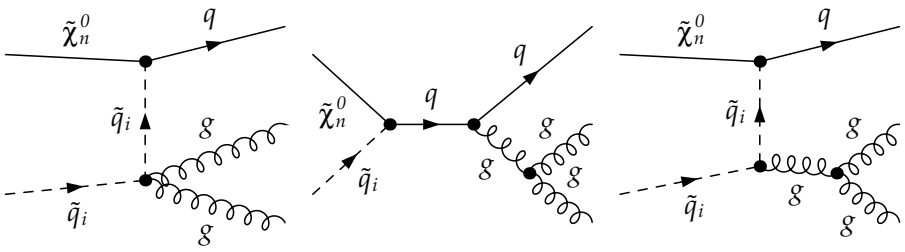

Figure 6.19.: Additional non-abelian real gluon emission diagrams contributing to neutralino-squark coannihilation into quarks gluon.

function renormalization constant of the gluon is given by

$$\delta Z = -\Re\left[\dot{\Pi}^g(m_g^2 = 0)\right] \tag{6.45}$$

where $\dot{\Pi}^g$ is the derivative of the two-point Green's function of the gluon. The strong coupling renormalization constant is then [193]

$$\delta g_s = \frac{\alpha_s}{8\pi}\frac{1}{\varepsilon}\left(n_f - 3\,C_V\right) \tag{6.46}$$

with $n_f = 6$ and $C_V = 3$.

6.6.2. Real corrections and collinear divergences

Since a real gluon can be emitted not only by squarks and quarks but also from the outgoing gluon there are additional real corrections diagrams contributing in the case of gluon final state (see Fig. 6.19). Because the gluon is massless the situation when both gluons are collinear to each other lead to a divergence. These new divergences will cancel with similar divergences present in the virtual corrections mentioned above. As it was done in the Sec. 6.3.2 in the case of soft divergences one has to extract the collinear divergences in an analytical form in order to perform the cancellation. To this end we use a more involved phase space slicing method called two cutoff method which is described in detail in App. C. This method makes use of the factorization of phase space and amplitudes to separate the soft, hard collinear and hard non collinear parts of the cross section. The soft part is treated in a similar manner as described in Sec. 6.3.2, with additional complications due to the possibility of double soft-collinear divergences, involving analytic angular integrals. The hard collinear part of the cross section is factorized using the collinear gluon approximation, leading to splitting functions which are analytically integrable, exhibiting single collinear poles. Lastly, the hard non collinear cross section is numerically integrated over the three-body phase space. These three parts are associated with regions of the phase space which are bounded by a soft and a collinear cutoff.

They therefore depend on the value of these cutoff, and the independence of the total cross section need again to be checked.

The first diagram of Fig. 6.19 is finite, whereas the two others lead to collinear divergences. For reasons discussed in App. C, when these diagrams are squared they give the only contribution to the hard-collinear gluon cross section (i.e. containing a single collinear pole), and they do not contribute to the soft gluon cross section. On the other hand, the interferences of these diagrams with soft diagrams, as the ones shown in Fig. 6.6, lead to soft-collinear double poles. Similarly to the discussion of Sec. 6.3.2 in the case of electroweak gauge and Higgs bosons, we now detail the cancellation of these additional collinear diagrams in the gluon case:

- The propagator and vertex counterterm diagrams now contain the gluon wave function renormalization constant, which has a hard-collinear single pole. The latter cancels with the hard-collinear integral discussed in App. C.2.

- The second box diagram of Fig. 6.18 has a soft-collinear double pole. When squared with the s-channel, it cancels with the soft-collinear integrals I_{24} times the squared s-channel and I_{34} times the s- and t-channels interference. When squared with the t-channel, it cancels with the soft-collinear integrals I_{34} times the squared t-channel and I_{24} times the s- and t-channels interference. The soft-collinear integrals are discussed in App. C.1.

- The second vertex correction diagram of Fig. 6.17 also has a soft-collinear double pole. When squared with the s-channel, it cancels with the soft-collinear integral I_{34} times the squared s-channel. When squared with the t-channel, it cancels with the soft-collinear integrals I_{24} times the squared s-channel and I_{34} times the s- and t-channels interference.

- Again, the fourth vertex correction diagram of Fig. 6.17 has a soft-collinear double pole. When squared with the s-channel, it cancels with the soft-collinear integrals I_{34} times the squared t-channel and I_{24} times the s- and t-channels interference. When squared with the t-channel, it cancels with the soft-collinear integral I_{24} times the squared t-channel.

- There is another real radiation diagram, not shown here, where the gluon split into a pair of massless quarks. When squared this diagram leads to a hard-collinear pole which cancels with the massless quark contribution to the gluon self-energy, involved in its wave function renormalization constant.

- All the other virtual correction diagrams are either IR finite, or obey the same cancellation rule as in the abelian case.

6.7. Conclusion

In order to keep up with the current and future experimental accuracies, a reduction of the theoretical uncertainty in the calculation of the dark matter relic density is necessary. The main source of uncertainty on the particle physics side comes from the calculation of the (co)annihilation cross section, which governs the Boltzmann equation and thus the prediction of the dark matter relic density. To this end, we have calculated the coannihilation of a neutralino with a stop into final states containing electroweak gauge or Higgs bosons at one-loop order in SUSY-QCD. In particular, we have defined a renormalization scheme, which can consistently be applied to all neutralino annihilation and coannihilation processes. Infrared singularities are handled using the phase-space slicing method. The present work is complementary to previous publications on radiative corrections to neutralino pair-annihilation [119, 136, 137] or coannihilation with a stop into a top quark and a gluon or a bottom quark and a W-boson [156].

We have seen that the one-loop corrections were significant and could reach 30% depending on the final states. We have also observed that the impact of the one-loop corrections on the predicted relic density of dark matter is more important than the current experimental uncertainty by the Planck observations. The presented corrections are therefore essential in predicting the neutralino relic density for a given parameter point or when extracting SUSY parameters from cosmological measurements. In order to obtain a consistent implementation of all coannihilation processes, including the missing case of a gluon final state is necessary. We have seen that additional treatment of the UV and IR divergences were necessary in this case. In particular we have described in details the two cutoff phase space slicing method used to cancel the soft and collinear divergences. Numerical results for this process will be presented in a later publication.

Appendix A.

The DM@NLO code

A.1. Structure of the code

NLO calculations involve several pieces which have to be combined together in order to obtain a consistent final numerical result: kinematic objects, relevant couplings and masses, expressions of one-loop and counterterm amplitudes, renormalization scheme, Passarino-Veltman integrals, soft and collinear integrals, etc. For clarity and convenience it is therefore mandatory to separate the computing code into several parts, each being dedicated to a specific aspect of the calculation. These different parts need of course to be linked to each other. The somewhat complicated structure of the code is shown in figure A.1. The core of the code, called "Main Code", is an interface between `micrOMEGAs` and all the needed files.

The file "main.c" is the `micrOMEGAs` file in which the different `micrOMEGAs` commands are called, like the calculation of the relic density for instance. In this file we use the built-in function "ImproveCrossSection" which allows us to give our own cross section instead of using the default one, calculated by `CalcHEP`. We first call a home-made subroutine called "SelectProcess" which checks if the processes needed in the calculation of the relic density is a neutralino-stop coannihilation process. In this case we call our interface function in the "Main Code", giving as inputs the PDG numbers of external particles, the center-of-mass momentum, the value of the phase space slicing cutoff, and other various settings. This function then calls several subroutines which perform important initializations and actions:

- `DMNLO_ModelPara` and `DMNLO_ModelIni` read MSSM parameters from `micrOMEGAs`.
- `Init_RenScheme` applies the renormalization scheme described in Sec. 6.2.3, i.e. computes the runing of α_s, self-energies of gluon, quarks and squarks, and their derivatives; computes the bottom and top quark masses in the relevant scheme; defines all needed renormalization constants.
- `NeuQ2qx_SetKinematics` identifies each external particle with a set of characteristic numbers (type, generation, mass eigenstate, etc.) and assigns the corresponding mass.

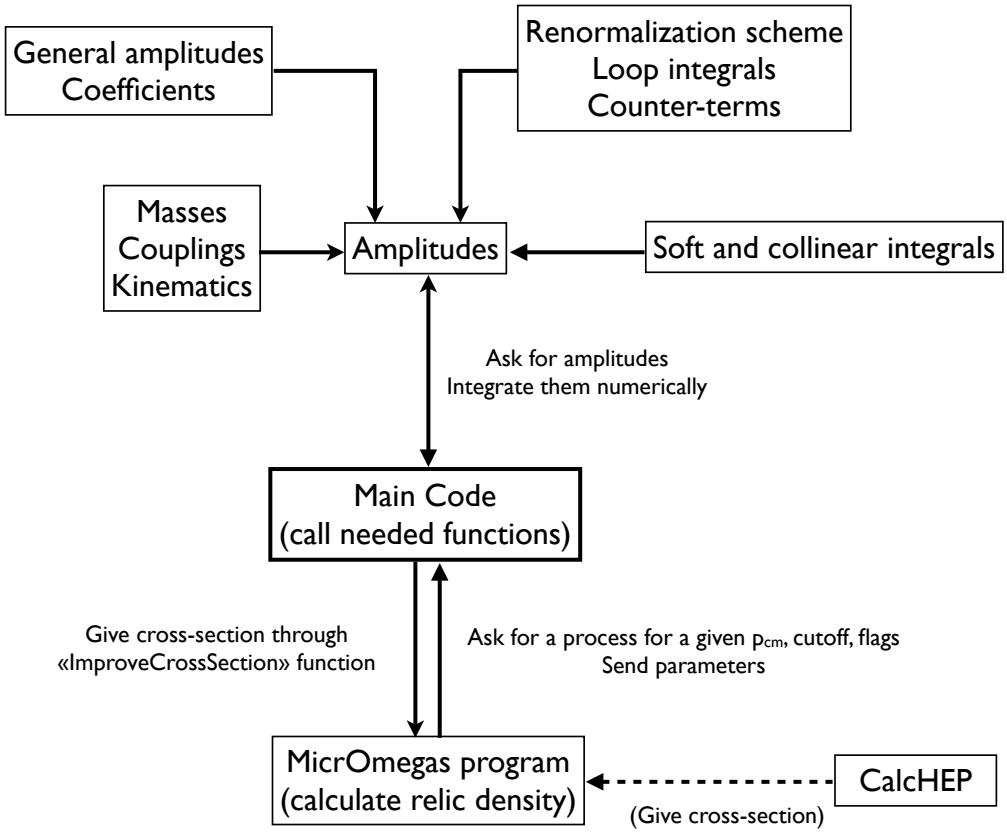

Figure A.1.: Simplified structure of the `DM@NLO` code. More details are given in the text.

- `NeuQ2qx_SetCouplings` defines all needed couplings as functions of the characteristic numbers of the involved particles.

- `NeuQ2qx_SetCounterterms` defines all propagator and coupling counterterms as a function of the renormalization constants.

- `NeuQ2qx_TreeCS` uses a Patterson integration subroutine to integrate the result obtained by calling `NeuQ2qx_DiffCS`. The latter returns as output the sum of several contributions to the differential cross section: tree-level, propagator corrections, propagator counterterms, vertex corrections, vertex counterterms, box corrections, soft gluon, soft photon in case of photon final state, hard collinear gluon in case of gluon final state.

- `NeuQ2qx_Bremsstrahlung` uses a Vegas Monte-Carlo integration (from the Cuba library [194]) to integrate the result obtained by calling `NeuQ2qx_Integrand`. The latter defines all needed kinematic variables (including scalar products) and integration boundaries, and returns as output the contribution from real gluon radiation.

- in addition, `DMNLO_LoopFunctions` contains the definition of all needed Passarino-Veltman scalar integrals as well as the reduction of tensor integrals.

These functions have either a prefix `DMNLO_` which means that this is a global function used for other processes in `DM@NLO`, or `NeuQ2qx_` which means that this is a specific function for Neutralino-stop coannihilation. The interface function returns as output the sum of all NLO cross sections, but also independent contributions in order to make debugging easier.

A.2. General amplitudes

In our general approach, at tree-level already, there is a high number of possible neutralino-squark coannihilation diagrams: 4 different neutralinos, 12 different squarks, 8 different gauge or Higgs bosons, s-, t- and u-channels. When considering all possible NLO correction diagrams (see Figs. 6.2, 6.3, 6.4, 6.5 and 6.6), it becomes mandatory to use a certain degree of generalization and automation so that implementing every single amplitude is not necessary. In this way not only the implementation and debugging are simplified, but also the compiling and execution of the code are made faster. The price to pay is a more complicated calculation and a non-trivial code structure. To this end we use what is called here "general amplitudes", which are valid for a certain class of processes and therefore usable several times for different contributions, just by assigning different values to the masses and couplings. First, all our amplitudes are separated into three categories: electroweak gauge bosons final states, Higgs bosons final states, and gluon final states. The main difference between the first and the second categories is of course the spin of one of the outgoing particle, while the last one contains additional non-abelian contributions. Then, for each of these categories and for each of the possible s-, t- and u-channel interferences, we define general amplitudes which can handle any possible structure of the propagator and vertex corrections.

For example, the general structure of the quark propagator is

$$P_p \equiv i \frac{1}{p^2 - m^2} \left(P_{vL} P_L \not{p} + P_{vR} P_R \not{p} + P_{sL} P_L + P_{sR} P_R \right) \tag{A.1}$$

where p is the momentum of the internal quark. In order to recover the tree-level propagator one needs to set $P_{sL} = P_{sR} = m$, $P_{vL} = P_{vR} = 1$, while the one-loop propagator correction will be obtained by expressing these coefficients in function of the left and right scalar and vector parts of the quark self-energy. There is no need for a general structure for the squark propagator correction since it is just a scalar number.

As we said the vertices also need to be generalized in order to take into account the one-loop corrections. The quark-quark-electroweak gauge boson coupling has the following structure:

$$\begin{aligned} B^{\mu}_{p_1p_2} \equiv i\Big(&\gamma^{\mu}(B_{sgL}P_L + B_{sgR}P_R) + (p_1+p_2)^{\mu}(B_{sm1L}P_L + B_{sm1R}P_R) \\ &+(p_1-p_2)^{\mu}(B_{sm2L}P_L + B_{sm2R}P_R) + \gamma^{\mu}(B_{vgL}P_L + B_{vgR}P_R)(\not{p}_1 - m_1) \\ &+(p_1+p_2)^{\mu}(B_{vm1L}P_L + B_{vm1R}P_R)(\not{p}_1 - m_1) + (p_1-p_2)^{\mu}(B_{vm2L}P_L + B_{vm2R}P_R)(\not{p}_1 - m_1)\Big). \end{aligned} \tag{A.2}$$

where p_1, m_1 are the momentum and mass of the incoming (off-shell) quark, p_2 is the momentum of the outgoing (on-shell) quark, and μ is the Lorentz index of the outgoing (on-shell) vector boson. Setting B_{sgL} and B_{sgR} to the tree-level left and right couplings, and all the other coefficients to zero, will return the tree-level vertex. On the other hand, NLO corrections or counterterms for this vertex will be obtained by setting these coefficients to the appropriate expressions. The general structure of the squark-squark-electroweak gauge boson coupling is:

$$C^{\mu}_{p_1p_2} \equiv i\Big(C_+(p_1+p_2)^{\mu} + C_-(p_1-p_2)^{\mu}\Big) \tag{A.3}$$

where p_1 is the momentum of the incoming (on-shell) squark, while p_2 is the momentum of the outgoing (off-shell) squark, and μ is the Lorentz index of the outgoing (on-shell) vector boson. Again, the tree-level coupling is obtained by setting $C_+ = C_{\text{tree}},\ C_- = 0$, and virtual corrections will be associated to more complicated expressions of these coefficients.

We then have general amplitudes for the boxes diagrams which can handle any possible structure of such correction. Again, as an example, the general box amplitude for a vector boson final state is the following:

$$\begin{aligned} \mathcal{M}_{\mu} \equiv \frac{1}{(4\pi)^2}\,\epsilon^{*}_{\mu}(p_4)\,\bar{u}(p_3)\Big(\quad & B_{v1L}\,p_1^{\mu}\not{p}_2\,P_L + B_{v1R}\,p_1^{\mu}\not{p}_2\,P_R + B_{s1L}\,p_1^{\mu}\,P_L + B_{s1R}\,p_1^{\mu}\,P_R \\ +\quad & B_{v2L}\,p_2^{\mu}\not{p}_2\,P_L + B_{v2R}\,p_2^{\mu}\not{p}_2\,P_R + B_{s2L}\,p_2^{\mu}\,P_L + B_{s2R}\,p_2^{\mu}\,P_R \\ +\quad & B_{v3L}\,p_3^{\mu}\not{p}_2\,P_L + B_{v3R}\,p_3^{\mu}\not{p}_2\,P_R + B_{s3L}\,p_3^{\mu}\,P_L + B_{s3R}\,p_3^{\mu}\,P_R \\ +\quad & B_{v0L}\,\gamma^{\mu}\not{p}_2\,P_L + B_{v0R}\,\gamma^{\mu}\not{p}_2\,P_R + B_{s0L}\,\gamma^{\mu}\,P_L + B_{s0R}\,\gamma^{\mu}\,P_R \quad \Big)u(p_1) \end{aligned} \tag{A.4}$$

where p_1, p_2, p_3 and p_4 are respectively the momenta of the incoming neutralino, incoming squark, outgoing quark, outgoing vector boson, all being on-shell, and μ is the Lorentz index of vector boson.

Appendix B.

Dipole subtraction method

The dipole subtraction formalism was developed in [188] and its general idea is the following. A total NLO cross section receive contributions from virtual and real corrections cross sections which are integrated over a two and a three final states phase space, respectively:

$$\sigma^{\mathrm{NLO}} = \int d\sigma^{\mathrm{NLO}} = \int_2 d\sigma^{\mathrm{Virtual}} + \int_3 d\sigma^{\mathrm{Real}}. \tag{B.1}$$

In the dipole formalism one introduce an auxiliary cross section $d\sigma^{\mathrm{Aux.}}$ which has a similar singular behavior as the virtual and real corrections cross sections. The total cross section is then expressed as

$$\sigma^{\mathrm{NLO}} = \int_2 d\sigma^{\mathrm{Virtual}} + \int_3 d\sigma^{\mathrm{Aux.}} + \int_3 \left(d\sigma^{\mathrm{Real}} - d\sigma^{\mathrm{Aux.}} \right). \tag{B.2}$$

On one hand the singularity present in $d\sigma^{\mathrm{Real}}$ is canceled by the one coming from $d\sigma^{\mathrm{Aux.}}$ and the numerical integration over the three final states phase space can be performed. On the other hand, integrating $d\sigma^{\mathrm{Aux.}}$ analytically (in dimensional reduction) over the one-particle subspace of the gluon gives explicit IR poles which cancel similar (but opposite) poles in the virtual part. This term can be then integrated numerically over the two final state phase space, and the two parts of the cross section (real and virtual) become separately convergent:

$$\sigma^{\mathrm{NLO}} = \int_2 \left(d\sigma^{\mathrm{Virtual}} + \int_1 d\sigma^{\mathrm{Aux.}} \right) + \int_3 \left(d\sigma^{\mathrm{Real}} - d\sigma^{\mathrm{Aux.}} \right). \tag{B.3}$$

The auxiliary cross section must fulfill several conditions:

- It might be universal, i.e. does not depend on a specific process.
- It must have an identical IR behavior as the real emission cross section.
- It must be analytically integrable over the one-particle phase space.

The dipole subtraction method is a recipe to construct a cross section with the required properties. The corresponding factorization formula involve, in addition to the tree-level cross

section, universal factors called dipoles. In [188] such dipoles are derived for massive or massless quarks, but also squarks and gluino. The case of initial-massive-scalar state radiation is however not covered since it is not needed for collider calculations, where squarks can only appear as final states. Nevertheless, this case is needed in our computation since the initial stop can emit a soft gluon. The implementation of a dedicated dipole subtraction method is work in progress and subject to a later publication.

Appendix C.

The two cutoff phase space slicing method

In this appendix we describe the two cutoff phase space slicing method, needed when collinear divergences appear, i.e. when the gluon is emitted by another gluon. This discussion is taken from [185]. In order to treat consistently the soft and collinear divergences, similarly as what has been done in Sec. 6.3.2 for the soft divergence, we split the cross section into different parts which will be treated differently:

$$\sigma_{2\to3}(\Delta E, \Delta\theta) = \sigma_{\text{soft}}(\Delta E, D) + \sigma_{\text{hard coll.}}(\Delta E, \Delta\theta, D) + \sigma_{\text{hard non coll.}}(\Delta E, \Delta\theta). \tag{C.1}$$

C.1. Soft part

The soft part is similar as what has been explained in Sec. 6.3.2, excepted from the fact that the angular part of the integration will be non trivial and eventually lead to collinear divergences. These additional divergences will appear only when the emitter is massless, which the case we consider here.

The three body phase space element factorization in dimensional regularization has been expressed in Eq. 6.37. Using

$$d^{D-1}p_5 = dE_5 E_5^{D-2} \sin^{D-3}\theta_1 \, d\theta_1 \sin^{D-4}\theta_2 \, d\theta_2 \Omega_{D-4} \tag{C.2}$$

we can make explicit the angular part of the integration:

$$d\Gamma_3^{\text{soft}} = d\Gamma_2 \frac{1}{(2\pi)^3} \frac{dE_5}{(2\pi)^{D-4}} \frac{E_5^{D-3}}{2} \sin^{D-3}\theta_1 \, d\theta_1 \sin^{D-4}\theta_2 \, d\theta_2 \, \Omega_{D-4}, \tag{C.3}$$

again valid for $E_5 \leq \Delta E$. Although the gluon can be soft and collinear at the same time, for the moment no additional cutoff $\Delta\theta$ is needed to separate the collinear from the non-collinear part of the phase space, in opposite to the hard-collinear case which will be described in the next section. Indeed, the soft gluon approximation is sufficient to simplify the amplitude (and

the phase space) and obtain integral which are analytically calculable. We therefore have only one cutoff ΔE.

As discussed in Sec. 6.3.2 using the soft gluon approximation lead to integrals which are expressed in Eq. 6.41. Denoting the momenta of the initial squark, final quark and final gluon respectively by p_2, p_3 and p_4, the only new integrals in comparison to Sec. 6.3.2 (i.e. the terms which give double soft-collinear divergences) are I_{24} and I_{34}, I_{44} being proportional to $p_4^2 = 0$. These two integrals are expressed as

$$I_{24} = \mu^{4-D} \int_{E_5 \leq \Delta E} \frac{dE_5 E_5^{D-3} \sin^{D-3}\theta_1 \, d\theta_1 \sin^{D-4}\theta_2 \, d\theta_2 \Omega_{D-4}}{(2\pi)^{D-4}} \frac{p_2 \cdot p_4}{(p_2 \cdot p_5)\,(p_4 \cdot p_5)}\,, \quad \text{(C.4)}$$

$$I_{34} = \mu^{4-D} \int_{E_5 \leq \Delta E} \frac{dE_5 E_5^{D-3} \sin^{D-3}\theta_1 \, d\theta_1 \sin^{D-4}\theta_2 \, d\theta_2 \Omega_{D-4}}{(2\pi)^{D-4}} \frac{p_3 \cdot p_4}{(p_3 \cdot p_5)\,(p_4 \cdot p_5)}. \quad \text{(C.5)}$$

After expressing the scalar products in function of $\sqrt{s}$, E_5, the involved masses and angles one obtains two terms: an integration over the energy, and another over the angles. The former one leads to

$$\left(\frac{4}{s}\right)^{-\varepsilon} \int_0^{\delta_s \sqrt{s}/2} dE_5 E_5^{1-2\varepsilon} \frac{1}{s E_5^2} = \frac{1}{s}\left(-\frac{1}{2\varepsilon}\right) \delta_s^{-2\varepsilon} \quad \text{(C.6)}$$

where we have defined $\delta_s \equiv 2\Delta E/\sqrt{s}$. Note that this energy integral depends on the soft cutoff, and contains a single IR pole in ε^{-1}. The term

$$\delta_s^{-2\varepsilon} = 1 - 2\varepsilon \ln \delta_s + 2\varepsilon^2 \ln^2 \delta_s + \mathcal{O}(\varepsilon^3) \quad \text{(C.7)}$$

gives additional finite contributions proportional to $\ln \delta_s$. The integration over the angles still remains to be done. The angular integrals will lead to integrals of the following form:

$$I_n^{(k,l)} = \int_0^\pi d\theta_1 \sin^{n-3}\theta_1 \int_0^\pi d\theta_2 \sin^{n-4}\theta_2 \frac{(a + b\cos\theta_1)^{-k}}{(A + B\cos\theta_1 + C\sin\theta_1 \cos\theta_2)^l}\,. \quad \text{(C.8)}$$

Some results for these angular integrals can be found for example in [185, App. B], [195, Sec. 5.3], [196, App. C], [197, App. B], [198, App. B], or [199, App. A]. The ones we need here are given in [197, Eq. (B.10)] and [195, Eq. (5.52)]. The latter one is given only to $\mathcal{O}(1)$, it was therefore needed to re-derive it to $\mathcal{O}(\varepsilon)$ since these terms combine with the soft pole in Eq. (C.6) to give a finite contribution. In the massless case the relation $A^2 = B^2 + C^2$ is valid; that leads to a special case of the integrals which contain a ε^{-1} pole. After combining it with the energy integral the final expression has a single soft pole together with a double soft-collinear pole. To the contrary, in the massive case this relation does not hold, so that the integral corresponds to a different case which has no ε^{-1} pole, the only pole comes then from the energy integration. In other words the mass of the emitter protect the process from the collinear divergence, but the soft divergence is still here. We recall that as the collinear

approximation has not been applied here yet these results are valid in all the soft part of the phase space (collinear or not) and there is no need to introduce a collinear cutoff, which is needed only in the hard part described below.

C.2. Hard collinear part

As explained in [200, App. B], using a light-cone gauge it is possible to show that the only contribution in the hard-collinear limit come from the squared amplitude where the gluon is emitted by the other gluon, and that all interference terms do not contribute. Therefore here we only have to consider the splitting of a gluon into two gluons.

We first introduce the notation p_{45} and E_{45} for the momentum and energy of the parent gluon 45, i.e. the one which splits into two final gluons. The 3−particles phase space element can be written as

$$d\Gamma_3 = d\Gamma_2 \frac{d^{D-1}p_5}{2E_5(2\pi)^{D-1}} \frac{E_{45}}{E_4}. \tag{C.9}$$

where $d\Gamma_2$ is the two-body phase space element of the particles 3 and 45. We then introduce two variables: z, which corresponds to the fraction of energy of the parent gluon taken by the gluon 4, and $s_{45} \equiv 2p_4 \cdot p_5$. The collinear condition is then $p_5 \approx (1-z)p_4$. This condition remove one degree of freedom and the integration over p_5 can be replaced by integrations over z and s_{45}. The collinear gluon approximation allows us to factorize the 3−particles phase space element into

$$d\Gamma_3^{\text{hard coll}} = d\Gamma_2 \frac{c_\varepsilon}{16\pi^2} \frac{dz\, ds_{45}}{[s_{45}z(1-z)]^{2-D/2}}\,, \tag{C.10}$$

with $c_\varepsilon = \Gamma(1+\varepsilon)(4\pi)^\varepsilon$. In the collinear limit $s_{45} \to 0$, and terms with s_{45}^{-1} will be responsible for collinear divergences. The hard collinear part is therefore separated from the hard non collinear part by the boundary condition $s_{45} < \delta_c\, s$, where δ_c is the collinear cutoff, which also specifies when the collinear approximation is valid.

In this approximation one can also simplify the squared amplitudes which factorizes into the leading order and so-called splitting functions [201]:

$$|M_3(1+2 \to 3+4+5)|^2 \simeq |M_2(1+2 \to 3+45)|^2 P_{gg}(z,D)\, g_s^2\, \mu^{4-D} \frac{2}{s_{45}}. \tag{C.11}$$

Here $P_{gg}(z,D)$ is the splitting function for a gluon splitting into a pair of gluons, calculated in D dimensions:

$$P_{gg}(z,D) = 2N\left[\frac{z}{1-z} + \frac{1-z}{z} + z(1-z)\right]. \tag{C.12}$$

The cross section then factorizes as:

$$\begin{aligned} d\sigma^{1+2\to3+4+5}_{\text{hard coll.}} &= d\sigma^{1+2\to3+45}_{\text{tree}}\left[\frac{\alpha_s}{2\pi}c_\varepsilon\left(\frac{\mu}{\sqrt{s}}\right)^{4-D}\right] &\text{(C.13)}\\ &\times \int_0^{\delta_c s}\frac{ds_{45}}{s_{45}}\left(\frac{\sqrt{s}}{\sqrt{s_{45}}}\right)^{4-D}\int dz[z(1-z)]^{D/2-2}P_{gg}(z,D). &\text{(C.14)}\end{aligned}$$

The integrations over s_{45} and z are independent. As explained above, the integration over s_{45} is done between two boundaries which are given by the collinear condition, and leads to the term

$$\int_0^{\delta_c s}\frac{ds_{45}}{s_{45}}\left(\frac{\sqrt{s}}{\sqrt{s_{45}}}\right)^{4-D} = -\frac{1}{\varepsilon}\,\delta_c^{-\varepsilon}. \tag{C.15}$$

The integration limits of z are defined in such a way that both gluons are hard:

$$\frac{\delta_s}{1-m_3^2/s} \le z \le 1 - \frac{\delta_s}{1-m_3^2/s}. \tag{C.16}$$

The splitting functions can be integrated over z and the final result is:

$$\begin{aligned} d\sigma^{1+2\to3+4+5}_{\text{hard coll.}} &= d\sigma^{1+2\to3+45}_{\text{tree}}\left[\frac{\alpha_s}{2\pi}c_\varepsilon\left(\frac{\mu}{\sqrt{s}}\right)^{4-D}\right] &\text{(C.17)}\\ &\times \left[\frac{N\,(11/6+2\ln\delta_s')}{2-D/2} + N\left[57/182-\pi^2/3-\ln^2\delta_s'-\ln\delta_c\left(11/6+2\ln\delta_s'\right)\right]\right]\\ &= d\sigma^{1+2\to3+45}_{\text{tree}}\left(\frac{\alpha_s}{2\pi}c_\varepsilon\right)\Big[N\big(11/6+2\ln\delta_s'\big)\big(\frac{1}{\varepsilon}+2\ln(\mu_r/\sqrt{s})\big) &\text{(C.18)}\\ &+ N\left(57/182-\pi^2/3-\ln^2\delta_s'-\ln\delta_c\left(11/6+2\ln\delta_s'\right)\right)\Big]\end{aligned}$$

where $\delta_s' \equiv \delta_s/(1-m_3^2/s)$. The $1/\varepsilon$ pole corresponds to the collinear divergence and will cancel with a similar pole in the virtual corrections.

C.3. Hard non collinear part

This part of the cross section is regular and can be numerically integrated over the relevant part of the three body phase space. This phase space region is defined by boundary conditions

which keep the integration far from the soft and collinear regions. In our case these conditions are applied on the energies of the final state particles and depends on two cutoff δ_s and δ_c:

- the usual soft cutoff is applied on the energy of the emitted gluon: $E_5 > \delta_s\sqrt{s}/2$,
- there is an additional soft cutoff applied on the energy of the tree-level gluon: $E_4 > \delta_s\sqrt{s}/2$,
- a cutoff is applied on the energy of the final quark, expressing the condition that the two gluons must not be collinear: $E_3 < \sqrt{s}/2 + m_3^2/(2\sqrt{s}) - \sqrt{s}\,\delta_c/2$.

Conclusion and outlook

In this thesis we have studied the neutralino-stop coannihilation and shown that the corresponding regions in various MSSM models have a rich phenomenology and are not fully excluded yet by experimental constraints. In particular the requirement of a small neutralino-stop mass splitting, which enhances the coannihilation and therefore reduces the relic density, pushes up the limits on the stop mass from the LHC. Also, it is compatible with a large stop mixing which is not in contradiction with the rather heavy mass of the Higgs boson, recently measured at the LHC. In addition it is well known that coannihilation regions lead to very small dark matter direct detection rates. We then tackled two different issues, both going beyond the usual framework of relic density in the MSSM.

We first studied the effect of Non Minimal Flavor Violation in the squark sector of the MSSM on the annihilation and coannihilation cross section of neutralino, and the related impact on the relic density of dark matter. Indeed, in the literature the framework of Minimal Flavor Violation (MFV) is generally assumed when computing the relic density in the MSSM. We have considered large flavor violating terms in the sectors of right handed third generation up and down squarks, and discussed the different effects that could affect the thermally averaged (co)annihilation cross section of the neutralino, and in consequence its predicted relic density. We have identified two kind of effects: the first one is the modification of the flavor content of the lightest squark, which opens new annihilation and coannihilation channels. This effect was particularly important when the corresponding flavor conserving channel was kinematically forbidden, as in the case of neutralino annihilation into top pairs for example. The second one is the modification of the mass eigenvalue of the squark, which enters the annihilation and coannihilation cross sections, but also the Boltzmann suppression factor in the case of coannihilation. The latter is the most important effect since the contribution of coannihilation strongly depends on the mass of the coannihilating NLSP. Performing a numerical analysis within the cMSSM, we have observed that these effects resulted in the reduction of the relic density in some part of the parameter space, leading to new favored regions absent in the case of MFV. In particular we have seen that a large mixing in the sector of down squark allow for coannihilation with the lightest down squark which is not possible in the usual cMSSM with MFV.

We then presented the calculation of the one-loop SUSY-QCD corrections to neutralino-stop coannihilation. Computing annihilation and coannihilation cross section at the Next-to-

leading Order becomes now necessary in order for the theoretical prediction to be as precise as the experimental measurement of the relic density. Our calculation has been presented in details, together with the corresponding implementation in a numerical code. We have seen that such calculation and implementation are non-trivial for several reasons. First, because of the large number of involved external states and of corresponding Feynman diagrams. Then, due to the difficulty of defining a consistent renormalization scheme in the MSSM, in particular in the sfermion sector, and the necessity to cancel Infra-Red divergences arising from different origins by using involved methods (in particular for the gluon final state). We have then shown numerical results for the electroweak gauge and Higgs boson final states and the one-loop corrections turned out to be significant, in particular in the case of the lightest Higgs boson final state, for which they reached 30% of the tree-level cross section. Our code was used to perform scans over the parameter space of a pMSSM model and we have seen that the impact of these corrections on the relic density was around 5 to 9% in the three considered scenarios, which is larger than the current experimental uncertainty from Planck (2%). These corrections need therefore to be taken into account when extracting parameters of supersymmetric models from the measurement of relic density.

Several deeper studies still need however to be performed. The calculation and implementation of the gluon final state will be finished soon, and significant corrections are expected. It could be then interesting to study the dependence of the results on the renormalization scale/scheme, and all relevant uncertainties. As was mentioned it is planned to implement a dipole subtraction method which would be numerically more stable and reliable than the phase space slicing method which is used. Again, it could be interesting to realize numerical comparisons between these two methods. We have also mentioned that this study is part of the DM@NLO project which includes the calculation of one-loop corrections to other processes like the annihilation of neutralino into heavy quarks. It is planned to perform a global analysis of the impact of such corrections in pMSSM scenario involving neutralino-stop coanihilation and neutralino annihilation into pair of top quarks, for example. However a renormalization scheme common to both processes still need to be defined. Members of the collaboration are involved in several projects, like the generalization of the correction in the case of neutralino annihilation process to the case of coannihilation of two different neutralino and chargino. Also, it is planned to adapt this calculation to the case of indirect detection. Lastly, the calculation of such corrections for the stop-stop annihilation processes, which contribute significantly in the neutralino-stop coannihilation region, is ongoing.

List of Figures

1.1. Rotation curve of the spiral galaxy NGC 6503. The dotted, dashed and dash-dotted lines are the contributions of gas, disk and dark matter, respectively. Figure taken from [5]. 3

1.2. Comoving number density of a WIMP in the early Universe. The dashed curves are the actual abundance, and the solid curve is the equilibrium abundance. Taken from [19]. 6

4.1. Cosmologically favored region in the (m_0, $m_{1/2}$) plane of the cMSSM for $\mu > 0$, $\tan\beta = 10$, $A_0 = 0$ GeV (left) and $A_0 = -3000$ GeV (right). 45

4.2. Evolution of different contributions to the relic density of neutralino with the neutralino-stop mass splitting. 50

4.3. Leading-order Feynman diagrams for neutralino-stop coannihilation into a quark and a Higgs boson ($\phi = h^0, H^0, A^0, H^\pm$) or a gauge boson ($V = g, \gamma, Z^0, W^\pm$). $q \equiv t$ or b if the outgoing boson is respectively neutral or charged. The u-channel is absent for a photon or a gluon in the final state. 51

4.4. Relative contributions of the neutralino-stop coannihilation channels for the generated parameter points as a function of the input parameters M_1, $M_{\tilde{q}_3}$, T_t, and $\tan\beta$ before (top) and after applying the relic density (middle) and Higgs mass (bottom) constraints. Shown are the contributions from th^0 (red), tg (green), tZ^0 (blue), tH^0 and tA^0 (yellow), bW^+ (cyan), bH^+ (pink), and $t\gamma$ (gray) final states. The parameters M_1, $M_{\tilde{q}_3}$, and T_t are given in GeV. The constraints are detailed in the text. 59

4.5. Relative contributions of the neutralino-stop coannihilation channels for the generated parameter points as a function of the input parameters M_1, $M_{\tilde{q}_3}$, T_t, and $\tan\beta$ after applying the flavor constraints (top), and all the mentioned constraints (bottom). Shown are the contributions from th^0 (red), tg (green), tZ^0 (blue), tH^0 and tA^0 (yellow), bW^+ (cyan), bH^+ (pink), and $t\gamma$ (gray) final states. The parameters M_1, $M_{\tilde{q}_3}$, and T_t are given in GeV. The constraints are detailed in the text. 60

5.1. Feynman diagrams for the annihilation of neutralinos into quark pairs through the exchange of a neutral Higgs boson $H_i^0 = h^0, H^0, A^0$ (left), a Z^0-boson (center left), or a squark (right and center right). 65

5.2. Cosmologically favored region and related exclusion limits in the (m_0, $m_{1/2}$) plane of the cMSSM for $\delta_{23}^{u,\mathrm{RR}} = 0$ (left) and $\delta_{23}^{u,\mathrm{RR}} = 0.98$ (right). 68

5.3. Cosmologically favored region and related exclusion limits for $\delta_{23}^{u,\mathrm{RR}} = 0.98$ in the ($m_{\tilde{\chi}_1^0}$, $m_{\tilde{u}_1} - m_{\tilde{\chi}_1^0}$) plane for fixed $A_0 = -500$ GeV and $\tan\beta = 10$ (left) and in the ($\delta_{23}^{u,\mathrm{RR}}$, A_0) plane for fixed $m_0 = 200$ GeV and $m_{1/2} = 400$ GeV (right). . 69

5.4. Cosmologically favored region and related exclusion limits in the ($\delta_{23}^{u,RR}, \delta_{23}^{u,LR}$) plane for fixed $m_0 = 200$ GeV, $m_{1/2} = 400$ GeV, and $A_0 = -500$ GeV. 71

5.5. Relic density of the neutralino (left) and contributing processes (right) as a function of $\delta_{23}^{u,\mathrm{RR}}$ for $m_0 = 1500$ GeV, $m_{1/2} = 680$ GeV, $A_0 = -500$ GeV, $\tan\beta = 10$, and $\mu > 0$. 72

5.6. Masses of the two lightest up-type squarks, gluino, and lightest neutralino (left) and flavor decomposition of lightest up-type squark (right) as a function of $\delta_{23}^{u,\mathrm{RR}}$ for $m_0 = 1500$ GeV, $m_{1/2} = 680$ GeV, $A_0 = -500$ GeV, $\tan\beta = 10$, and $\mu > 0$. 72

5.7. Cosmologically favored region and related exclusion limits in the (m_0, $m_{1/2}$) plane of the cMSSM for $\delta_{23}^{u,\mathrm{RR}} = 0$, $\delta_{23}^{d,\mathrm{RR}} = 0.98$ (left) and $\delta_{23}^{u,\mathrm{RR}} = \delta_{23}^{d,\mathrm{RR}} = 0.98$ (right). 73

6.1. Leading-order Feynman diagrams for neutralino-squark coannihilation into a quark and Higgs (ϕ) or electroweak gauge (V) bosons. The u-channel is absent for a photon in the final state. 81

6.2. Self-energy corrections for the quarks and squarks at one-loop level in QCD contributing to neutralino-squark coannihilation. 81

6.3. Vertex corrections at one-loop level contributing to neutralino-squark coannihilation into quarks and Higgs (ϕ) or electroweak gauge (V) bosons. The diagram involving the $V - g - \tilde{q} - \tilde{q}$ vertex is present only for the case of a gauge boson in the final state. 81

6.4. Four-point diagrams at one-loop level contributing to neutralino-squark coannihilation into quarks and Higgs (ϕ) or electroweak gauge (V) bosons. The last diagram involving the four-vertex is absent for a scalar in the final state. 81

6.5. Counterterms diagrams for the quarks and squarks propagators, the $\tilde{\chi}-\tilde{q}-q$, $q-q-V/\phi$ and $\tilde{q}-\tilde{q}-V/\phi$ vertices contributing to neutralino-squark coannihilation into quarks and Higgs (ϕ) or electroweak gauge (V) bosons. Again, the last diagram is absent in the case of photon final state. 85

6.6. Real gluon emission diagrams at one-loop level contributing to neutralino-squark coannihilation into quarks and Higgs (ϕ) or electroweak gauge (V) bosons. The last diagram involving the four-vertex is absent for a scalar in the final state. . 93

6.7. Soft and hard gluon radiation cross sections and their sum (left plot) in function of the soft cutoff for the process $\tilde{\chi}_1^0\ \tilde{t}_1 \to t\ Z^0$ with $p_{cm} = 100$ GeV. On the right plot is shown only the sum of soft and hard cross sections on a smaller scale. The spectrum corresponds to the pMSSM scenario II introduced later in Sec. 6.4.1. 96

6.8. Real gluon emission diagrams with a Wb final state where an internal top quark can become on-shell, as indicated by a double line. 97

6.9. Contribution of the different diagrams (s-, t-, and u-channels) depicted in Fig. 4.3. For the studied scenarios of Tab. 6.1 we show for selected coannihilation channels the tree-level cross section as well as the contribution of the different squared diagrams (ss, tt, uu) and the interference terms (st, su, tu). 100

6.10. Contribution of the different corrections to the total next-to-leading order correction for the case of coannihilation into th^0 for scenario I and into tZ^0 for scenario II. The real contribution σ^{real} is defined as the sum of the hard radiation and the soft gluon part with a cut on the gluon energy of $\Delta E = 10^{-3}\sqrt{s}$. The gray area indicates the thermal distribution (in arbitrary units). 102

6.11. Tree-level (black dashed line), full one-loop (blue solid line) and `micrOMEGAs` (orange solid line) cross sections for selected coannihilation channels in the scenarios of Tab. 6.1. The upper part of each plot shows the absolute value of σv together with the thermal distribution (in arbitrary units), whereas the lower part shows the corresponding relative shifts (second item in the legend). 103

6.12. The neutralino relic density $\Omega_\chi h^2$ as a function of M_1 (left) and T_t (right) in our scenario I calculated using different coannihilation cross sections: default `micrOMEGAs` (orange solid line), tree-level (black dashed line), and full one-loop (blue solid line). The gray band indicates the favored range according to Eq. (1.6) within 1σ. The lower part shows the relative impact of the one-loop correction on the relic-density compared to the tree-level calculation (second item in the legend). 105

6.13. 1σ Planck-compatible relic density bands from the default `micrOMEGAs` calculation (orange) and our one-loop calculation for coannihilation (blue) in the $(M_{\tilde{q}_3}, M_1)$ (left) and (T_t, M_1) (right) planes. In the plots on the left hand side the relative contribution of coannihilation processes is shown in green contour, and the relative impact of the one-loop corrections on the relic density in black lines. The plots on the right hand side show the LSP-NLSP mass difference in green contour. 106

6.14. The neutralino relic density $\Omega_\chi h^2$ as a function of $M_{\tilde{q}_3}$ (left) and T_t (right) in our scenario II calculated using different coannihilation cross sections: default `micrOMEGAs` (orange solid line), one-loop correction only for the th^0 final state (blue solid line), and one-loop correction only for the tZ^0 final state (blue dashed line). The gray band indicates the favored range according to Eq. (1.6). The lower part of the figure shows the relative impact of the one-loop correction on the relic-density compared to `micrOMEGAs` (second item in the legend). 108

6.15. Leading-order Feynman diagrams for neutralino-squark coannihilation into a gluon. 109

6.16. Self-energy corrections for the gluon at one-loop level in QCD contributing to neutralino-squark coannihilation via the counterterms. 110

6.17. Additional non-abelian vertex corrections at one-loop level contributing to neutralino-squark coannihilation into quarks and gluon. The lower right diagram does not contribute because of a zero color factor. 110

6.18. Additional non-abelian four-point diagrams at one-loop level contributing to neutralino-squark coannihilation into quarks and gluon. 110

6.19. Additional non-abelian real gluon emission diagrams contributing to neutralino-squark coannihilation into quarks gluon. 111

A.1. Simplified structure of the `DM@NLO` code. More details are given in the text. . . 116

List of Tables

3.1. Chiral supermultiplets in the Minimal Supersymmetric Standard Model. 28

3.2. Gauge supermultiplets in the Minimal Supersymmetric Standard Model. 28

3.3. Interaction and mass eigenstates of the superpartners of the Standard Model particles. 36

6.1. Three characteristic scenarios chosen in the pMSSM, which will be considered in this study. Given are the input parameters as described in the text, the lightest neutralino mass $m_{\tilde{\chi}_1^0}$, the lightest stop mass $m_{\tilde{t}_1}$, and the masses of the light and heavy CP-even Higgs bosons m_{h^0} and m_{H^0}. All values except for $\tan\beta$ are given in GeV. 98

6.2. Neutralino relic density and relative contributions of neutralino-stop coannihilation into a quark and a Higgs or electroweak gauge boson for the characteristic scenarios of Tab.6.1. The last column gives the sum of the listed contributions. 99

Bibliography

[1] P. Ade *et al.* (Planck Collaboration) (2013), arXiv:1303.5076 [astro-ph.CO]

[2] G. Bertone, D. Hooper, and J. Silk, Phys.Rept. **405**, 279 (2005), arXiv:hep-ph/0404175 [hep-ph]

[3] F. Zwicky, Helv.Phys.Acta **6**, 110 (1933)

[4] D. Clowe, M. Bradac, A. H. Gonzalez, M. Markevitch, S. W. Randall, *et al.*, Astrophys.J. **648**, L109 (2006), arXiv:astro-ph/0608407 [astro-ph]

[5] K. Begeman, A. Broeils, and R. Sanders, Monthly Notices of the Royal Astronomical Society **249**, 523 (1991)

[6] E. Komatsu *et al.* (WMAP Collaboration), Astrophys.J.Suppl. **192**, 18 (2011), arXiv:1001.4538 [astro-ph.CO]

[7] W. Rau, Phys.Part.Nucl. **42**, 650 (2011), arXiv:1103.5267 [astro-ph.HE]

[8] L. Bergstrom, Annalen Phys. **524**, 479 (2012), arXiv:1205.4882 [astro-ph.HE]

[9] M. W. Goodman and E. Witten, Phys.Rev. **D31**, 3059 (1985)

[10] E. Aprile *et al.* (XENON100 Collaboration), Phys.Rev.Lett. **107**, 131302 (2011), arXiv:1104.2549 [astro-ph.CO]

[11] R. Bernabei *et al.* (DAMA Collaboration), Eur.Phys.J. **C56**, 333 (2008), arXiv:0804.2741 [astro-ph]

[12] C. Aalseth *et al.* (CoGeNT collaboration), Phys.Rev.Lett. **106**, 131301 (2011), arXiv:1002.4703 [astro-ph.CO]

[13] C. Aalseth, P. Barbeau, J. Colaresi, J. Collar, J. Diaz Leon, *et al.*, Phys.Rev.Lett. **107**, 141301 (2011), arXiv:1106.0650 [astro-ph.CO]

[14] G. Angloher, M. Bauer, I. Bavykina, A. Bento, C. Bucci, *et al.*, Eur.Phys.J. **C72**, 1971 (2012), arXiv:1109.0702 [astro-ph.CO]

[15] Z. Ahmed *et al.* (CDMS-II Collaboration), Science **327**, 1619 (2010), arXiv:0912.3592

[astro-ph.CO]

[16] Z. Ahmed *et al.* (CDMS-II Collaboration), Phys.Rev.Lett. **106**, 131302 (2011), arXiv:1011.2482 [astro-ph.CO]

[17] Z. Ahmed *et al.* (CDMS Collaboration) (2012), arXiv:1203.1309 [astro-ph.CO]

[18] E. Armengaud *et al.* (EDELWEISS Collaboration), Phys.Rev. **D86**, 051701 (2012), arXiv:1207.1815 [astro-ph.CO]

[19] E. W. Kolb and M. S. Turner, *The Early universe*, Vol. 69 (1990) pp. 1–547

[20] K. Griest and D. Seckel, Nucl.Phys. **B283**, 681 (1987)

[21] P. Gondolo and G. Gelmini, Nucl.Phys. **B360**, 145 (1991)

[22] K. Griest and D. Seckel, Phys.Rev. **D43**, 3191 (1991)

[23] P. Binetruy, G. Girardi, and P. Salati, Nucl.Phys. **B237**, 285 (1984)

[24] J. Edsjo and P. Gondolo, Phys.Rev. **D56**, 1879 (1997), arXiv:hep-ph/9704361 [hep-ph]

[25] G. Belanger, F. Boudjema, A. Pukhov, and A. Semenov, Comput.Phys.Commun. **149**, 103 (2002), arXiv:hep-ph/0112278 [hep-ph]

[26] G. Belanger, F. Boudjema, A. Pukhov, and A. Semenov, Comput.Phys.Commun. **177**, 894 (2007)

[27] P. Gondolo, J. Edsjo, P. Ullio, L. Bergstrom, M. Schelke, *et al.*, JCAP **0407**, 008 (2004), arXiv:astro-ph/0406204 [astro-ph]

[28] H. Baer and M. Brhlik, Phys.Rev. **D53**, 597 (1996), arXiv:hep-ph/9508321 [hep-ph]

[29] H. Baer, C. Balazs, and A. Belyaev, 1138 (2002), arXiv:hep-ph/0211213 [hep-ph]

[30] F. Mahmoudi, Comput.Phys.Commun. **180**, 1579 (2009), arXiv:0808.3144 [hep-ph]

[31] J. Hamann, S. Hannestad, M. S. Sloth, and Y. Y. Wong, Phys.Rev. **D75**, 023522 (2007), arXiv:astro-ph/0611582 [astro-ph]

[32] A. Arbey and F. Mahmoudi, Phys.Lett. **B669**, 46 (2008), arXiv:0803.0741 [hep-ph]

[33] A. Arbey and F. Mahmoudi, JHEP **1005**, 051 (2010), arXiv:0906.0368 [hep-ph]

[34] J. R. Ellis, J. E. Kim, and D. V. Nanopoulos, Phys.Lett. **B145**, 181 (1984)

[35] K. Rajagopal, M. S. Turner, and F. Wilczek, Nucl.Phys. **B358**, 447 (1991)

[36] T. Teubner, *The standard model* (2008) pp. 112–206

[37] M. E. Peskin and D. V. Schroeder, *An Introduction to quantum field theory* (1995)

[38] C. Burgess and G. Moore, *The standard model: A primer* (2007)

[39] D. Gross and F. Wilczek, Phys.Rev. **D8**, 3633 (1973)

[40] D. Gross and F. Wilczek, Phys.Rev. **D9**, 980 (1974)

[41] H. D. Politzer, Phys.Rept. **14**, 129 (1974)

[42] L. Faddeev and V. Popov, Phys.Lett. **B25**, 29 (1967)

[43] S. Glashow, Nucl.Phys. **22**, 579 (1961)

[44] S. Weinberg, Phys.Rev.Lett. **19**, 1264 (1967)

[45] A. Salam, Conf.Proc. **C680519**, 367 (1968)

[46] J. Goldstone, Nuovo Cim. **19**, 154 (1961)

[47] F. Englert and R. Brout, Phys.Rev.Lett. **13**, 321 (1964)

[48] P. W. Higgs, Phys.Rev.Lett. **13**, 508 (1964)

[49] J. M. Cornwall, D. N. Levin, and G. Tiktopoulos, Phys.Rev. **D10**, 1145 (1974)

[50] C. Vayonakis, Lett.Nuovo Cim. **17**, 383 (1976)

[51] B. W. Lee, C. Quigg, and H. Thacker, Phys.Rev. **D16**, 1519 (1977)

[52] N. Cabibbo, Phys.Rev.Lett. **10**, 531 (1963)

[53] M. Kobayashi and T. Maskawa, Prog.Theor.Phys. **49**, 652 (1973)

[54] Z. Maki, M. Nakagawa, and S. Sakata, Prog.Theor.Phys. **28**, 870 (1962)

[55] S. P. Martin (1997), arXiv:hep-ph/9709356 [hep-ph]

[56] J. Edsjo, M. Schelke, P. Ullio, and P. Gondolo, JCAP **0304**, 001 (2003), arXiv:hep-ph/0301106 [hep-ph]

[57] M. Klasen, C. E. Yaguna, J. D. Ruiz-Alvarez, D. Restrepo, and O. Zapata, JCAP **1304**, 044 (2013), arXiv:1302.5298 [hep-ph]

[58] J. L. Feng, K. T. Matchev, and F. Wilczek, Phys.Lett. **B482**, 388 (2000), arXiv:hep-ph/0004043 [hep-ph]

[59] J. R. Ellis, T. Falk, and K. A. Olive, Phys.Lett. **B444**, 367 (1998), arXiv:hep-ph/9810360 [hep-ph]

[60] J. R. Ellis, T. Falk, K. A. Olive, and M. Srednicki, Astropart.Phys. **13**, 181 (2000), arXiv:hep-ph/9905481 [hep-ph]

[61] C. Boehm, A. Djouadi, and M. Drees, Phys.Rev. **D62**, 035012 (2000), arXiv:hep-ph/9911496 [hep-ph]

[62] J. R. Ellis, K. A. Olive, and Y. Santoso, Astropart.Phys. **18**, 395 (2003), arXiv:hep-ph/0112113 [hep-ph]

[63] V. Bertin, E. Nezri, and J. Orloff, JHEP **0302**, 046 (2003), arXiv:hep-ph/0210034 [hep-ph]

[64] G. Belanger, F. Boudjema, A. Cottrant, A. Pukhov, and A. Semenov, Nucl.Phys. **B706**, 411 (2005), arXiv:hep-ph/0407218 [hep-ph]

[65] A. Birkedal-Hansen and B. D. Nelson, Phys.Rev. **D64**, 015008 (2001), arXiv:hep-ph/0102075 [hep-ph]

[66] S. Profumo and C. Yaguna, Phys.Rev. **D69**, 115009 (2004), arXiv:hep-ph/0402208 [hep-ph]

[67] J. R. Ellis, T. Falk, K. A. Olive, and Y. Santoso, Nucl.Phys. **B652**, 259 (2003), arXiv:hep-ph/0210205 [hep-ph]

[68] H. Baer, A. Mustafayev, S. Profumo, A. Belyaev, and X. Tata, JHEP **0507**, 065 (2005), arXiv:hep-ph/0504001 [hep-ph]

[69] S. Profumo, Phys.Rev. **D68**, 015006 (2003), arXiv:hep-ph/0304071 [hep-ph]

[70] A. Delgado, G. F. Giudice, G. Isidori, M. Pierini, and A. Strumia, Eur.Phys.J. **C73**, 2370 (2013), arXiv:1212.6847 [hep-ph]

[71] J. Camargo-Molina, B. O'Leary, W. Porod, and F. Staub (2013), arXiv:1307.1477 [hep-ph]

[72] A. Pukhov (2004), arXiv:hep-ph/0412191 [hep-ph]

[73] A. Pukhov, E. Boos, M. Dubinin, V. Edneral, V. Ilyin, *et al.* (1999), arXiv:hep-ph/9908288 [hep-ph]

[74] W. Porod, Comput.Phys.Commun. **153**, 275 (2003), arXiv:hep-ph/0301101 [hep-ph]

[75] W. Porod and F. Staub, Comput.Phys.Commun. **183**, 2458 (2012), arXiv:1104.1573 [hep-ph]

[76] A. Djouadi, J.-L. Kneur, and G. Moultaka, Comput.Phys.Commun. **176**, 426 (2007), arXiv:hep-ph/0211331 [hep-ph]

[77] B. Allanach, Comput.Phys.Commun. **143**, 305 (2002), arXiv:hep-ph/0104145 [hep-ph]

[78] B. Allanach, C. Balazs, G. Belanger, M. Bernhardt, F. Boudjema, *et al.*, Comput.Phys.Commun. **180**, 8 (2009), arXiv:0801.0045 [hep-ph]

[79] D. Restrepo, M. Taoso, J. Valle, and O. Zapata, Phys.Rev. **D85**, 023523 (2012), arXiv:1109.0512 [hep-ph]

[80] C. E. Yaguna, Phys.Rev. **D81**, 075024 (2010), arXiv:1003.2730 [hep-ph]

[81] L. Lopez Honorez and C. E. Yaguna, JHEP **1009**, 046 (2010), arXiv:1003.3125 [hep-ph]

[82] A. Goudelis, B. Herrmann, and O. Stål (2013), arXiv:1303.3010 [hep-ph]

[83] J. Ellis and K. A. Olive, Eur.Phys.J. **C72**, 2005 (2012), arXiv:1202.3262 [hep-ph]

[84] `https://twiki.cern.ch/twiki/bin/view/AtlasPublic/CombinedSummaryPlots`

[85] `https://twiki.cern.ch/twiki/bin/view/CMSPublic/PhysicsResultsSUS`

[86] W. Beenakker, M. Kramer, T. Plehn, M. Spira, and P. Zerwas, Nucl.Phys. **B515**, 3 (1998), arXiv:hep-ph/9710451 [hep-ph]

[87] K. Huitu, L. Leinonen, and J. Laamanen, Phys.Rev. **D84**, 075021 (2011), arXiv:1107.2128 [hep-ph]

[88] M. A. Ajaib, T. Li, and Q. Shafi, Phys.Rev. **D85**, 055021 (2012), arXiv:1111.4467 [hep-ph]

[89] Z.-H. Yu, X.-J. Bi, Q.-S. Yan, and P.-F. Yin (2012), arXiv:1211.2997 [hep-ph]

[90] S. Bornhauser, M. Drees, S. Grab, and J. Kim, Phys.Rev. **D83**, 035008 (2011), arXiv:1011.5508 [hep-ph]

[91] C. Kilic and B. Tweedie (2012), arXiv:1211.6106 [hep-ph]

[92] M. Adeel Ajaib, T. Li, and Q. Shafi, Phys.Lett. **B701**, 255 (2011), arXiv:1104.0251 [hep-ph]

[93] A. Belyaev, T. Lastovicka, A. Nomerotski, and G. Lastovicka-Medin, Phys.Rev. **D81**, 035011 (2010), arXiv:0912.2411 [hep-ph]

[94] E. Alvarez and Y. Bai, JHEP **1208**, 003 (2012), arXiv:1204.5182 [hep-ph]

[95] G. Aad *et al.* (ATLAS Collaboration), Phys.Lett. **B716**, 1 (2012), arXiv:1207.7214 [hep-ex]

[96] S. Chatrchyan *et al.* (CMS Collaboration), Phys.Lett. **B716**, 30 (2012), arXiv:1207.7235

[hep-ex]

[97] A. Collaboration, ATLAS-CONF-2013-009, ATLAS-COM-CONF-2013-014 (2013)

[98] C. Collaboration, CMS-PAS-HIG-13-005 (2013)

[99] A. Arbey, M. Battaglia, A. Djouadi, F. Mahmoudi, and J. Quevillon, Phys.Lett. **B708**, 162 (2012), arXiv:1112.3028 [hep-ph]

[100] A. Arbey, M. Battaglia, A. Djouadi, and F. Mahmoudi, JHEP **1209**, 107 (2012), arXiv:1207.1348 [hep-ph]

[101] F. Brummer, S. Kraml, and S. Kulkarni, JHEP **1208**, 089 (2012), arXiv:1204.5977 [hep-ph]

[102] H. Baer, V. Barger, and A. Mustafayev, JHEP **1205**, 091 (2012), arXiv:1202.4038 [hep-ph]

[103] J. Ellis, F. Luo, K. A. Olive, and P. Sandick (2012), arXiv:1212.4476 [hep-ph]

[104] M. Badziak, E. Dudas, M. Olechowski, and S. Pokorski, JHEP **1207**, 155 (2012), arXiv:1205.1675 [hep-ph]

[105] M. Carena, S. Gori, N. R. Shah, C. E. M. Wagner, and L.-T. Wang (2013), arXiv:1303.4414 [hep-ph]

[106] Y. Amhis *et al.* (Heavy Flavor Averaging Group) (2012), arXiv:1207.1158 [hep-ex]

[107] F. Mahmoudi, S. Neshatpour, and J. Orloff, JHEP **1208**, 092 (2012), arXiv:1205.1845 [hep-ph]

[108] A. Arbey, M. Battaglia, F. Mahmoudi, and D. Martinez Santos, Phys.Rev. **D87**, 035026 (2013), arXiv:1212.4887 [hep-ph]

[109] R. Aaij *et al.* (LHCb Collaboration), Phys.Rev.Lett. **110**, 021801 (2013), arXiv:1211.2674

[110] R. Aaij *et al.* (LHCb collaboration) (2013), arXiv:1307.5024 [hep-ex]

[111] S. Chatrchyan *et al.* (CMS Collaboration) (2013), arXiv:1307.5025 [hep-ex]

[112] The ATLAS, CMS and LHCb Collaborations, LHCb-CONF-2012-017, CMS-PAS-BPH-12-009, ATLAS-COM-CONF-2012-090 (2012)

[113] G. Bennett *et al.* (Muon G-2 Collaboration), Phys.Rev. **D73**, 072003 (2006), arXiv:hep-ex/0602035 [hep-ex]

[114] J. Beringer *et al.* (Particle Data Group), Phys.Rev. **D86**, 010001 (2012)

[115] M. Davier, A. Hoecker, B. Malaescu, and Z. Zhang, Eur.Phys.J. **C71**, 1515 (2011), arXiv:1010.4180 [hep-ph]

[116] S. Bodenstein, C. Dominguez, K. Schilcher, and H. Spiesberger (2013), arXiv:1302.1735 [hep-ph]

[117] G.-C. Cho, K. Hagiwara, Y. Matsumoto, and D. Nomura, JHEP **1111**, 068 (2011), arXiv:1104.1769 [hep-ph]

[118] J. A. Aguilar-Saavedra, A. Ali, B. C. Allanach, R. L. Arnowitt, H. A. Baer, *et al.*, Eur.Phys.J. **C46**, 43 (2006), arXiv:hep-ph/0511344 [hep-ph]

[119] B. Herrmann and M. Klasen, Phys.Rev. **D76**, 117704 (2007), arXiv:0709.0043 [hep-ph]

[120] L. Hall and L. Randall, Phys.Rev.Lett. **65**, 2939 (1990)

[121] G. D'Ambrosio, G. Giudice, G. Isidori, and A. Strumia, Nucl.Phys. **B645**, 155 (2002), arXiv:hep-ph/0207036 [hep-ph]

[122] W. Altmannshofer, A. J. Buras, and D. Guadagnoli, JHEP **0711**, 065 (2007), arXiv:hep-ph/0703200 [hep-ph]

[123] G. Bozzi, B. Fuks, B. Herrmann, and M. Klasen, Nucl.Phys. **B787**, 1 (2007), arXiv:0704.1826 [hep-ph]

[124] B. Fuks, B. Herrmann, and M. Klasen, Nucl.Phys. **B810**, 266 (2009), arXiv:0808.1104 [hep-ph]

[125] T. Hurth and W. Porod, JHEP **0908**, 087 (2009), arXiv:0904.4574 [hep-ph]

[126] A. Bartl, K. Hidaka, K. Hohenwarter-Sodek, T. Kernreiter, W. Majerotto, *et al.*, Phys.Lett. **B679**, 260 (2009), arXiv:0905.0132 [hep-ph]

[127] M. Bruhnke, B. Herrmann, and W. Porod, JHEP **1009**, 006 (2010), arXiv:1007.2100 [hep-ph]

[128] A. Bartl, H. Eberl, B. Herrmann, K. Hidaka, W. Majerotto, *et al.*, Phys.Lett. **B698**, 380 (2011), arXiv:1007.5483 [hep-ph]

[129] D. Choudhury, R. Garani, and S. K. Vempati, JHEP **1206**, 014 (2012), arXiv:1104.4467 [hep-ph]

[130] B. Herrmann, M. Klasen, and Q. Le Boulc'h, Phys.Rev. **D84**, 095007 (2011), arXiv:1106.6229 [hep-ph]

[131] F. Gabbiani, E. Gabrielli, A. Masiero, and L. Silvestrini, Nucl.Phys. **B477**, 321 (1996), arXiv:hep-ph/9604387 [hep-ph]

[132] J. S. Hagelin, S. Kelley, and T. Tanaka, Nucl.Phys. **B415**, 293 (1994)

[133] M. Ciuchini, E. Franco, D. Guadagnoli, V. Lubicz, M. Pierini, *et al.*, Phys.Lett. **B655**, 162 (2007), arXiv:hep-ph/0703204 [hep-ph]

[134] A. Crivellin (2012), arXiv:1205.4881 [hep-ph]

[135] M. Blanke, G. F. Giudice, P. Paradisi, G. Perez, and J. Zupan, JHEP **1306**, 022 (2013), arXiv:1302.7232 [hep-ph]

[136] B. Herrmann, M. Klasen, and K. Kovarik, Phys.Rev. **D79**, 061701 (2009), arXiv:0901.0481 [hep-ph]

[137] B. Herrmann, M. Klasen, and K. Kovarik, Phys.Rev. **D80**, 085025 (2009), arXiv:0907.0030 [hep-ph]

[138] T. E. W. Group (CDF Collaboration, D0 Collaboration) (2009), arXiv:0903.2503 [hep-ex]

[139] K. Nakamura *et al.* (Particle Data Group), J.Phys. **G37**, 075021 (2010)

[140] F. Staub (2008), arXiv:0806.0538 [hep-ph]

[141] F. Staub, Comput.Phys.Commun. **181**, 1077 (2010), arXiv:0909.2863 [hep-ph]

[142] C. Pallis, Nucl.Phys. **B678**, 398 (2004), arXiv:hep-ph/0304047 [hep-ph]

[143] M. Klasen, C. E. Yaguna, and J. D. Ruiz-Alvarez, Phys.Rev. **D87**, 075025 (2013), arXiv:1302.1657 [hep-ph]

[144] M. Drees, J. Kim, and K. Nagao, Phys.Rev. **D81**, 105004 (2010), arXiv:0911.3795 [hep-ph]

[145] M. Drees and J. Gu, Phys.Rev. **D87**, 063524 (2013), arXiv:1301.1350 [hep-ph]

[146] J. Hisano, S. Matsumoto, M. Nagai, O. Saito, and M. Senami, Phys.Lett. **B646**, 34 (2007), arXiv:hep-ph/0610249 [hep-ph]

[147] A. Hryczuk, R. Iengo, and P. Ullio, JHEP **1103**, 069 (2011), arXiv:1010.2172 [hep-ph]

[148] M. Beneke, C. Hellmann, and P. Ruiz-Femenia, JHEP **1303**, 148 (2013), arXiv:1210.7928 [hep-ph]

[149] C. Hellmann and P. Ruiz-Femenia (2013), arXiv:1303.0200 [hep-ph]

[150] A. Hryczuk, Phys.Lett. **B699**, 271 (2011), arXiv:1102.4295 [hep-ph]

[151] N. Baro, F. Boudjema, and A. Semenov, Phys.Lett. **B660**, 550 (2008), arXiv:0710.1821 [hep-ph]

[152] N. Baro, G. Chalons, and S. Hao, AIP Conf.Proc. **1200**, 1067 (2010), arXiv:0909.3263 [hep-ph]

[153] N. Baro, F. Boudjema, G. Chalons, and S. Hao, Phys.Rev. **D81**, 015005 (2010), arXiv:0910.3293 [hep-ph]

[154] F. Boudjema, G. Drieu La Rochelle, and S. Kulkarni, Phys.Rev. **D84**, 116001 (2011), arXiv:1108.4291 [hep-ph]

[155] A. Chatterjee, M. Drees, and S. Kulkarni, Phys.Rev. **D86**, 105025 (2012), arXiv:1209.2328 [hep-ph]

[156] A. Freitas, Phys.Lett. **B652**, 280 (2007), arXiv:0705.4027 [hep-ph]

[157] J. Harz, B. Herrmann, M. Klasen, K. Kovarik, and Q. Le Boulc'h, Phys.Rev. **D87**, 054031 (2013), arXiv:1212.5241 [hep-ph]

[158] I. Gogoladze, S. Raza, and Q. Shafi, JHEP **1203**, 054 (2012), arXiv:1111.6299 [hep-ph]

[159] R. L. Arnowitt, B. Dutta, and Y. Santoso, Nucl.Phys. **B606**, 59 (2001), arXiv:hep-ph/0102181 [hep-ph]

[160] V. Bednyakov, H. Klapdor-Kleingrothaus, and V. Gronewold, Phys.Rev. **D66**, 115005 (2002), arXiv:hep-ph/0208178 [hep-ph]

[161] T. Hahn, Comput.Phys.Commun. **140**, 418 (2001), arXiv:hep-ph/0012260 [hep-ph]

[162] R. Mertig, M. Bohm, and A. Denner, Comput.Phys.Commun. **64**, 345 (1991)

[163] J. Vermaseren (2000), arXiv:math-ph/0010025 [math-ph]

[164] W. Siegel, Phys.Lett. **B84**, 193 (1979)

[165] G. 't Hooft and M. Veltman, Nucl.Phys. **B153**, 365 (1979)

[166] G. Passarino and M. Veltman, Nucl.Phys. **B160**, 151 (1979)

[167] S. Dittmaier, Nucl.Phys. **B675**, 447 (2003), arXiv:hep-ph/0308246 [hep-ph]

[168] A. Denner and S. Dittmaier, Nucl.Phys. **B844**, 199 (2011), arXiv:1005.2076 [hep-ph]

[169] T. Hahn and M. Perez-Victoria, Comput.Phys.Commun. **118**, 153 (1999), arXiv:hep-ph/9807565 [hep-ph]

[170] N. Baro and F. Boudjema, Phys.Rev. **D80**, 076010 (2009), arXiv:0906.1665 [hep-ph]

[171] S. Heinemeyer, H. Rzehak, and C. Schappacher, Phys.Rev. **D82**, 075010 (2010), arXiv:1007.0689 [hep-ph]

[172] K. Kovarik, C. Weber, H. Eberl, and W. Majerotto, Phys.Rev. **D72**, 053010 (2005), arXiv:hep-ph/0506021 [hep-ph]

[173] K. Melnikov and A. Yelkhovsky, Phys.Rev. **D59**, 114009 (1999), arXiv:hep-ph/9805270 [hep-ph]

[174] A. Hoang, Phys.Rev. **D61**, 034005 (2000), arXiv:hep-ph/9905550 [hep-ph]

[175] M. Beneke and A. Signer, Phys.Lett. **B471**, 233 (1999), arXiv:hep-ph/9906475 [hep-ph]

[176] A. Penin and A. Pivovarov, Nucl.Phys. **B549**, 217 (1999), arXiv:hep-ph/9807421 [hep-ph]

[177] H. Baer, J. Ferrandis, K. Melnikov, and X. Tata, Phys.Rev. **D66**, 074007 (2002), arXiv:hep-ph/0207126 [hep-ph]

[178] K. Chetyrkin, Phys.Lett. **B390**, 309 (1997), arXiv:hep-ph/9608318 [hep-ph]

[179] P. Baikov, K. Chetyrkin, and J. H. Kuhn, Phys.Rev.Lett. **96**, 012003 (2006), arXiv:hep-ph/0511063 [hep-ph]

[180] K. Chetyrkin and A. Kwiatkowski, Nucl.Phys. **B461**, 3 (1996), arXiv:hep-ph/9505358 [hep-ph]

[181] M. S. Carena, D. Garcia, U. Nierste, and C. E. Wagner, Nucl.Phys. **B577**, 88 (2000), arXiv:hep-ph/9912516 [hep-ph]

[182] J. Guasch, P. Hafliger, and M. Spira, Phys.Rev. **D68**, 115001 (2003), arXiv:hep-ph/0305101 [hep-ph]

[183] H. Eberl, K. Hidaka, S. Kraml, W. Majerotto, and Y. Yamada, Phys.Rev. **D62**, 055006 (2000), arXiv:hep-ph/9912463 [hep-ph]

[184] C. Weber, K. Kovarik, H. Eberl, and W. Majerotto, Nucl.Phys. **B776**, 138 (2007), arXiv:hep-ph/0701134 [hep-ph]

[185] B. Harris and J. Owens, Phys.Rev. **D65**, 094032 (2002), arXiv:hep-ph/0102128 [hep-ph]

[186] W. Giele and E. N. Glover, Phys.Rev. **D46**, 1980 (1992)

[187] A. Denner, Fortsch.Phys. **41**, 307 (1993), arXiv:0709.1075 [hep-ph]

[188] S. Catani, S. Dittmaier, M. H. Seymour, and Z. Trocsanyi, Nucl.Phys. **B627**, 189 (2002), arXiv:hep-ph/0201036 [hep-ph]

[189] G. 't Hooft and M. Veltman, Nucl.Phys. **B153**, 365 (1979)

[190] W. Beenakker, R. Hopker, M. Spira, and P. Zerwas, Nucl.Phys. **B492**, 51 (1997),

arXiv:hep-ph/9610490 [hep-ph]

[191] T. M. Tait, Phys.Rev. **D61**, 034001 (2000), arXiv:hep-ph/9909352 [hep-ph]

[192] D. Goncalves-Netto, D. Lopez-Val, K. Mawatari, T. Plehn, and I. Wigmore, Phys.Rev. **D87**, 014002 (2013), arXiv:1211.0286 [hep-ph]

[193] H. Eberl, Ph.D. thesis (1998), `www.hephy.at/user/helmut/diss.ps.gz`

[194] T. Hahn, Comput.Phys.Commun. **168**, 78 (2005), arXiv:hep-ph/0404043 [hep-ph]

[195] I. Bojak, Ph.D. thesis (2000), arXiv:hep-ph/0005120 [hep-ph]

[196] W. Beenakker, H. Kuijf, W. van Neerven, and J. Smith, Phys.Rev. **D40**, 54 (1989)

[197] B. Harris and J. Smith, Nucl.Phys. **B452**, 109 (1995), arXiv:hep-ph/9503484 [hep-ph]

[198] J. Smith, D. Thomas, and W. van Neerven, Z.Phys. **C44**, 267 (1989)

[199] W. van Neerven, Nucl.Phys. **B268**, 453 (1986)

[200] M. L. Mangano, P. Nason, and G. Ridolfi, Nucl.Phys. **B373**, 295 (1992)

[201] G. Altarelli and G. Parisi, Nucl.Phys. **B126**, 298 (1977)

Abstract

The Minimal Supersymmetric Standard Model (MSSM), the most studied model of Physics beyond the Standard Model, provides a candidate for dark matter: the neutralino. It however has often a too large predicted relic density, which can be reduced to the experimental range of WMAP and Planck thanks to several known mechanisms, like the coannihilation between the neutralino and the stop. In this thesis, we first make short reviews of WIMP dark matter and the Standard Model of particle Physics, introduce the MSSM and discuss the phenomenology of the neutralino relic density. We then focus on two different aspects related to the prediction of the relic density in the neutralino-stop coannihilation region and the calculation of the corresponding annihilation and coannihilation cross sections. First, we study the phenomenology of non minimal flavor violation in the squark sector in the context of the neutralino relic density. We consider flavor violating terms in the sectors of right-handed third generation up and down squarks and show that they can have an important impact on the thermally averaged (co)annihilation cross section of the neutralino, and therefore on its relic density. Then, following earlier studies which have shown that the impact of radiative corrections to the annihilation of neutralinos was larger than the experimental uncertainty, we calculate one-loop SUSY-QCD corrections for the neutralino-stop coannihilation into electroweak gauge and Higgs bosons. We study the phenomenological impact of these corrections on the relic density, which turns out to be larger than the current experimental uncertainty from the Planck experiment.

Résumé

Le Modèle Standard Supersymétrique Minimal (MSSM), le plus étudié des modèles de Nouvelle Physique, contient un candidat à la matière noire : le neutralino. Sa densité relique prédite est cependant habituellement trop élevée, mais peut être réduite jusqu'à l'intervalle expérimental de WMAP et de Planck grâce à certains mécanismes connus, comme la coannihilation entre le neutralino et le stop. Dans cette thèse nous présentons tout d'abord la matière noire en tant que WIMP ainsi que le Modèle Standard de la Physique des Particules, puis nous abordons le MSSM ainsi que la phénoménologie de la densité relique de neutralino. Nous étudions ensuite deux aspects différents liés à la prédiction de la densité relique dans la région de coannihilation neutralino-stop, ainsi qu'au calcul des sections efficaces d'annihilation et de coannihilation correspondantes. Nous étudions tout d'abord la phénoménologie de la violation de saveur non minimale dans le secteur des squarks dans le contexte de la densité relique de neutralino. Nous considérons des termes violant la saveur dans le secteur des squarks up et down de chiralité droite et de troisième génération et montrons qu'ils peuvent avoir un impact important sur les sections efficaces d'annihilation et de coannihilation du neutralino, et en conséquence sur la densité relique. En se basant ensuite sur des travaux antérieurs qui ont montré que l'impact des corrections radiatives pour l'annihilation de neutralino était supérieur à l'incertitude expérimentale, nous calculons les corrections SUSY-QCD à une boucle pour la coannihilation neutralino-stop en bosons de jauge électrofaibles et bosons de Higgs. Nous étudions l'impact phénoménologique de ces corrections sur la densité relique, qui s'avère être supérieur à l'incertitude expérimentale donnée par l'expérience Planck.